CASE INSTITUTE OF TECHNOLOGY

CLEVELAND, OHIO

ENGINEERING DESIGN CENTER

This Research Was Sponsored by

THE NATIONAL AERONAUTICS AND SPACE ADMINISTRATION

A COMPENSATED PULSE-DATA RELAY SERVOMECHANISM

Report No. EDC 1 - 65 - 32

by

William Doyle McLeod

C. K. Taft
Assistant Professor of Engineering
Co-Investigator

Harry W. Mergler
Professor of Engineering
Principal Investigator

Digital
Systems
Laboratory

Ns G 36 - 60

ABSTRACT

To obtain digital accuracy in a position control system it is necessary to quantize the measured variable. The minimum resolution required by the system specifications dictates the quanta size. This quantization process reduces the information content in a signal which severely limits the dynamics performance of the controlled system. In addition, fine quantization of a signal is not feasible in some physical systems and this would appear to limit the usefullness of a digital controller.

A means of retaining the full information content in a quantized variable by use of a high frequency dither is developed. This dither signal does not involve adding a dither to the input to the quantizer and consequently the quantizer circuitry is not required to process information at high rates so that reliability of the digital portion of the control loop is maintained. This technique also makes it possible to obtain a resolution which is smaller than the quanta size. This method of quantization is combined with a relay control element in a digital feedback system. The relay is effectively linearized by a high frequency dither. This provides the capability of satisfying a wide range of performance specifications and eliminates some of the stability problems normally associated with digital systems.

ACKNOWLEDGMENT

The author wishes to thank his advisor, Dr. C. K. Taft, for his guidance.

The research described in this report was supported by funds from Research Grant No. NsG - 36 - 60 supplied by The National Aeronautics and Space Administration under the direction of Dr. H. W. Mergler.

TABLE OF CONTENTS

LIST OF FIGURES

LIST OF TABLES

LIST OF SYMBOLS

A	Limit cycle amplitude
A	Quantizer output channel
A_{1T}	Trigger element for quantizer channel A_1
A_{2T}	Trigger element for quantizer channel A_2
a_n	Fourier coefficient
B	Limit cycle amplitude
B	Quantizer output channel
B_T	Trigger element for quantizer channel B
B	Boolean equation
b_n	Fourier coefficient
c_n	Circulating register n^{th} bit
D	Relay dead zone
D	Damping coefficient
$d_n(t)$	Dither signal
E_{sat}	Saturation level
e(t)	System error
$e_o(t)$	Relay output

$e_i(t)$	Relay input
$F(t)$	Fourier series
f	Boolean equation
$G(s)$	Transfer function
i(a)	Armature current
J	Inertia
j	$\sqrt{-1}$
K_{eq}	Equivalent gain
K_q	Describing function gain
K	Open loop gain
K'	Damped natural frequency
K_n	Gain
K_t	Torque constant
K_B	Back emf constant
L_a	Inductance
M	Binary equivalent of (n - 1)
M	Weighting function
m	Dither amplitude
n	Integer
P	Dither amplitude

Q^*	Incremental quantizer
q	Quanta size
R_a	Armature resistance
$r(t)$	Input signal
S	Laplace transform (d/dt)
S	Boolean variable
s_n	Denominator polynomial roots
T_d	Period of dither
T_r	Input pulse period
T_L	Load torque
t	Time
u	Unit step function
V_{bemf}	Armature back emf
V_0	Source voltage
Z_0	Source impedance
α	0 → 1 flip-flop transition
β	1 → 0 flip-flop transition
β	Phase angle
Δ_p	Output ripple
$\Delta(t)$	Quantization error

δ	Unit impulse function
μ_n	Phase angle
Σ	Implies summation
τ	Time
τ	Torque
ψ	Time
$\Omega_q(t)$	Output signal
Ω_{ave}	Average output
$\Omega(t)$	Output signal
$\dot{\Omega}(t)$	$d\Omega(t)/dt$
ω	Phase angle
ω_d	Damped natural frequency

LOGIC ELEMENT SYMBOLS

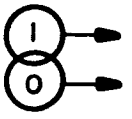

FREE-RUNNING MULTIVIBRATOR

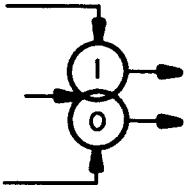

FLIP FLOP

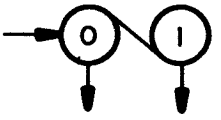

ONE SHOT MULTIVIBRATOR

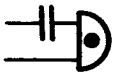

GATED PULSE GENERATOR

ANALOG "EITHER OR" GATE

AND

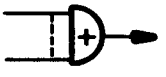

OR

NOR

STEERING GATE

TIME DELAY

CHAPTER I
INTRODUCTION

A pulse-data system is a special case within the general class of digital systems. The name is derived from the fact that the information transfer is accomplished by means of pulses. The information is stored by counting the pulses and registering the totals in the form of a coded number. The main reasons for using a pulse-data system are that the system can be implemented economically and the input data can be produced relatively simply by storing electrical pulses on magnetic tape, although the input pulses can be generated in many other ways. These pulses contain both position and velocity information. Each pulse commands an incremental change in the plant output, and the pulse repetition rate determines the rate of change of the plant output. This incremental change is termed a quanta.

A typical pulse-data system is shown in block diagram form in figure 1. The reference or input signal $r(t)$, in the form of electrical pulses, drives one input of a bidirectional counter. These pulses must be direction-sensitive so that the counter can discriminate between forward and reverse command pulses. The state of the counter is fed to a digital-to-analog converter, which converts a coded number to an analog signal capable of controlling the plant. The output of this plant is fed

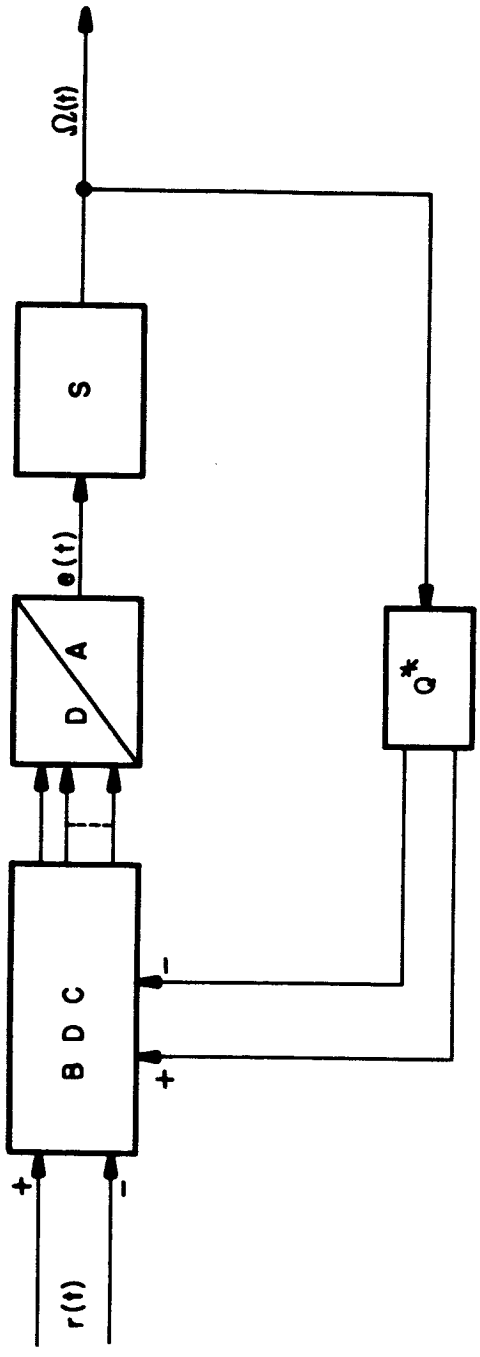

FIG. I CONVENTIONAL PULSE-DATA SYSTEM

to a quantizer Q^* , which emits frequency-modulated, direction-sensitive pulses. The positions of the output variable when the quantizer emits a pulse are termed quanta points. Pulses produced by the quantizer are subtracted from the count in the bidirectional counter. Thus, the bidirectional counter is a memory element which stores the error in the system between the required reference position and the actual output position to an integral number of quanta. The quanta size is determined by the accuracy requirement for the controlled plant, and the pulses from the quantizer carry the same information as the reference input pulses.

There are several disadvantages inherent in this type of system. Since the data is necessarily discontinuous, there is a ripple produced in $\Omega(t)$, which can be quite large when the input reference velocity is low. This occurs because the pulse repetition rate on the input signal can approach the band pass frequency of the system being controlled. The input ripple, therefore, will be passed through the system. It is possible to eliminate the discontinuities in the feedback signal. This can be accomplished by allowing the controller information on the state of the plant between quanta points, using a high frequency dither signal added to the plant output. The discontinuous nature of the input signal can be minimized. Since this information is stored as a series of pulses, it is not possible to obtain an exact indication of the input signal between

pulses. If, however, the resolution of each pulse is decreased, a substantial decrease in the plant output ripple is obtained.

Another disadvantage is the use of a digital-to-analog converter in the forward loop. The requirements for component tolerances within this device are relatively high. Any change of component values or voltages causes problems with drift and noise, with a consequent loss in accuracy. The digital-to-analog conversion can be replaced by using the digital indication of the error to time modulate a square wave signal. This signal can then be used to operate a dead zone relay. The time average of the relay output would then be proportional to the error. Relay control systems have many advantages over continuous systems.[1] They provide a more efficient usage of power, require a minimum of components to implement and are inexpensive.

The third disadvantage is a lack of closed form expressions allowing synthesis or analysis of this system. The sample data techniques have been well exploited in the use of the Z transform, but those techniques do not apply in this case since we have no knowledge of the time at which the feedback pulse will occur and no information on the output between the quanta points.

---

[1]Superscript numerals refer to the Bibliography.

This thesis proposes a pulse-data system that is compensated to provide complete information on the state of the plant output and replaces the digital-to-analog converter by a linearized dead zone relay.

CHAPTER II

GENERAL SYSTEM DESCRIPTION

This chapter presents a general discussion of the compensated pulse-data relay system presented in this thesis. For a more detailed discussion, the reader is referred to appendix A.

Figure 2 is a schematic block diagram of the system. The reference input to the bidirectional counter (BDC) is in the form of pulses with sign information. The feedback signal from the plant output $\Omega(t)$ is quantized by the Q' block. The quantized information in the form of pulses and sign information is then fed to the bidirectional counter. The bidirectional counter stores the error to an integral number of quanta in binary notation. The state of this counter is fed to the summation block Σ which, in combination with the signal $d_1(t)$, produces a time-modulated rectangular wave. This rectangular wave operates a dead zone relay which is used as the input to the plant.

Since all relay systems exhibit instabilities in the form of limit cycles unless they are compensated by the addition of a dead zone around the null position,[2] a dead zone relay is used where the dead zone is equal to D. The signal $d_1(t)$, shown in figure 2, is a chain of equally spaced pulses. The

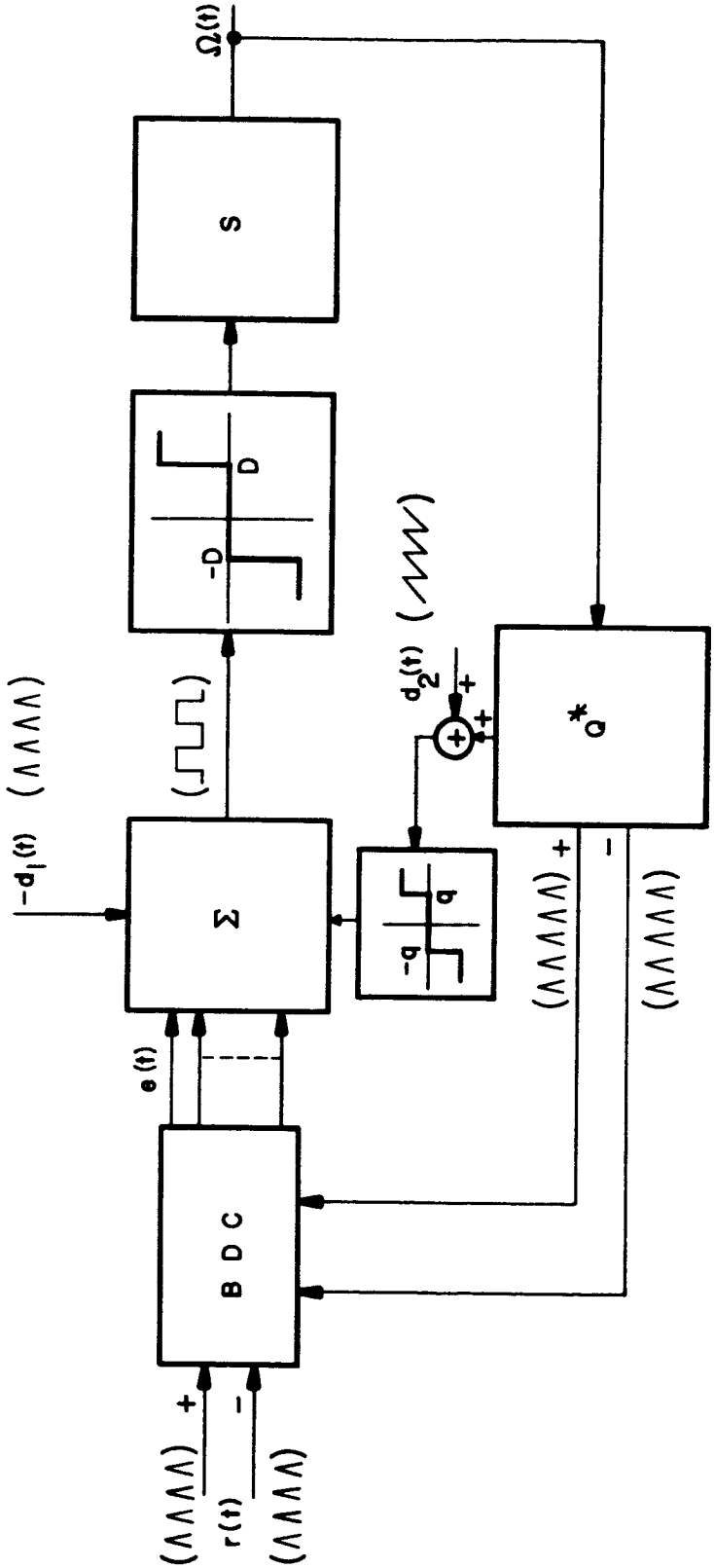

FIG. 2 SCHEMATIC BLOCK DIAGRAM OF THE COMPENSATED PULSE-DATA RELAY SYSTEM

summation block counts the number of pulses of $d_1(t)$. The first pulse sets the input to the relay equal to $\pm D$, provided there is a non-zero error. The sign of D is determined by the sign of the error. When the number of pulses of $d_1(t)$ is equal to the quantized error, the output to the relay is set equal to zero. The block can be represented by an integrator and adder combination. The first pulse sets the integrator to its saturation level and the input to the relay to $\pm D$. The succeeding pulses cause the integrator output to be a decreasing staircase wave form. When the sum of the quantized error and the integrator output is equal to or less than the dead zone of the relay, the relay is turned off. Since the error is limited to integral values due to the quantization of the input and the feedback, the block and the relay may be represented by a dead zone relay with a sawtooth wave form added to its input. The capacity of the Σ block is limited. When this capacity is exceeded, the relay input is again set equal to $\pm D$ and a new count sequence is initiated. The saturation level of the system is, therefore, set by the capacity of the Σ block. The effect of this signal addition is to linearize the dead zone relay, as described in chapter 3.

The usage of a linearized relay controller as described above can cause a ripple in the plant output. The magnitude of this ripple is dependent upon the frequency of the dither signal relative to the band pass of the plant being controlled. If a

high-frequency, low amplitude ripple can be tolerated by the system, it can be used to advantage to eliminate stiction problems. A solid state relay was used and was, therefore, capable of very high frequency operation, which allows the output ripple amplitude to be controlled by selecting its frequency.

The second dither signal is designated as $d_2(t)$. This signal is added to one output from the quantizer Q'. The quantizer designed for this system provides an analog signal which is proportional to the distance between quanta points. By adding $d_2(t)$ to this analog signal, it is possible to compensate the input to the relay for the feedback quantization error. This is accomplished by feeding this signal into a relay with a dead zone equal to one quanta. The average output from this relay is then proportional to the distance of the plant output between quanta points. Mathematically, this is the same as linearizing the quantizer by the addition of a dither signal to its input. All pulse-data systems are vulnerable to the loss of pulses. Lost pulses cause accumulative errors. If the addition of the dither signal were implemented at the input to the quantizer, the bidirectional counter would be dithered at this frequency, increasing the danger of losing pulses.

Figure 3 shows the equivalent continuous loop for the compensated system of figure 2. Chapter 3 verifies the

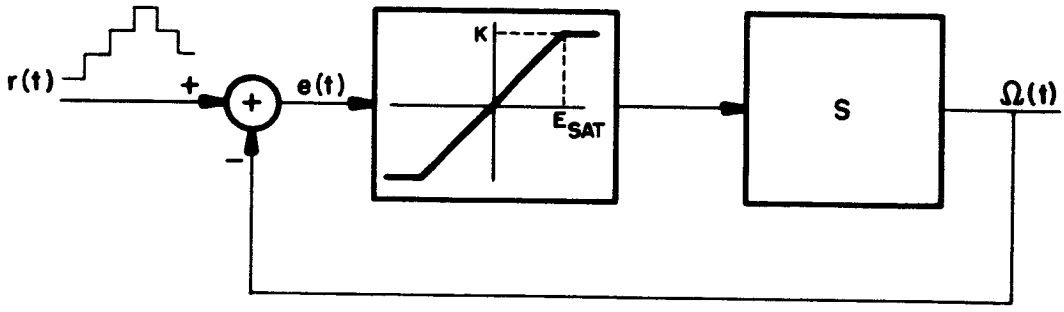

FIG. 3 EQUIVALENT SYSTEM

linearization of the quantizer so that the feedback loop can be shown as a single loop with a unity gain. The saturation element has ideal saturation characteristics determined by the dead zone of the relay. No information is lost, however, due to saturation since the bidirectional counter has sufficient capacity to contain the maximum possible error expected in the system. This is illustrated in figure 4, which shows the bidirectional counter performing the function of integration in the input path and in the feedback path.[3]

The ability to represent the compensated pulse-data system by the equivalent continuous system of figure 3 allows analysis in closed form of this system for ramp inputs by means of the steady-state Laplace transformation techniques.[4 and 5]

With the pulse-data system as shown, it is possible to have a step input applied in two ways. The first and the simplest to implement is to have the input reference signal in the form of pulses with a repetition rate much greater than the response rate of the system. This will look like a step input with a very large but finite slope. The second method is to have a presettable bidirectional counter. This allows a true step input. Consideration of step response behavior is essential for a pulse-data system. Any application in the machine control field would require a path control system for a machining operation and, in order to have a repetition of

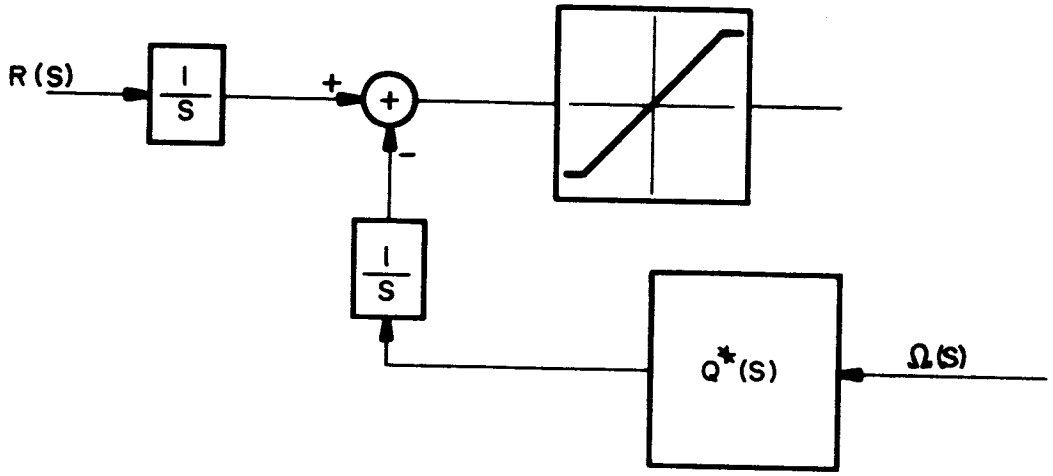

FIG. 4 SCHEMATIC SHOWING FUNCTIONAL REPRESENTATION OF THE BIDIRECTIONAL COUNTER

one operation, it is necessary to return the machine tool to a reference position at the completion of the operation. With a system of this kind, the reference position can be entered in the counter at the completion of the operation, and the system will travel at maximum velocity back to the given reference.

CHAPTER III
MATHEMATICAL DESCRIPTION OF THE QUANTIZER AND THE RELAY

A quantizer is a transducer that emits an electrical pulse whenever the controlled variable takes on values which are one quanta apart. One quanta represents the minimum resolution required commensurate with system accuracy specifications. In order to simplify the following discussion and subsequent analysis, the input and output variables will be expressed in quanta. The main effect of the quantization process is to subdivide the entire range of the controlled variable into increments. Figure 5 shows the quantizer input-output characteristics. As shown, the input to the quantizer is an analog quantity and the output is a chain of pulses, each pulse representing a transition of the input from one quanta to the next. The position of the controlled plant between quanta points is unknown, and the quantity c must then be defined as follows:

$$0 < c < 1 \qquad (1)$$

Figure 6A shows the equivalent quantizer representation with the quantizer of figure 5A combined with an integration. The input-output relationships for this quantizer are shown in figure 6B. This definition of the quantizer is somewhat arbitrary.

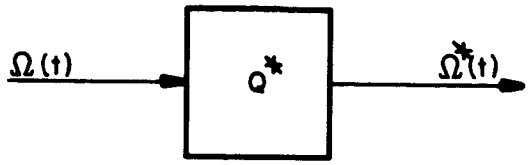

A: QUANTIZER BLOCK DIAGRAM

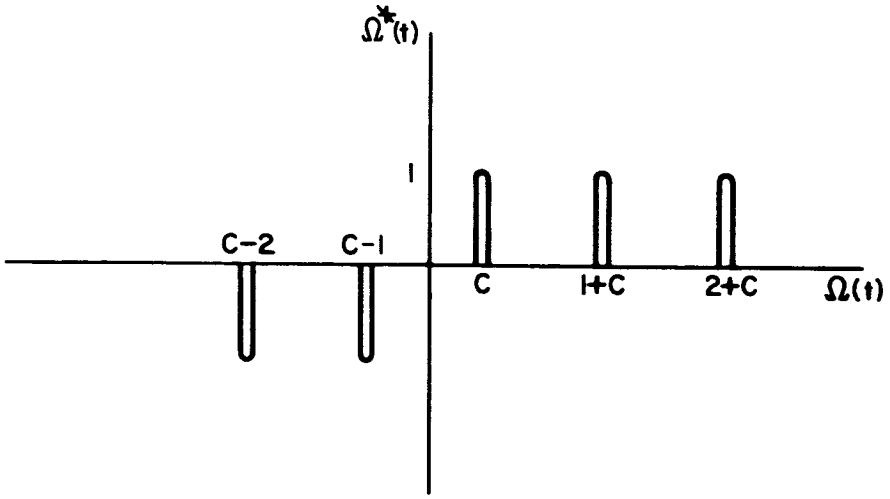

B: QUANTIZER INPUT—OUTPUT CURVE

FIG. 5 QUANTIZER

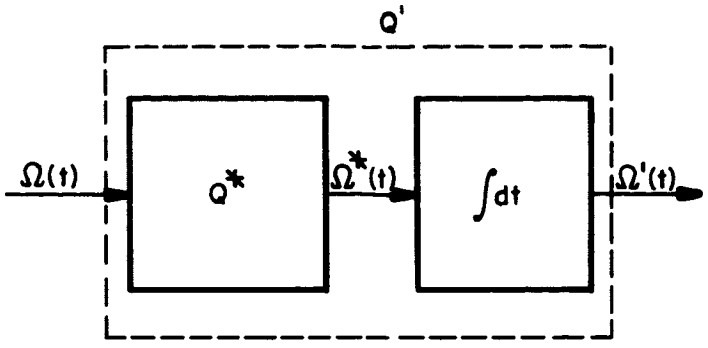

A: QUANTIZER AND INTEGRATOR COMBINED

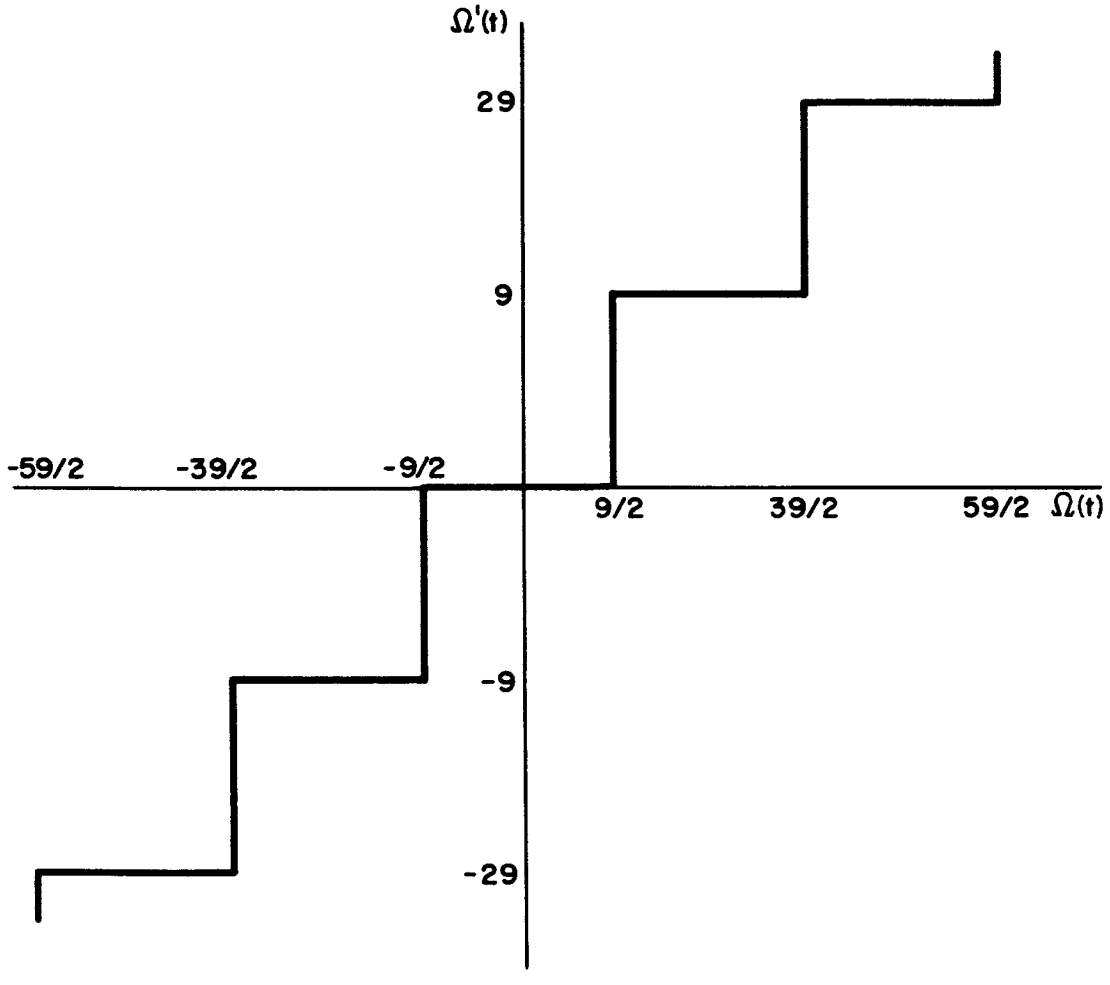

B: INPUT-OUTPUT RELATIONSHIPS

FIG.6 QUANTIZER MODEL

It can be noticed from figure 5B that the first output pulse occurs at

$$\Omega(t) = c$$

where c is limited by equation (1). For convenience, the definition given for the quantizer in figure 6B arbitrarily sets

$$c = 0.5$$

This definition has been chosen in order to allow stability investigation by the describing function analysis that follows later in this chapter.

The quantizer fits within the general class of highly nonlinear transducers. The idea of linearizing these highly nonlinear transducers by means of an externally applied signal has been investigated by several people. Loeb[6] has suggested that any nonlinear system can be linearized in this manner. A question of linearizing a quantizer has been raised by G. G. Furman.[7] He has used a sinusoidal dither in attempting a linearization of a quantizer and has shown that exact linearization can be obtained using a sawtooth dither. Furman did not, however, suggest any means of implementation of this dither nor did he show any of the effects of varying the dither amplitude due to drift.

Any system that quantizes information is subject to instabilities in the form of limit cycles for a limited class of input conditions. The limit cycle behavior of this system in

response to step inputs will be investigated by describing function techniques. A low frequency pulse input will also produce a limit cycle. This limit cycle will be referred to as a ripple on the plant output, and its characteristics can be determined by using the steady-state Laplace transform calculus.

A describing function will be developed for the quantizer. In order to include the effects of the dither, it will be necessary to use the dual-input describing function.[8] The methodology in the dual-input describing function approach is to ensure that the dither frequency is much greater than the frequency of the limit cycle assumed for the system. This allows use of the approximate dual-input describing function developed by Boyer.[9] The dither effectively alters the quantizer input-output characteristics and allows replacement of the quantizer by an alternate set of characteristics. The assumed sinusoidal limit cycle can then be applied to the altered quantizer to investigate the stability of the system. The advantage of this technique is that it is not necessary to use the describing function approach in order to utilize the altered quantizer in the system loop. These altered characteristics in no way depend upon the shape of the assumed limit cycle and, therefore, will be valid for any input whose frequency is much less than the dither frequency. In the following analysis, the altered quantizer characteristics are first developed and,

secondly, the describing function for the altered quantizer is determined.

Furman has shown that the sawtooth dither that will exactly linearize the quantizer should be as follows:

$$d(t) = m\left[1 - \frac{2t}{T_d}\right]$$

for $0 < t < T_d$.

In general:

$$d(t) = m\left[1 - \frac{2t}{T_d}\right] + \sum_{n=0}^{\infty} mu(t - T_d)$$

where: n = 0, 1, 2, 3 . . .

m = 0.5, 1.0, 1.5, 2.0 . . .

This wave is shown in figure 7A.

When using a dither signal to linearize the quantizer, it is not desirable (and in many cases not possible) to dither the input to the quantizer. If the input to the quantizer is dithered, this causes the bidirectional counter to be dithered at a pulse repetition rate 2m times the dither frequency, where m is the dither amplitude. As described in chapter 2, the dither signal bypasses the bidirectional counter. In order to accomplish this efficiently, a dither signal which is either positive or negative was chosen. The sign is determined by the sign of the error.

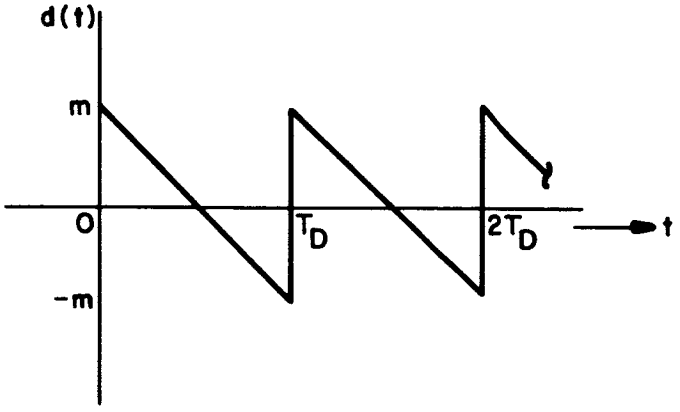

A : LINEARIZING DITHER SUGGESTED BY G.G. FURMAN

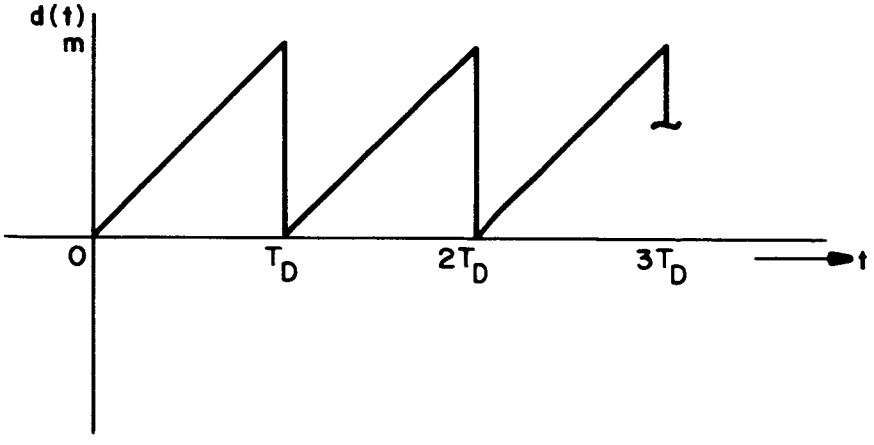

B : LINEARIZING DITHER USED IN THIS THESIS

FIG. 7 DITHER SIGNALS

The dither used is shown in figure 7B and can be expressed as:

$$d(t) = \pm m \left[\frac{t}{T_d} - \sum_{n=0}^{\infty} u(t - nT_d) \right]$$

where: $n = 0, 1, 2, 3 \ldots$

Figure 8 shows the block diagram used for the describing function analysis. Since the quantizer has been considered in the forward loop, the dither is subtracted. The reason is as follows:

$$\Omega(t) = \Omega_q(t) + \Delta(t)$$

where: $\Delta(t) = \Omega(t) - nq$

for $nq < \Omega(t) < (n + 1)q$

and $\Omega_q(t) = nq$

$$e(t) = r(t) - \Omega(t)$$

$$e(t) = \{r(t) - \Omega_q(t)\} - \Delta(t)$$

$\Delta(t)$ represents the quantization error and is that part of the error corrected for by the dither.

If the rate of change of $\Omega(t)$ is much less than the rate of change of $d(t)$, then the altered characteristics for the quantizer are obtained by assuming $\Omega(t)$ is constant over one

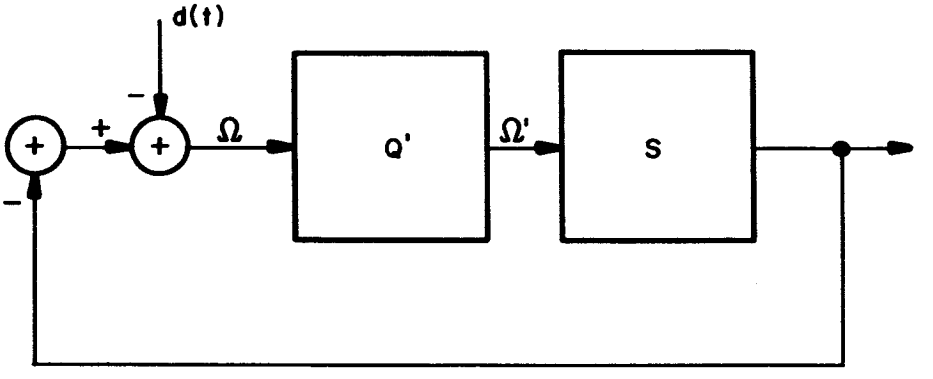

FIG. 8 BLOCK DIAGRAM FOR DESCRIBING FUNCTION ANALYSIS

cycle of the dither. The equivalent gain can be calculated for this value as follows:

$$K_{eq} = \frac{\Omega'_{ave}}{\Omega}$$

where: $$\Omega'_{ave} = \frac{1}{T_d}\int_0^{T_d} \Omega' \, dt$$

Integration over the one period T_d of the dither is valid since the dither signal is periodic with period T_d. That is

$$d(t) = d(t + T_d)$$

In addition to this, the quantizer output is periodic with period one quanta. Therefore, it is only necessary to calculate the equivalent gain for values of $\Omega(t)$ as follows:

$$0 \leq \Omega(t) \leq 1$$

The equivalent gain can be determined from figure 9:

$$K_{eq} = \int_0^1 \frac{\Omega' d\left(\frac{t}{T_d}\right)}{\Omega}$$

$$= \frac{1}{\Omega}\int_{\frac{\psi}{T_d}}^1 d\,\frac{t}{T_d}$$

Therefore, $$K_{eq} = \frac{1 - \frac{\psi}{T_d}}{\Omega}$$

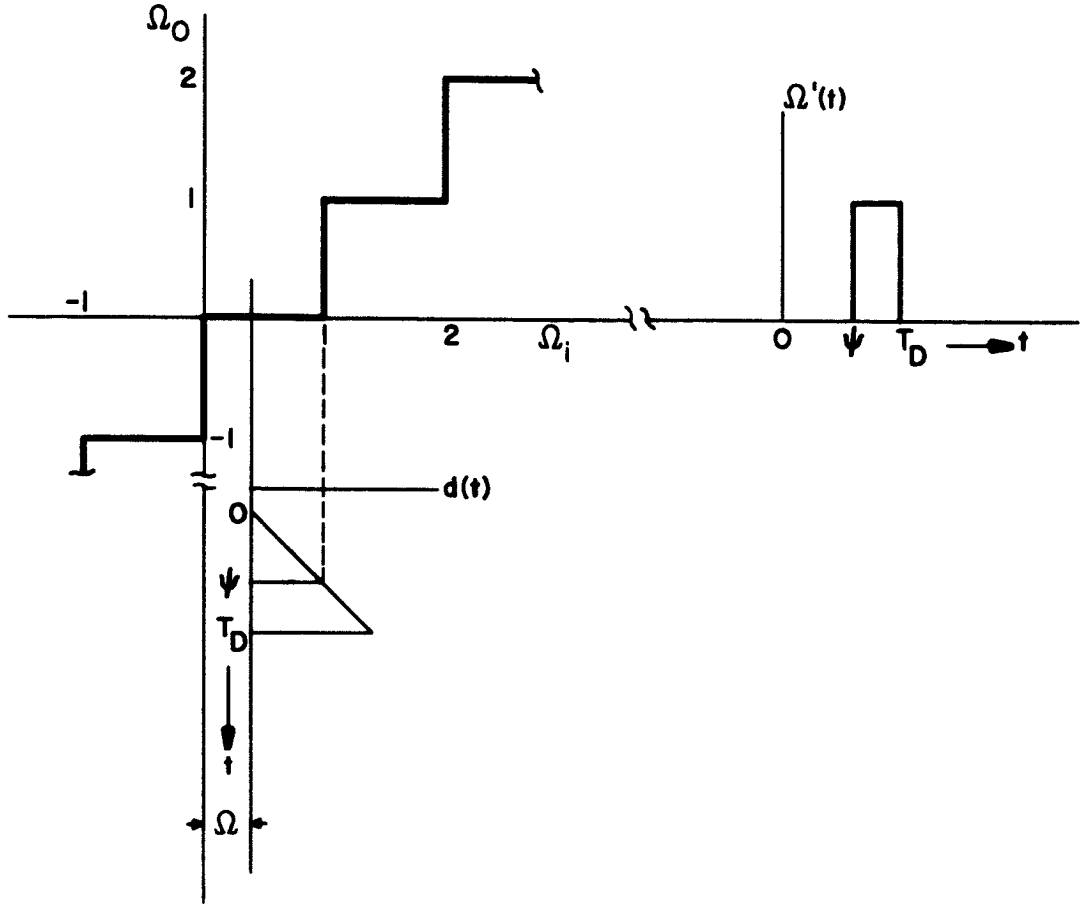

FIG. 9 EFFECT OF DITHER SIGNAL ON QUANTIZER

From the equation for the dither:

$$d(t) = m \frac{t}{T_d}$$

for $0 \leq t \leq T_d$

Therefore: $\Omega + \frac{m\psi}{T_d} = 1$; i.e. $\frac{\psi}{T_d} = \frac{1 - \Omega}{m}$

Therefore, $K_{eq} = \frac{1 - \frac{(1 - \Omega)}{m}}{\Omega}$

This is a straight line with a slope of $\frac{1}{m}$.

In general, when $\Omega(t) = n + \Delta(t)$

for $0 \leq \Delta(t) < 1$

$n = 0, 1, 2, 3 \ldots$

$$K_{eq} = \frac{n}{\Omega(t)} + \frac{1 - \frac{n + 1 - \Omega(t)}{m}}{\Omega(t)}$$

Note: This equation is not defined for

$$\frac{n + 1 - \Omega(t)}{m} > 1$$

Since K_{eq} would be a negative quantity for $n = 0$, we therefore need two equations.

$$K_{eq} = \frac{n}{\Omega(t)} + \frac{1 - \frac{n + 1 - \Omega(t)}{m}}{\Omega(t)}$$

for $\frac{n + 1 - \Omega(t)}{m} \leq 1$

$$K_{eq} = \frac{n}{\Omega(t)}$$

for $\frac{n + 1 - \Omega(t)}{m} > 1$

Figure 10 shows the altered characteristics for various values of m. For $m > 1$, the quantizer with the dither added, as defined in this thesis, has the following saturation characteristic:

$$\Omega(t) + m \leq n + 1$$

where: $\Omega(t) = n + \Delta(t)$

for $0 \leq \Delta < 1$; $n = 0, 1, 2, 3 \ldots$

With this limitation, the quantizer exhibits a region of infinite gain at a quanta point for $m > 1$. If the system is to be used for positioning, this condition is intolerable since a limit cycle will always exist. Therefore, the dither amplitude must be kept equal to or less than 1. This ensures a region of zero gain (i.e., a dead zone) at a quanta point and will allow the plant to be positioned within $\pm(1 - m)$ of an integral number of quanta.

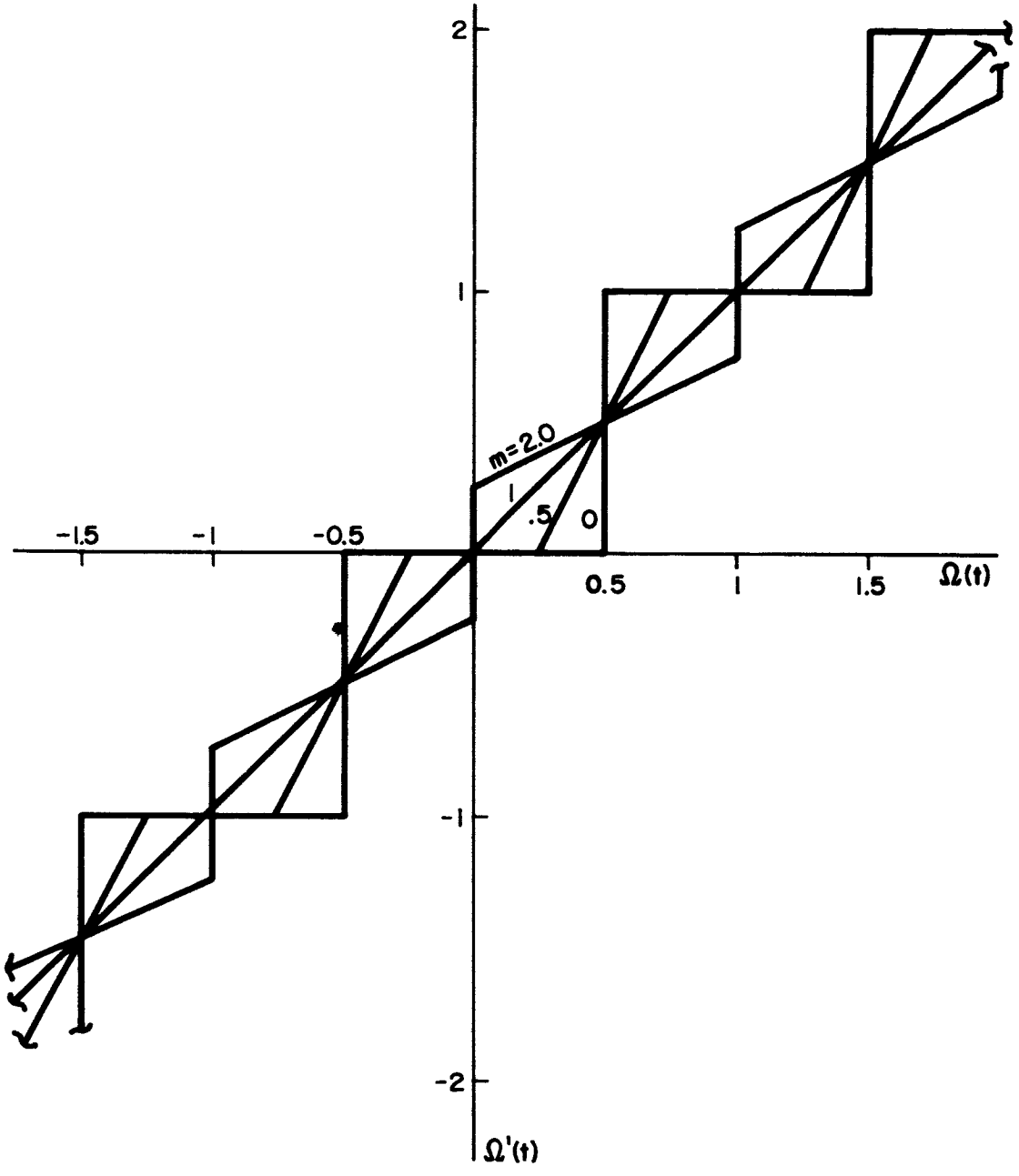

FIG. 10 ALTERED QUANTIZER INPUT-OUTPUT CHARACTERISTICS

The effect of a variation in dither amplitude can be easily demonstrated by observing the change in the describing function for the altered quantizer. The describing function allows replacement of the quantizer by an equivalent gain K_q. This gain is determined by assuming that a self-sustained oscillation of $\Omega(t)$ exists and that this oscillation is a sine wave. The output of the quantizer is expressed in a Fourier series, and all harmonics higher than the first are ignored. The K_q is then the ratio of the output amplitude to the input amplitude. A general describing function for the dithered quantizer is developed below. The input-output relationships for the quantizer are shown in figure 11.

The quantizer output may be expressed as a Fourier series, as follows:

$$F(t) = \frac{a_0}{2} + \sum_{n=1}^{\infty} a_n \operatorname{Cos}(n\omega t) + \sum_{n=1}^{\infty} b_n \operatorname{Sin}(n\omega t)$$

where: $a_0 = \frac{1}{2\pi}\int_0^{2\pi} F(\omega t)\, d(\omega t)$

$$a_n = \frac{1}{\pi}\int_0^{2\pi} F(\omega t) \operatorname{Cos}(n\omega t)\, d(\omega t)$$

$$b_n = \frac{1}{\pi}\int_0^{2\pi} F(\omega t) \operatorname{Sin}(n\omega t)\, d(\omega t)$$

Since $F(\omega t)$ is an odd function, $a_0 = a_n = 0$.

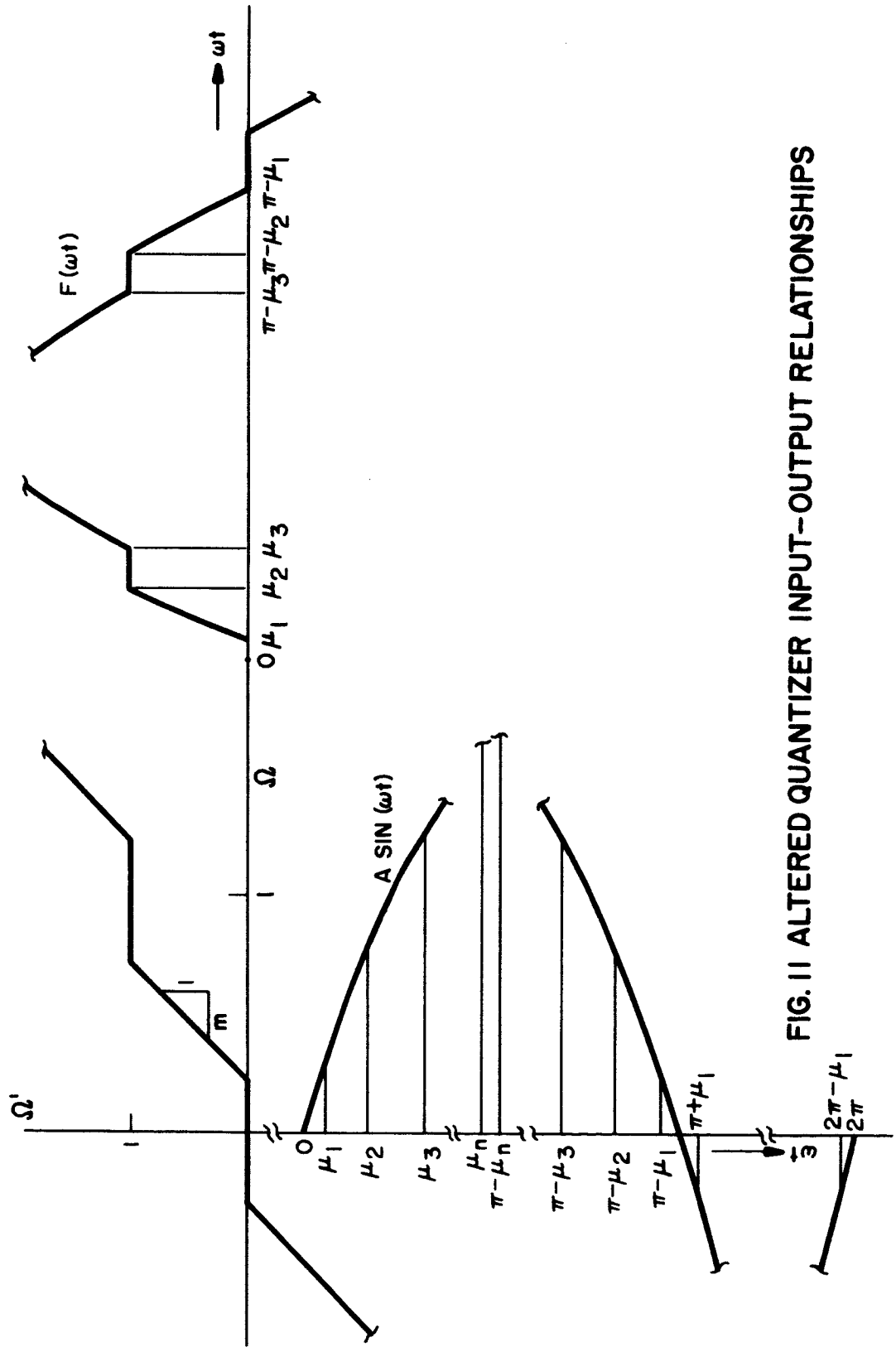

FIG. 11 ALTERED QUANTIZER INPUT-OUTPUT RELATIONSHIPS

Consequently,

$$b_1 = \frac{2}{\pi}\int_0^{\pi} F(\omega t)\,\mathrm{Sin}(\omega t)\,d(\omega t)$$

$$= \frac{2}{\pi}\left[\int_{\mu_1}^{\mu_2}\frac{1}{m}\left[A\,\mathrm{Sin}^2(\omega t) - A\,\mathrm{Sin}(\mu_1)\,\mathrm{Sin}(\omega t)\right]d(\omega t)\right.$$

$$+\int_{\mu_2}^{\pi-\mu_2}\mathrm{Sin}(\omega t)\,d(\omega t)$$

$$+\int_{\mu_3}^{\mu_4}\frac{1}{m}\left[A\,\mathrm{Sin}^2(\omega t) - A\,\mathrm{Sin}(\mu_3)\,\mathrm{Sin}(\omega t)\right]d(\omega t)$$

$$+\int_{\mu_4}^{\pi-\mu_4}\mathrm{Sin}(\omega t)\,d(\omega t) + \text{-------} +$$

$$+\int_{\pi-\mu_4}^{\pi-\mu_3}\frac{1}{m}\left[A\,\mathrm{Sin}^2(\omega t) - A\,\mathrm{Sin}(\mu_3)\,\mathrm{Sin}(\omega t)\right]d(\omega t)$$

$$\left.+\int_{\pi-\mu_2}^{\pi-\mu_1}\frac{1}{m}\left[A\,\mathrm{Sin}^2(\omega t) - A\,\mathrm{Sin}(\mu_2)\,\mathrm{Sin}(\omega t)\right]d(\omega t)\right]$$

By integrating:

$$b_1 = \frac{2}{\pi}\left[\frac{A}{m}\left[\frac{\omega t}{2} - \frac{\mathrm{Sin}(2\omega t)}{4} + \mathrm{Sin}(\mu_1)\,\mathrm{Cos}(\omega t)\right]_{\mu_1}^{\mu_2}\right.$$

$$- \left[\mathrm{Cos}(\omega t)\right]_{\mu_2}^{\pi-\mu_2}$$

$$+ \frac{A}{m}\left[\frac{\omega t}{2} - \frac{\mathrm{Sin}(2\omega t)}{4} + \mathrm{Sin}(\mu_3)\,\mathrm{Cos}(\omega t)\right]_{\mu_3}^{\mu_4}$$

$$- \left[\mathrm{Cos}(\omega t)\right]_{\mu_4}^{\pi-\mu_4} + \text{-------} +$$

$$\left.+ \frac{A}{m}\left[\frac{\omega t}{2} - \frac{\mathrm{Sin}(2\omega t)}{4} + \mathrm{Sin}(\mu_3)\,\mathrm{Cos}(\omega t)\right]_{\pi-\mu_4}^{\pi-\mu_3}\right.$$

$$+ \frac{A}{m}\left[\frac{\omega t}{2} - \frac{\mathrm{Sin}(2\omega t)}{4} + \mathrm{Sin}(\mu_1)\,\mathrm{Cos}(\omega t)\right]_{\pi-\mu_2}^{\pi-\mu_1}\Bigg]$$

In general,

$$b_1 = \frac{2}{\pi}\Bigg[\frac{A}{m}\{\mu_2 - \mu_1 + \mu_4 - \mu_3 + \text{-----} + (-1)^n \mu_n\}$$

$$+ \frac{A}{m}\{2\mathrm{Sin}(\mu_1)\,\mathrm{Cos}(\mu_2) - 2\mathrm{Sin}(\mu_1)\,\mathrm{Cos}(\mu_1) + \text{---} +$$

$$+ 2\mathrm{Sin}(\mu_{2n-1})\,\mathrm{Cos}(\mu_{2n}) - 2\mathrm{Sin}(\mu_{2n-1})\,\mathrm{Cos}(\mu_{2n-1})\}$$

$$+ 2\mathrm{Cos}(\mu_2) + 2\mathrm{Cos}(\mu_4) + \text{---} + 2\mathrm{Cos}(\mu_n)$$

$$+ \frac{\pi}{4} + (-1)^n \frac{\pi}{4}\Bigg]$$

for $n = 0, 1, 2, 3, 4 \ldots$

Where: $A\,\mathrm{Sin}(\mu_1) = \frac{1-m}{2}$; $\quad \mu_1 = \mathrm{Sin}^{-1}\frac{1-m}{2A}$

$A\,\mathrm{Sin}(\mu_2) = \frac{1+m}{2}$; $\quad \mu_2 = \mathrm{Sin}^{-1}\frac{1+m}{2A}$

$A\,\mathrm{Sin}(\mu_3) = \frac{3-m}{2}$; $\quad \mu_3 = \mathrm{Sin}^{-1}\frac{3-m}{2A}$

. . . .

$A\,\mathrm{Sin}(\mu_n) = \frac{n-m}{2}$; $\quad \mu_n = \mathrm{Sin}^{-1}\frac{n-m}{2A}$

for $n = 1, 3, 5, 7 \ldots$

$$A \, \mathrm{Sin}(\mu_n) = \frac{(n-1)+m}{2}; \qquad \mu_n = \mathrm{Sin}^{-1} \frac{(n-1)+m}{2A}$$

for $n = 2, 4, 6, 8 \ldots$

The special case when $m = 0$ gives the expression for the non-linearized quantizer. For this case,

$$m = 0; \quad \mu_{2n} = \mu_{2n-1}$$

$$\lim_{m \to 0} \frac{A}{m} \{\mu_2 - \mu_1 + \mu_4 - \mu_3 \ldots\} = \frac{0}{0}$$

Therefore:

$$\lim_{m \to 0} \frac{d}{dm} \{\mu_2 - \mu_1 + \mu_4 - \mu_3 \ldots\} = 0$$

Similarly,

$$\lim_{m \to 0} \frac{A}{m} \left[\frac{1-m}{A} \sqrt{1 - \left(\frac{1+m}{2A}\right)^2} - \frac{1-m}{A} \sqrt{1 - \left(\frac{1-m}{2A}\right)^2} + \ldots \right] = \frac{0}{0}$$

Therefore:

$$\lim_{m \to 0} \frac{d}{dm} \left[A \left(\frac{1-m}{A} \sqrt{1 - \left(\frac{1+m}{2A}\right)^2} - \frac{1-m}{A} \sqrt{1 - \left(\frac{1-m}{2A}\right)^2} + \ldots \right) \right] = 0$$

Therefore, in this case,

$$b_1 = \frac{4}{\pi} \{\mathrm{Cos}(\mu_2) + \mathrm{Cos}(\mu_4) + \ldots + \mathrm{Cos}(\mu_n)\}$$

From these equations, the describing function can be determined

$$K_q = \frac{b_1}{A}$$

Figure 12 shows the plot of K_q versus A for various values of m. The following observation can be made from these curves:

$$\lim_{A \to \infty} K_q = 1$$

For dither amplitudes other than 1, the altered quantizer is still nonlinear. If the limit cycle that was assumed for the describing function were considered as a dither signal, the above fact shows that a large amplitude sine wave dither signal tends to linearize the quantizer.

This family of curves indicates the effect of a change in the dither amplitude on the stability of the system. If $G(j\omega)$ is the system transfer function of the plant, then the closed loop transfer function between input and output is:

$$\frac{R(j\omega)}{\Omega(j\omega)} = \frac{K_q G(j\omega)}{1 + K_q G(j\omega)}$$

A sufficient condition for existence of a sustained oscillation in the system is:

$$G(j\omega) = -\frac{1}{K_q}$$

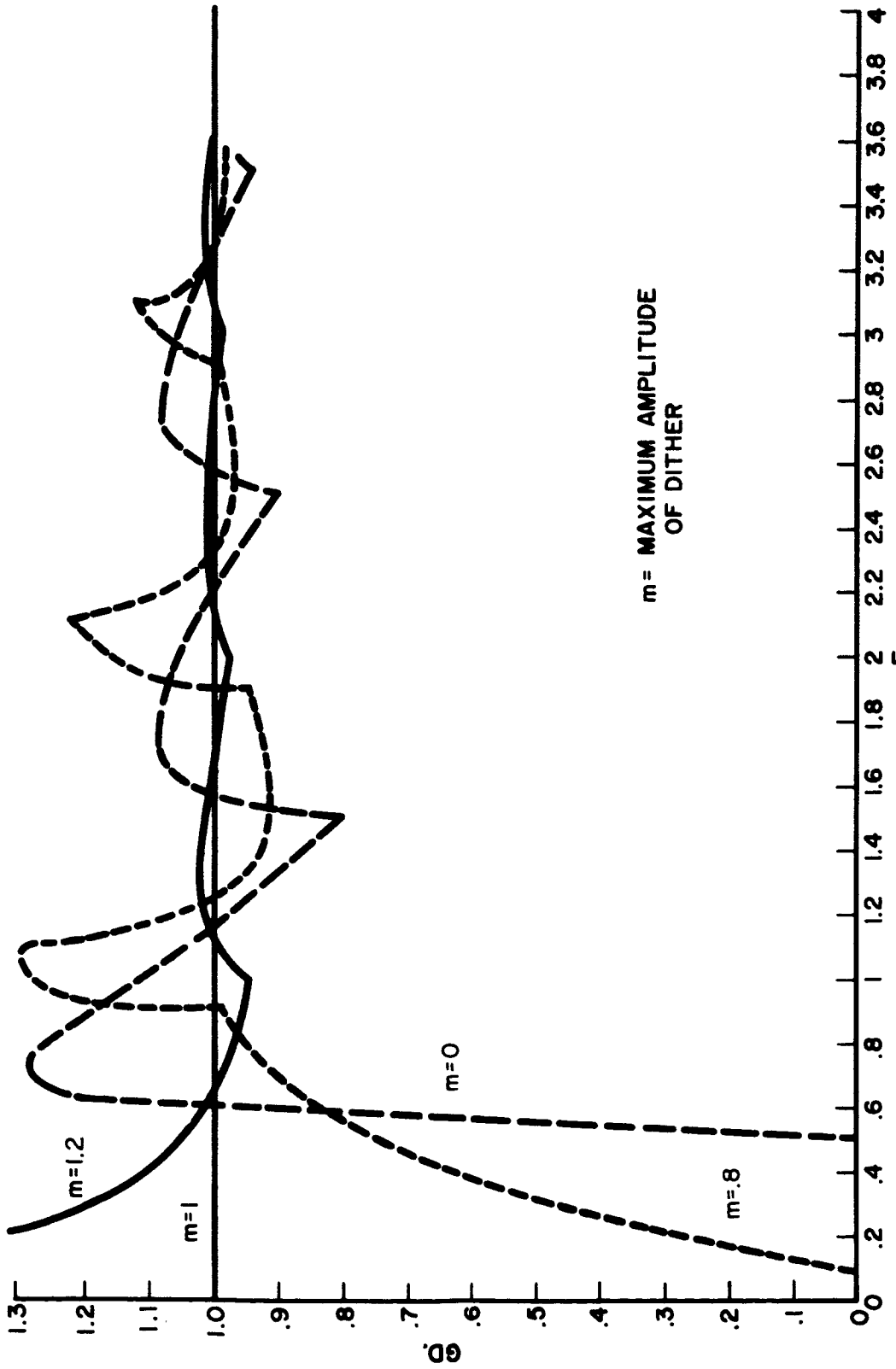

FIG.12 DESCRIBING FUNCTION FOR QUANTIZER PLUS DITHER

For the case where $m = 1$, the quantizer is exactly linearized and can be replaced by a unity gain in the loop. This fact allows the stability of the system to be checked by any of the familiar linear stability criteria, such as the Nyquist, Routh Hurwitz, root locus, etc.[10]

If $|G(j\omega)|$ is $< \frac{1}{K_q}$, the system will be stable. Since at the point of interest, $G(j\omega)$ is real and $\angle G(j\omega) = -180^\circ$, the $\frac{1}{G(j\omega)}$ line can be drawn in figure 12 for a given $G(j\omega)$. A limit cycle can exist if K_q is greater than $\frac{1}{G(j\omega)}$ at any point. The amplitude of the limit cycle, if it exists, is determined by the point of intersection of the K_q and the $\frac{1}{G(j\omega)}$ lines. In most cases, as can be seen from the curves, there will be two points of intersection for each crossing of the $\frac{1}{G(j\omega)}$ line. The amplitude of the stable limit cycle that will exist is the larger of the two. The frequency of this limit cycle is that frequency which will cause $\angle G(j\omega) = -180^\circ$. These limit cycles are only possible with step disturbances or initial conditions since an autonomous system was assumed, and they are only approximate due to the neglect of all harmonics higher than the first in the Fourier analyses of the quantizer output wave form. These curves do, however, give a qualitative idea of the effects of the dither amplitude.

The input signal to the plant is applied by a relay, shown in figure 2. The relay is another highly nonlinear element which can be linearized by adding a dither to its input signal. Figure 13A shows the input-output characteristics of a dead zone relay. This relationship for $|e_i(t)| < D$ is analogous to the first period of the quantizer. The dual-input describing function methods can be applied to replace the relay with the dither added by an alternate relay. From figure 13C, for a fixed value of $e(t)$:

$$e_{0\ ave}(t) = \int_0^1 e_0(t)d(t/T_d)$$

$$= \int_{\psi/T_d}^1 K d(t/T_d) = K - \psi/T_d$$

Therefore:

$$K_{eq} = \frac{K(1 - \psi/T_d)}{e_i(t)}$$

Where: $\frac{D\psi}{T_d} + e_i(t) = D$

$$K_{eq} = K\left\{\frac{1 - \frac{\{D - e_i(t)\}}{P}}{e_i(t)}\right\}$$

Therefore: $Pe_0(t) = R\{P - D + e_i(t)\}$

If $D = P$,

$$e_0(t) = \frac{K}{P}\{e_i(t)\}$$

for $|e_i(t)| \leq P$

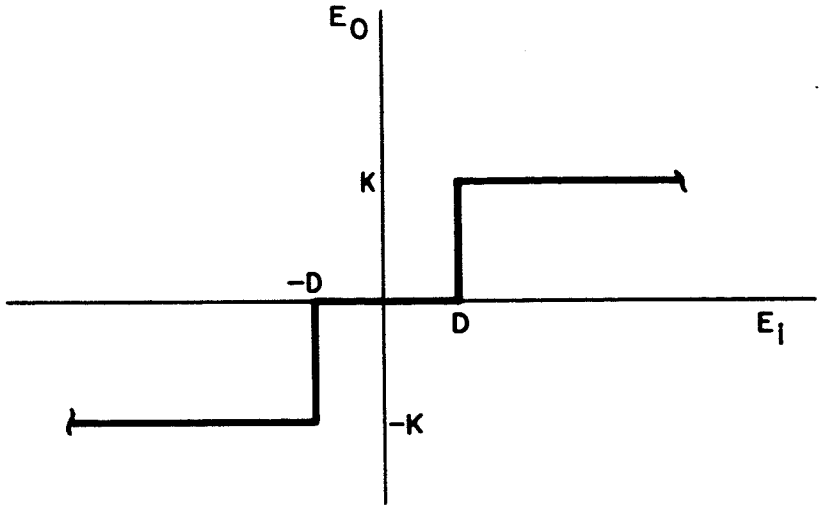

A: DEAD ZONE RELAY INPUT–OUTPUT CHARACTERISTICS

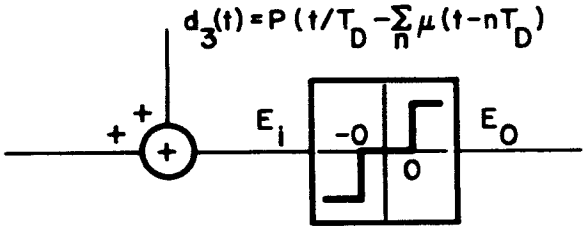

B: LINEARIZING MODEL FOR RELAY

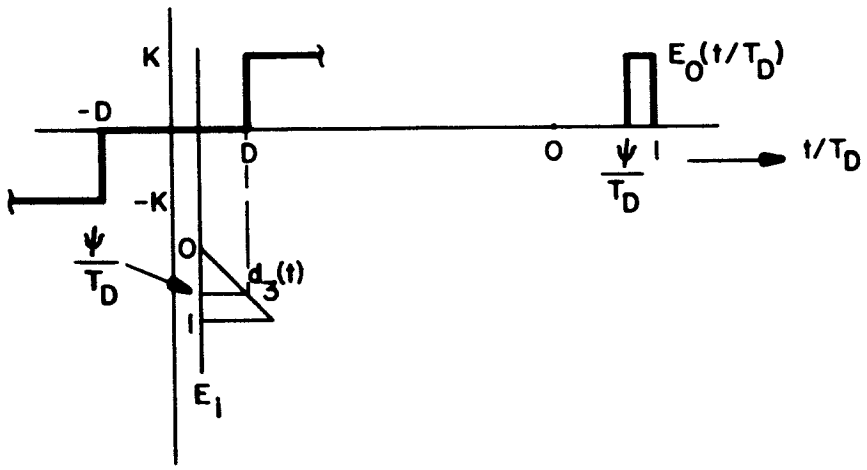

C: EFFECT OF ADDING $d_3(t)$ TO THE RELAY

FIG.13 RELAY MODEL

The relay can then be considered as a linear gain. There will, however, be a ripple in the plant output of the same frequency as $d_3(t)$. If the frequency is high relative to the band pass of the system, the ripple is quite small. It will, however, have an effect on the quantizer linearization.

As noted above, the manner in which $d_2(t)$, the quantizer dither, was implemented causes an infinite gain at a quanta point when the dither amplitude exceeds 1. In addition, it is desirable to have a small dead zone or region of zero gain at the quanta points. For these reasons, the amplitude of the dither is less than 1, and its altered characteristics are shown in figure 10.

The ripple caused by the linearized relay will produce a second dither signal which can be assumed to be a sine wave. The effect of the dither is additive and again alters the quantizer characteristics. Its effects can be assessed in a manner similar to that given above for the sawtooth dither. The equivalent gain can be calculated from figure 11, as follows, noting that the amplitude of this dither is very small since the frequency of $d_3(t)$ is high relative to the band pass of the plant.

$$\Omega_{0\ ave} = \frac{1}{2\pi}\int_{\mu_1}^{\mu_2} \frac{C}{m} \operatorname{Sin}(\beta t)\, d(\beta t)$$

$$= \frac{C}{2\pi m}\left[-\operatorname{Cos}(\beta t)\right]_{\mu_1}^{\pi-\mu_1}$$

$$= \frac{C}{2\pi m}\left[2\cos(\mu_1)\right]$$

$$\Omega_{0\ ave} = \frac{C}{\pi m}\cos(\mu_1)$$

Since $B\sin(\mu_1) = \frac{1-m}{2} - \Omega_i$

Therefore: $\mu_1 = \sin^{-1}\left(\frac{1-m}{2B} - \Omega_i\right)$

Therefore: $\Omega_{0\ ave} = \frac{C}{\pi m}\sqrt{1 - \left(\frac{1-m}{2B} - \Omega_i\right)^2}$

and $K_{eq} = \frac{C}{\pi m \Omega_i}\sqrt{1 - \left(\frac{1-m}{2B} - \Omega_i\right)^2}$

The altered characteristics are shown in figure 14 for $m = .9$ and $C = .1$. As can be seen, the discontinuities have been eliminated and for

$$.9 \leq m \leq 1$$

and $C = 0.1$

the quantizer characteristics are very nearly linear. For the remaining analysis in the thesis, it will be considered a linear gain of 1.

The assumption that the approximate dual-input describing function can be used is valid since

$$d_2(t) = 10d_3(t)$$

and $d_3(t)$ is at least ten times the band pass of the plant.

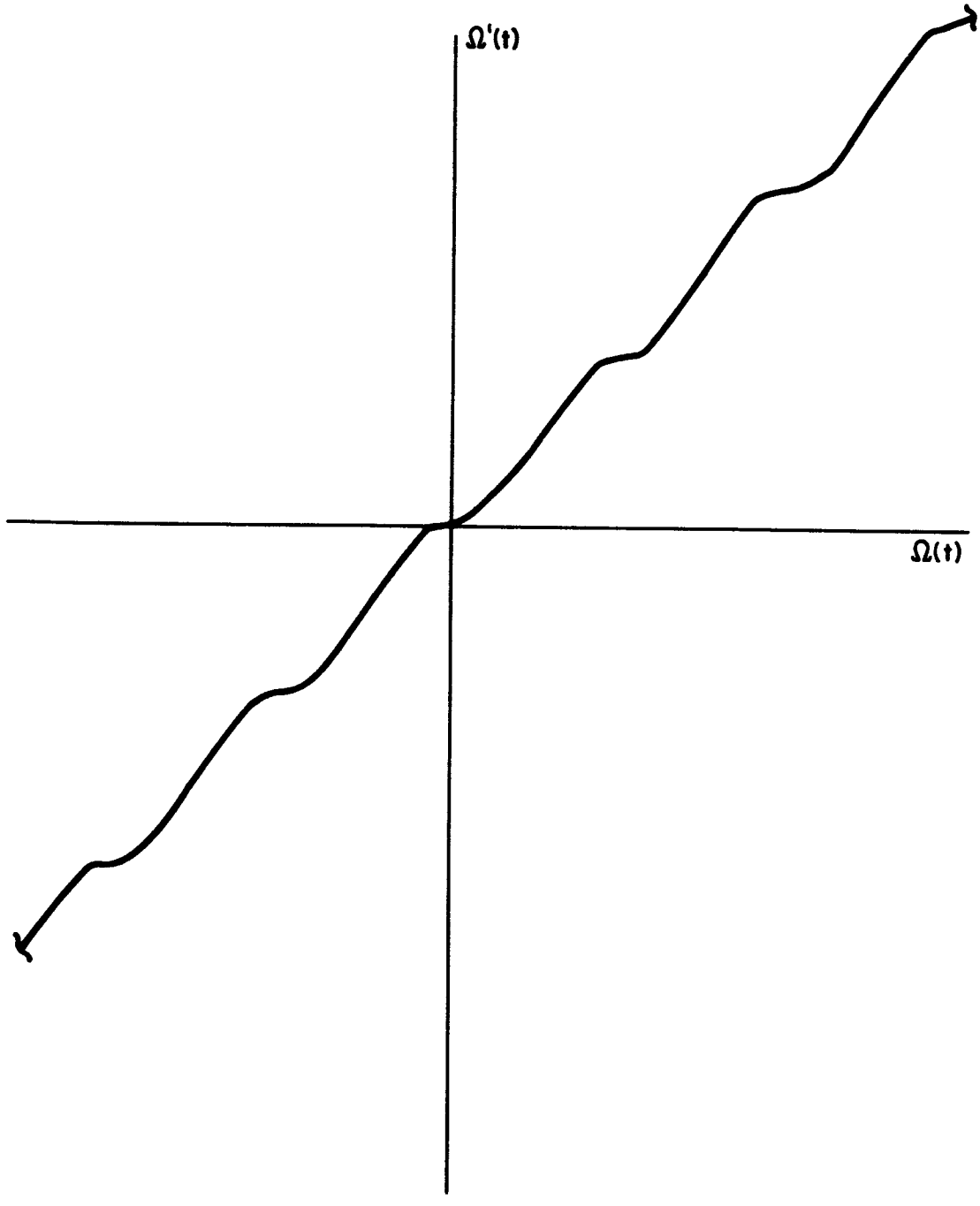

FIG. 14 QUANTIZER CHARACTERISTICS DUE TO OUTPUT RIPPLE

This change in the quantizer characteristics has a beneficial effect on the describing function. Figure 12 shows that the equivalent gain for the case where m is slightly less than one has a rather high peak over the region of the dead zone. The ripple in the plant output has the effect of substantially reducing this peak.

CHAPTER IV
LINEARIZED SYSTEM ANALYSIS

The object of this chapter is to develop a synthesis technique for the system proposed which will allow satisfaction of a limited class of specifications on the response to both ramp inputs and step inputs. Following the justification given for the linearization of the dead zone relay in the forward loop and the quantizer in the feedback loop, the system may now be represented as shown in figure 15. The reference input signal is in the form of a chain of pulses, with each pulse commanding the system output to change one quanta. The pulse repetition rate, therefore, is a measure of the velocity required for the system. Due to the nature of this input, it is impossible to have a completely smooth output, and the system gain must be designed so that the output generated will be satisfactory or commensurate with the plant requirements over a reasonable range of input rates. As can be seen from figure 15, the system forward loop gain depends upon the saturation level. The maximum possible saturation level in the system is determined by the capacity of the counter; however, the saturation level can be varied from this maximum down to zero.

The procedure for determining the gain requirement for a satisfactory response to the ramp input is as follows. Since

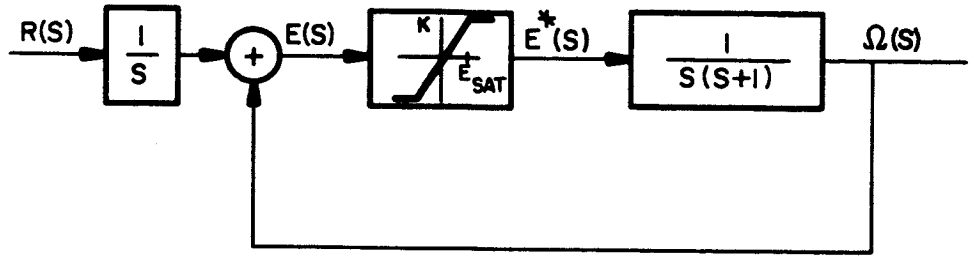

A: LINEARIZED SYSTEM SHOWING SATURATION AND A FIRST ORDER PLANT

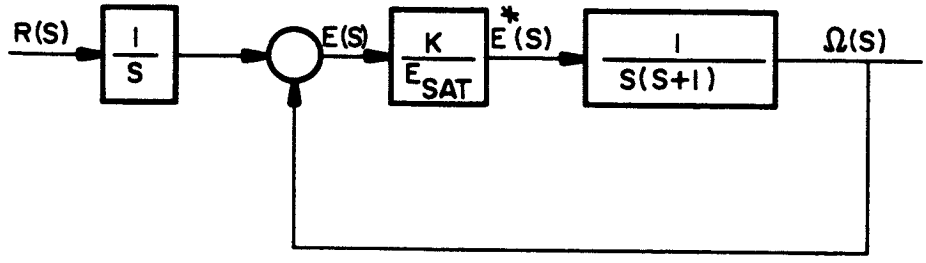

B: SYSTEM MODEL FOR STEADY STATE SOLUTION

FIG. 15 SYSTEM BLOCK DIAGRAMS

the input signal for a constant velocity of the output would be a chain of pulses equally spaced in time, the Laplace transform of the input signal can be expressed in closed form. The methods of the steady-state Laplace transform calculus[11] can then be applied, which will allow determination of the steady-state output from the system as a function of time. From this solution curve, the maximum peak-to-peak ripple can be determined for any given system gain and input rate. The range of input rates for satisfactory response can now be easily determined. The best procedure is to calculate the error rather than the output since the solution curve is not valid if the error exceeds the assumed saturation level at any time during a cycle. The plant output can be determined directly from the error signal since a linearized quantizer has been assumed.

In order to employ the methods of the steady-state Laplace transform calculus, it is necessary to assume that the error does not reach the saturation level in response to a ramp input. This must be checked in each case to ensure that the results are valid. Therefore, the system of figure 15B is assumed for the following development.

Since $r(t)$ is a chain of equally spaced pulses,

$$r(t) = \Sigma \delta(t - nT_r)$$

Where: δ is the impulse function

Laplace transforming,

$$R(s) = \sum_{n=0}^{\infty} e^{-nsT_r}$$

which is an infinite series and can be reduced to closed form, i.e.

$$R(s) = \frac{1}{1 - e^{-sT_r}}$$

The open loop transfer function for the plant is assumed to be:

$$G(s) = \frac{K/E_{sat}}{s(s + 1)}$$

and the closed loop function between $R(s)$ and $E(s)$ is:

$$\frac{E(s)}{R(s)} = \frac{(s + 1)}{s(s + 1) + K/E_{sat}}$$

Therefore:

$$E(s) = \frac{1}{1 - e^{-sT_r}} \left(\frac{(s + 1)}{s(s + 1) + K/E_{sat}} \right)$$

The method of the steady-state Laplace transform calculus is first to determine the transient portion of the $e(t)$. Since the transient is due to the poles of the denominator polynomial,

$$s^2 + s + K/E_{sat} = (s - s_1)(s - s_2)$$

it is not necessary to evaluate the residues for the pole at

$s = 0$. Therefore, the transient portion of the solution,

$$e(t)_{tr} = \frac{(s_1 + 1)e^{s_1 t}}{(1 - e^{-T_r s_1})(s_1 - s_2)} + \frac{(s_2 + 1)e^{s_2 t}}{(1 - e^{-T_r s_2})(s_2 - s_1)}$$

The next step is to evaluate the total response of the system from $t = 0$ to $t = T_r$. For this time period, $R(s) = 1$ and the transcendental function $(1 - e^{sT_r})$ can be neglected. The total response is:

$$e(t)_{tot} = \frac{(s_1 + 1)e^{s_1 t}}{(s_1 - s_2)} + \frac{(s_2 + 1)e^{s_2 t}}{(s_2 - s_1)}$$

for $0 \leq t \leq T_r$

The steady-state response of the system for one period of the input can be determined by subtracting the transient portion from the total response. The steady-state response is:

$$e(t)_{ss} = \frac{(s_1 + 1)e^{s_1 t}}{(s_1 - s_2)} \left(1 - \frac{1}{1 - e^{-T_r s_1}}\right) + \frac{(s_2 + 1)e^{s_2 t}}{(s_2 - s_1)} \left(1 - \frac{1}{1 - e^{-T_r s_2}}\right)$$

Where: $s = -0.5 \pm j\sqrt{K/E_{sat} - 0.25}$

for $K/E_{sat} > 0.25$

By substitution and reduction, this equation can be expanded:

$$e(t)_{ss} = \frac{e^{-0.5(t - T_r)}}{C} \left[A \cos(K't) + B \sin(K't) \right]$$

for $0 \leq t \leq T_r$

Where: $K' = \sqrt{\frac{K}{E_{sat}} - 0.25}$

$$A = 0.5 \sin(K'T_r) - K' \cos(K'T_r) + K'e^{0.5T_r}$$

$$B = 0.5e^{0.5T_r} - 0.5 \cos(K'T_r) - K' \sin(K'T_r)$$

$$C = K \left[1 - e^{T_r} - 2e^{0.5T_r} \cos(K'T_r) \right]$$

If $\frac{K}{E_{sat}} < 0.25$, the roots of the denominator polynomial are real and the final expression is simpler. Since the cases of interest to this thesis are those capable of response rates above the maximum produced by this condition, the results are restricted to

$$\frac{K}{E_{sat}} > 0.25$$

The performance of the system can be assessed by determining the maximum peak-to-peak ripple Δ_p of the output variable. The equation given for the error is the difference between a step function and the output. This step function is a quantized ramp function. To determine the ripple in the plant

output from the error equation given above, it is necessary to add a term, as follows:

$$\Omega(t)_{ss} = r(t)_{ss} - e(t)_{ss}$$

The desired steady-state input:

$$r_d(t)_{ss} = \frac{t}{T_r}$$

Where: T_r is the period of the step function

Therefore: $$\Omega(t)_{ss} = \frac{t}{T_r} - e(t)_{ss}$$

Figure 16 plots the peak-to-peak ripple as a function of $K'T_r$ for a range of values of the forward loop gain. These curves were determined by the computer program given in appendix D. The equation used for determining the peak-to-peak ripple is:

$$\Delta_p = \left[\frac{t}{T_r} - e(t)_{ss}\right]_{max.} - \left[\frac{t}{T_r} + e(t)_{ss}\right]_{min.}$$

The conditions for a maximum or a minimum are:

$$\frac{d\left(\Omega(t)_{ss}\right)}{dt} = 0$$

If $\frac{d^2\left(\Omega(t)_{ss}\right)}{dt^2}$ is positive, a maximum occurs. Conversely, if $\frac{d^2\left(\Omega(t)_{ss}\right)}{dt^2}$ is negative, a minimum occurs.

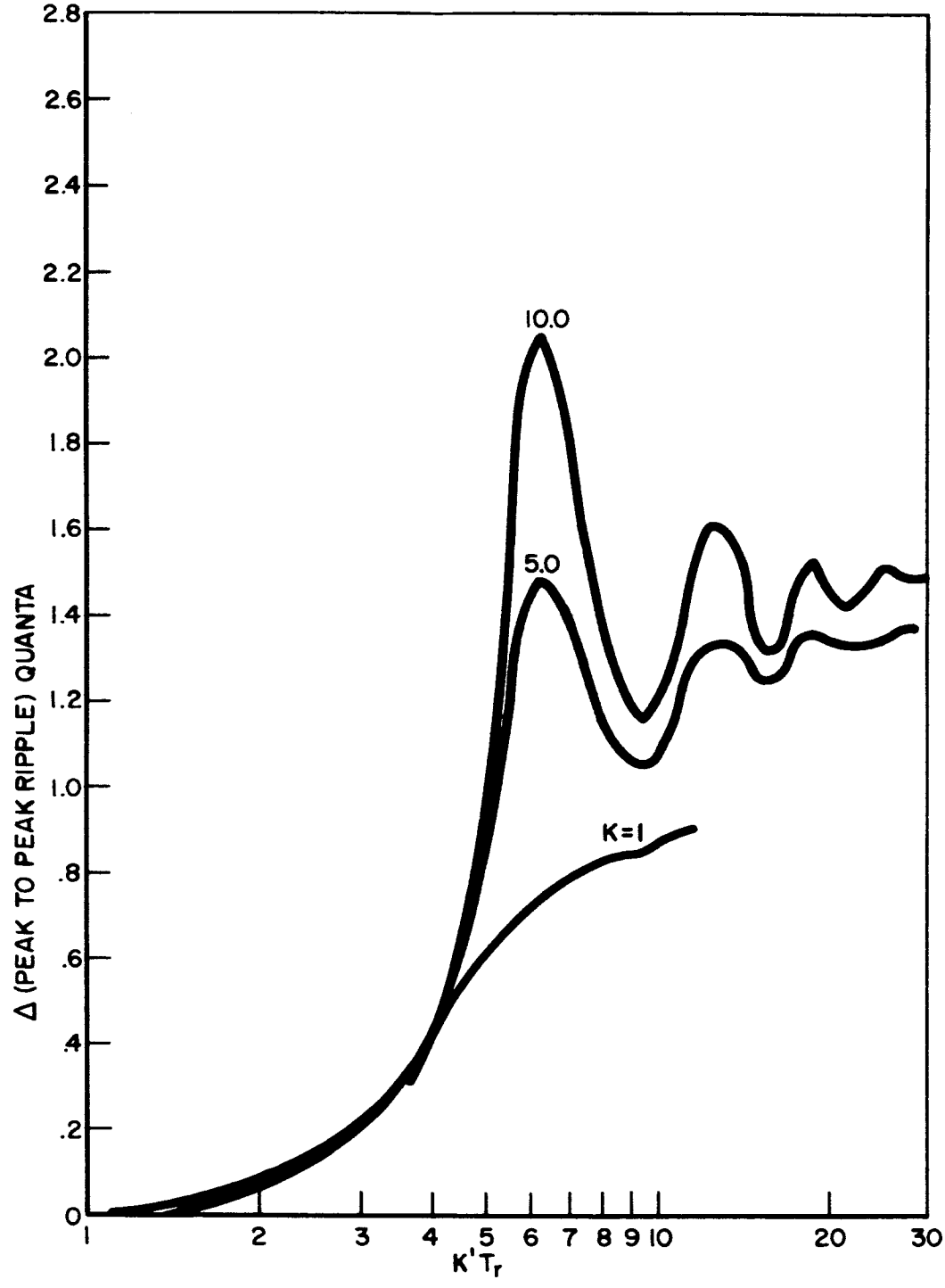

FIG. 16 $K'T_r$ VS. PEAK TO PEAK RIPPLE (IN QUANTA)

Therefore:

$$\frac{de(t)}{dt} = e^{-0.5(t - T_r)} \left[\text{Cos}(K't)\{K'B - 0.5A\} - \text{Sin}(K't)\{0.5B + K'A\} \right]$$

Therefore, the condition for maxima or minima is:

$$K't = \text{Tan}^{-1} \frac{K'B - 0.5A}{0.5B + AK'}$$

Since the function is a sinusoidal function, the maximum and minimum points occur $\pi/2$ degrees apart. The performance index requires determination of both maxima and minima; therefore, the above condition need only be satisfied at one point.

Figure 17 plots the maximum peak-to-peak ripple in the time rate of change of the output variable. The equations from which these curves were generated are given below:

$$\dot{\Omega}(t)_{ss} = \frac{Ke^{-0.5(t - T_r)}}{C} \left[M \text{ Cos}\{K'(T_r - t)\} + N \text{ Sin}\{K'(T_r - t)\} \right]$$

for $0 \leq t \leq T_r$

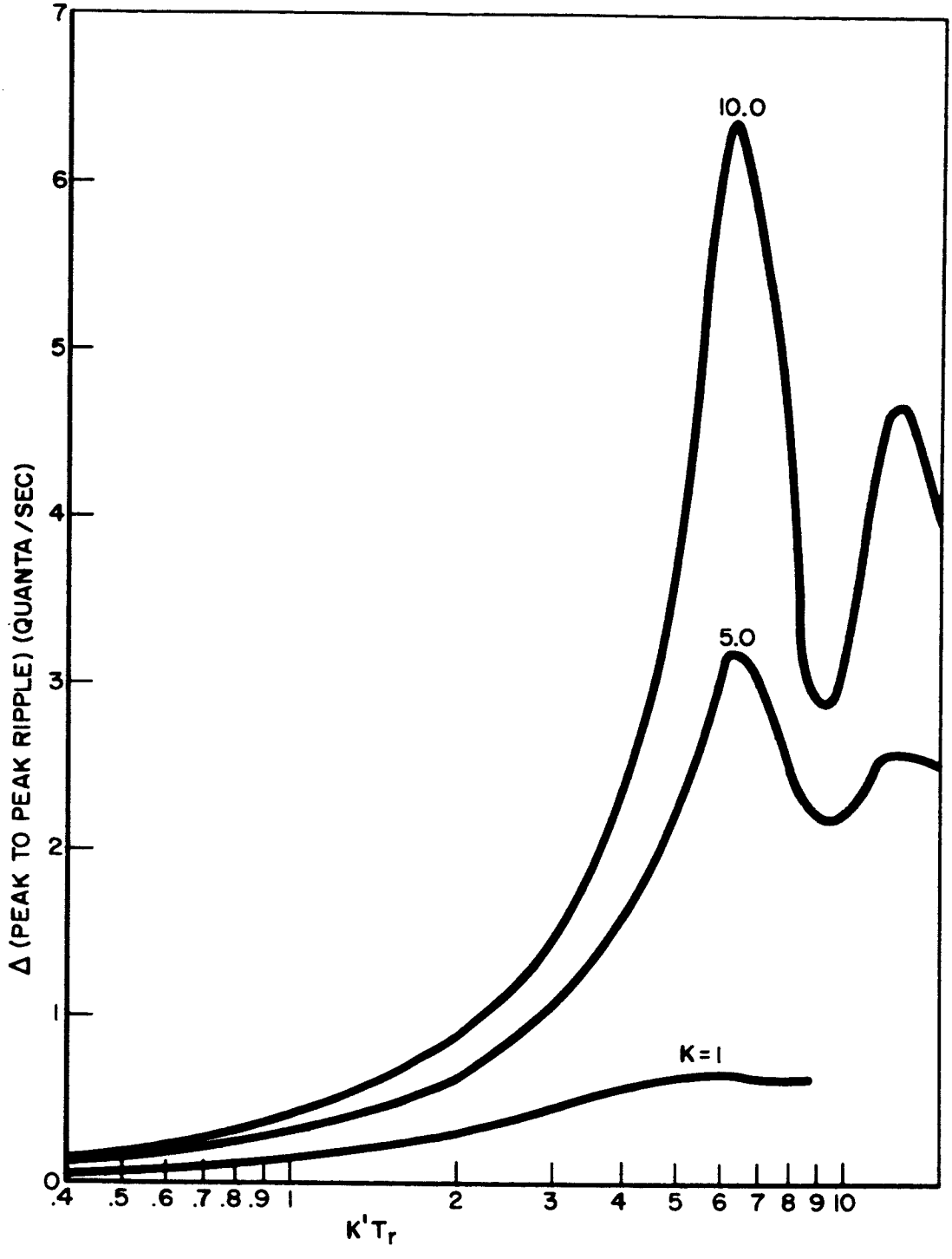

FIG. 17 $K'T_r$ VS. PEAK TO PEAK RIPPLE (QUANTA/SEC)

Where: $M = e^{0.5T_r} \text{Sin}(K'T_r)$

$$N = 1 - e^{0.5T_r} \text{Cos}(K'T_r)$$

$$C = K'\{1 + e^{T_r} - 2e^{0.5T_r} \text{Cos}(K'T_r)\}$$

The conditions for maxima or minima along this trajectory are:

$$K'(T_r - t) = \text{Tan}^{-1} \frac{0.5M + K'N}{K'M - 0.5N}$$

Both figures 16 and 17 demonstrate a resonance in the peak-to-peak ripple at a value for $K' = 2n\pi$, where $n = 1, 2, 3 \ldots$ Reference to the system transfer function will show that K' represents the damped natural frequency of the system. Since T_r is in units of seconds per cycle, it is not unreasonable that the resonant peaks should occur as shown. The maximum ripple is kept below 0.1 quanta from $0 \leq K'T_r \leq 2$. It is obvious that there is an input rate below which the output ripple is unsatisfactory depending on the system specifications. The range of input rates over which a satisfactory output is obtained may be substantially increased by the addition to the control circuit of a weighting factor M. The system as defined up until now has weighted each input pulse to be equivalent to a change in the output position of one quanta. If this rating were reduced by one tenth, the peak-to-peak ripple, as shown in figures 16 and 17, would be reduced to one tenth of their value.

In other words, the addition of this weighting factor appears as a gain on the input line ahead of the closed-loop transfer function, as shown in figure 18. In order to command the same velocity of the output variable $\Omega(t)$, as in the other case, the pulse repetition rate of the input must be increased by a factor of 1/M. The means of implementing this additional gain is discussed in appendix A. The net result of this new circuit is to increase the operating range of the system. A satisfactory range can be determined from figures 16 and 17 by multiplying the ordinates of these curves by M.

A system that is designed for a path-control operation should be capable of responding to step inputs. A satisfactory criterion for the step response would be specification of the maximum overshoot. A second possible criterion would be the number of sign reversals of the error. Both of these criteria can be satisfied by use of the phase plane if the system is of second order. In systems higher than second order, simultaneous phase planes can be used, but the method becomes much too complex for consideration and other techniques must be employed. Nonlinear techniques must be used to analyze this response since there is a saturation characteristic in the forward loop. It is also feasible to consider adaption within the loop that will use one saturation level for path control and one for step response. This is particularly valid within the machine tool control field. In order to use the phase plane, the system differential equation is best expressed as follows:

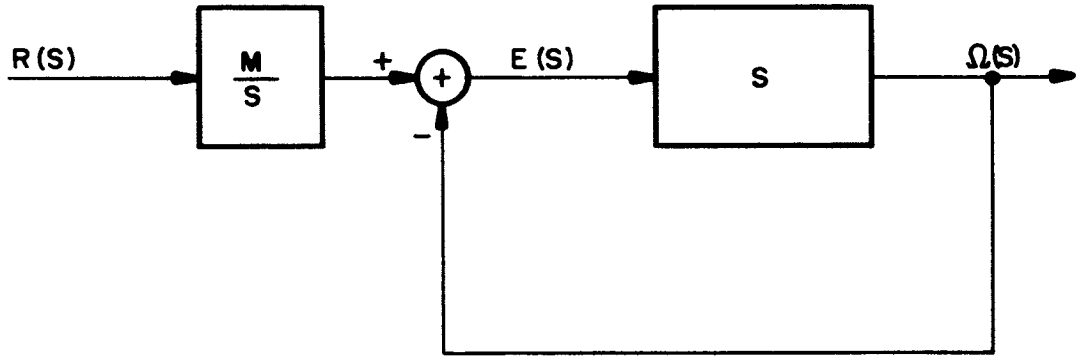

FIG. 18 SCHEMATIC BLOCK DIAGRAM SHOWING WEIGHTING FACTOR USED TO INCREASE SATISFACTORY OPERATING RANGE OF SYSTEM

$$\frac{d^2\{e(t)\}}{dt^2} + \frac{d\{e(t)\}}{dt} + \{K/E_{sat}\}e(t) = 0$$

for $e(t) < E_{sat}$

and $$\frac{d^2\{e(t)\}}{dt^2} + \frac{d\{e(t)\}}{dt} + K/E_{sat} = 0$$

for $e(t) > E_{sat}$

The isoclines for the unsaturated operation are:

$$\frac{d\dot{e}(t)}{de(t)} = -\left[1 + \frac{\{K/E_{sat}\}e(t)}{\dot{e}(t)}\right]$$

for $e(t) \leq E_{sat}$

Where: $\dot{e} = \frac{d\{e(t)\}}{dt}$

or $$\frac{d\dot{e}(t)}{de(t)} = -\left[1 + \frac{K}{\dot{e}(t)}\right]$$

for $e(t) \geq E_{sat}$

Since the equations for the isoclines are straight lines, the phase plane is relatively simple to plot. However, the isoclines are a function of the saturation level, and this requires replotting of the phase plane isoclines for each value of E_{sat}

that is to be investigated. Since the system exhibits a saturation characteristic, the maximum output velocity is limited. This maximum velocity can be determined as follows by observing that, when the error is saturated, the input to the open loop transfer function is a step input with an amplitude equal to K.

$$\Omega(s) = \frac{\{K/E_{sat}\}E(s)}{s(s+1)}$$

Let $E(s) = \frac{E_{sat}}{s}$

Therefore: $\Omega(s) = \frac{K}{s^2(s+1)}$

and $\lim_{t \to \infty} \dot{\Omega}(t) = \lim_{s \to 0} s\{s\Omega(s)\} = K$

The step response in its worst case is for the $\dot{e}(t)$ to be a maximum when the system enters the linear region. This would occur for large step inputs. If the specifications for step response limited only the overshoot, it would be necessary to plot the phase portrait in the first or third quadrants only on the phase plane for each value of saturation level that is to be investigated. Figure 19 has a sample phase portrait plotted on it showing an overshoot of 2.2 quanta. As mentioned above, a system of an order higher than two requires an extremely difficult analysis in the phase plane, and the reader is referred to several alternate analytical techniques that can handle the

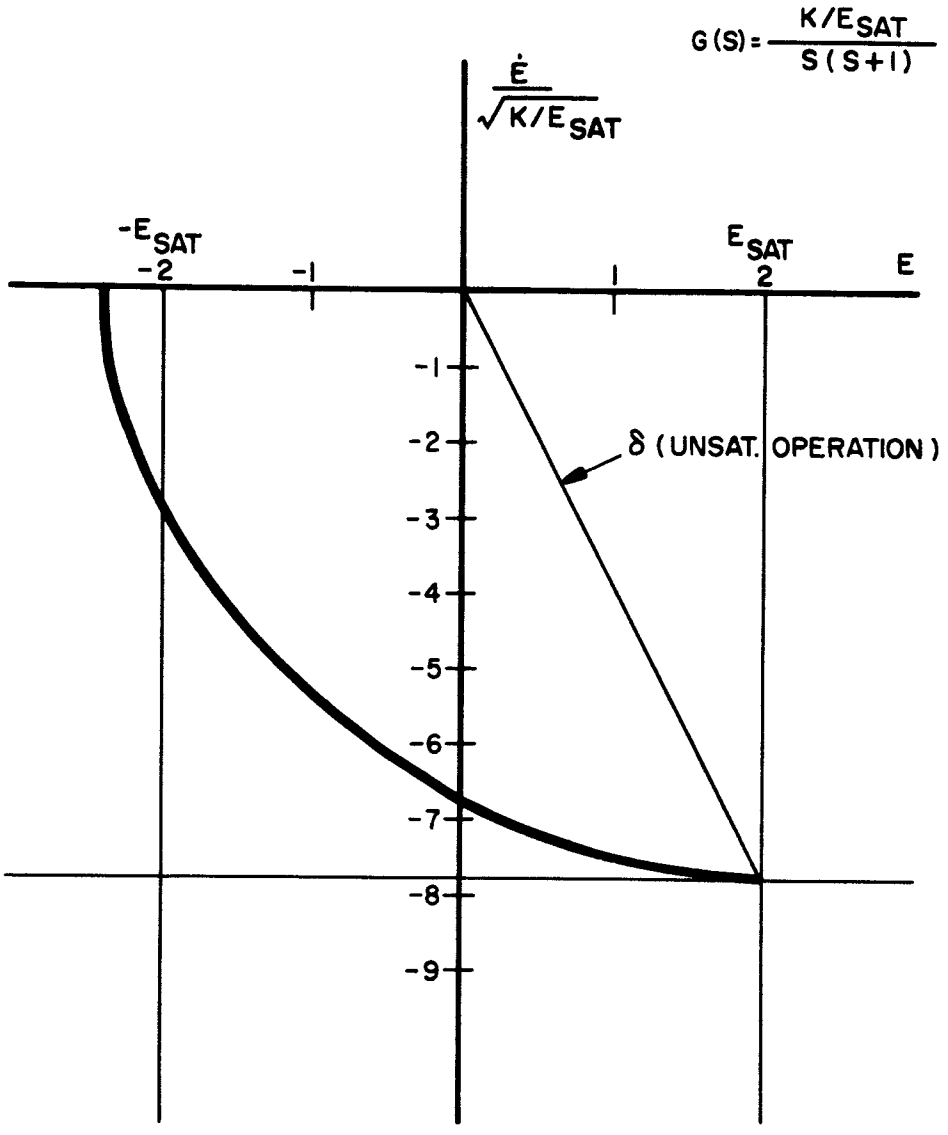

FIG. 19 PHASE PORTRAIT FOR STEP RESPONSE

saturation characteristic very well. Several of these are described by Thaler and Pastel and by Graham and McRuer.[12]

This chapter has presented techniques for designing the system to follow an input path and to design the system to have satisfactory step response. Both of these methods will be compared to an experimental model in chapter 5.

CHAPTER V

EXPERIMENTAL INVESTIGATION

This chapter introduces a physical model to verify the mathematical model developed in chapters 3 and 4.

In order to use the same form of transfer function chosen as an example in chapters 3 and 4, a d-c motor with armature control was selected as the controlled plant. Figure 20 shows the block diagram for the experimental model. The parameters in this figure are identified as follows:

R = input data (quanta)

E^* = controlled plant input (volts)

Ω = system output (radians)

K_1 = maximum armature voltage (volts)

E_{sat} = saturation level (quanta)

K_2 = open loop plant gain (radians/volt)

K_3 = feedback gain (quanta/radian)

The transfer function for the motor, developed in appendix C, is as follows:

$$\frac{\Omega(S)}{E^*(S)} = \frac{2.26}{S(0.0379S + 1)}$$

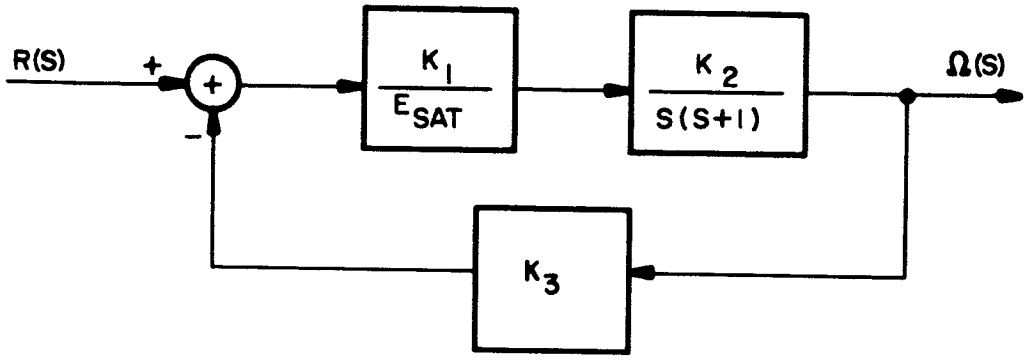

FIG. 20 BLOCK DIAGRAM OF EXPERIMENTAL MODEL

For the experimental tests,

$$K_1 = 6.5$$
$$E_{sat} = 10.0$$
$$K_3 = 63.6$$

By reducing the block diagram of figure 20, the closed loop transfer function is obtained.

$$\frac{\Omega(S)}{R(S)} = \frac{38.6}{S^2 + 26.6S + 2460}$$

The damped natural frequency of the closed loop response is:

$$\omega_d = 7.6 \text{ cycles/second}$$

Figure 21 shows the experimental step response for the above set of parameters. From this figure, the damped natural frequency measured is 7.5 cycles per second.

To obtain a step response that would give a good measure of the damped natural frequency, it was necessary to subject the system to a large step input which exceeded the saturation level. A step input of 32 quanta was used. This step size was satisfactory for a system loop gain of 38.6 because the system did not overshoot into saturation.

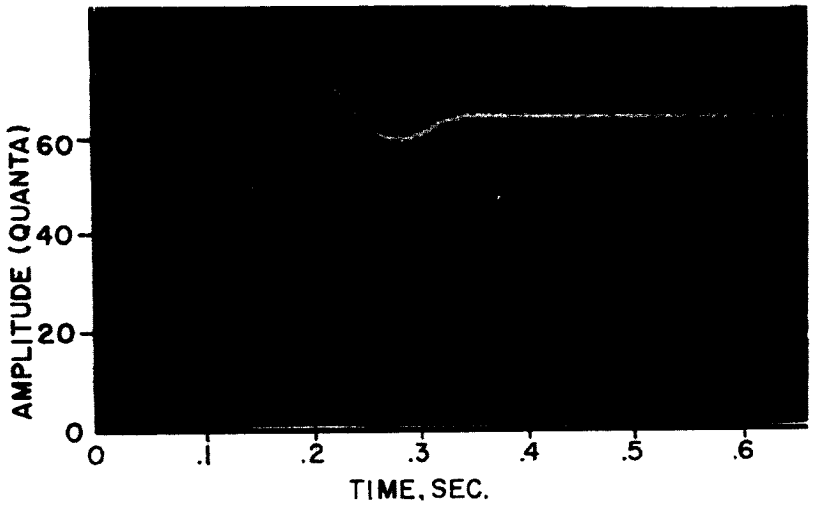

FIG. 21 EXPERIMENTAL STEP RESPONSE

In order to verify the overshoot obtained, a phase portrait of the experimental model was constructed. It is shown in figure 22. The measured overshoot was 6.4 quanta. This differs from the value determined from figure 22 by 9.4%, which is within the measurement accuracy of the experimental model.

The step response test reported above was checked at higher values of loop gain. The gain was increased by decreasing the saturation level. The only parameter checked from these other tests was the damped natural frequency since the first overshoot was in the saturation region. In all cases, good correspondence existed between the theoretical and the measured frequencies. All measured values were within 5% of the corresponding theoretical values.

The ramp response of the system was also checked. A pulse generator provided a constant frequency pulse input to the system. Figure 23 shows both the theoretical response for the system and the experimentally determined values.

At the low input pulse rates, the experimental values are somewhat lower than the theoretical, and no sharp resonant peak could be determined. Both of these characteristics are due to the friction in the system. In order to obtain a linear transfer function for the system, the friction properties were lumped

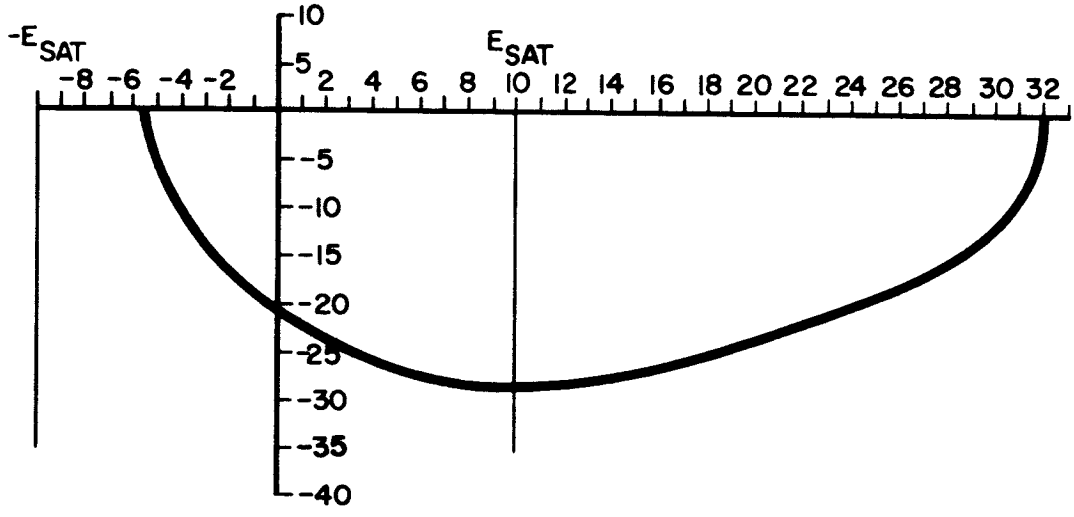

FIG. 22 PHASE PORTRAIT OF THE EXPERIMENTAL MODEL

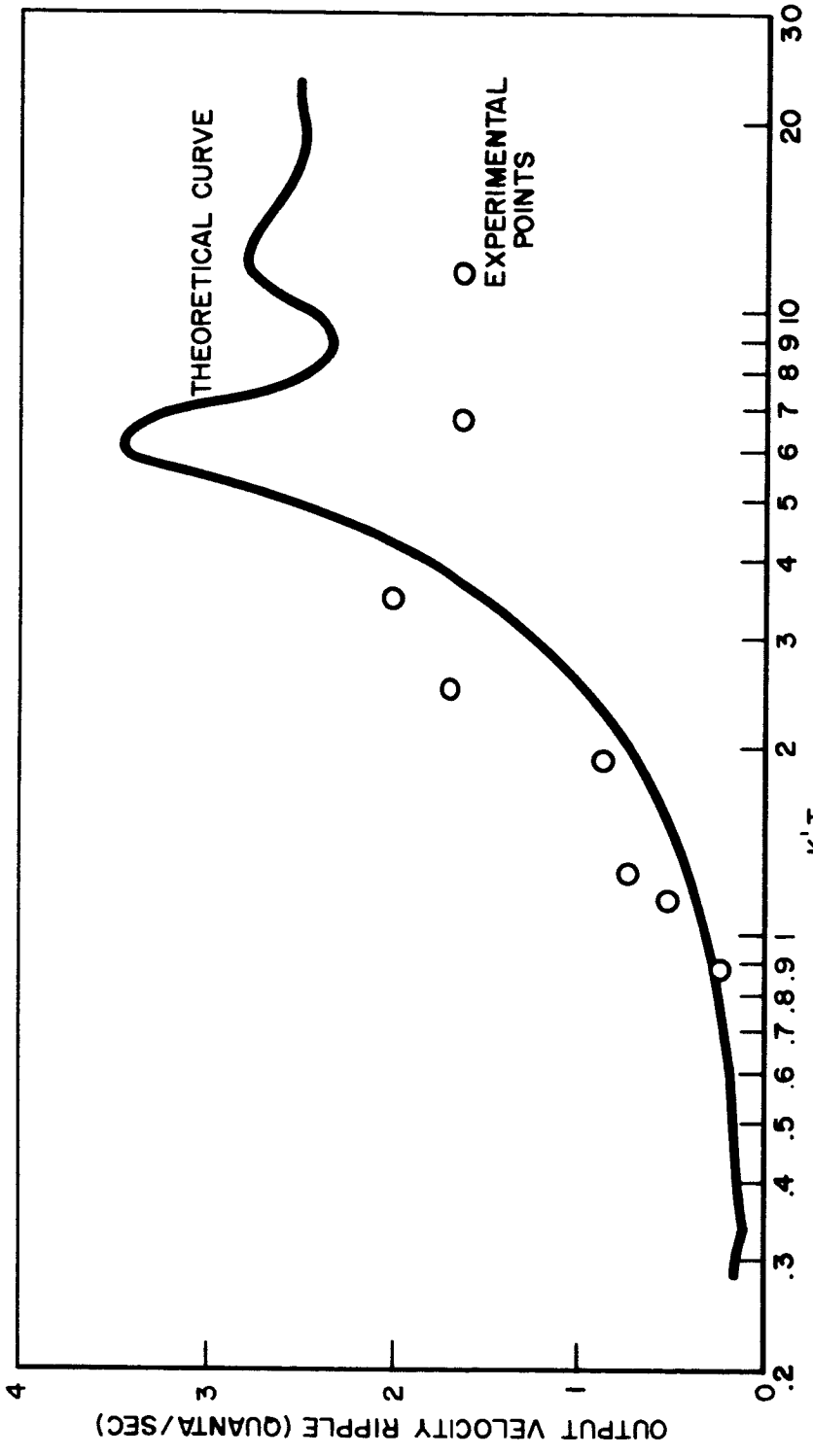

FIG. 23 VELOCITY RIPPLE OF EXPERIMENTAL SYSTEM

with the damping coefficient. The friction does not allow the system to overshoot in response to very small step inputs. This characteristic limits the peak-to-peak velocity ripple to a value somewhat less than the model will predict and will not allow the system to resonate at the damped natural frequency.

At the lower input rates, the velocity ripple was not constant. The points shown on figure 23 are the average values. The variation is caused mainly by the variation in armature resistance. This resistance varies from 17 ohms to a maximum of 70 ohms, depending upon the angular position of the rotor. The transfer function was modeled on the average resistance of 25 ohms. This variation in resistance would not affect the step response data given above because the step input was large enough to average the resistance.

Figure 23 plots the velocity ripple due to the input pulses. The theoretical curve assumes that the time between the input pulses is constant. The pulse generator used to generate the input signal was subject to a low frequency drift which caused the output to exhibit a limit cycle. This phenomenon was most evident at input rates from two to four times the system damped natural frequency. Other limit cycles were observed as the input rate approached a sub-multiple of the relay input frequency.

The maximum output rate for the system can be determined from the open loop transfer function, assuming the maximum error signal exists:

$$S\Omega(S) = \frac{S6.5(2.26)}{S^2(0.0379S + 1)}$$

By the final value theorem of Laplace transform calculus, the maximum steady-state output rate is:

14.7 radians/second.

The results presented in this chapter verify the use of a linear model in predicting the system response. They also point out the need for a means of adapting the system to compensate for limit cycles in the output.

CHAPTER VI
CONCLUSIONS

This thesis has shown that satisfactory performance for a pulse-data relay system can be obtained by linearization of the quantizer and of the relay. This was shown theoretically and was verified by an experimental model. The digital-to-analog converter can be successfully eliminated from the conventional system, and the ripple produced in the output by the linearized relay can be minimized by using a solid-state relay, which is capable of extremely high frequency operation relative to the band pass of the system. The logic required to implement this type of system is described in appendix A. The quantizer used to effect the linearization was a commercially produced unit. It is shown in appendix A that the dither can be added to this quantizer without allowing the dither frequency to affect the count in the bidirectional counter or to dither the system at this frequency.

There are many advantages in linearizing a quantizer. The net result depends upon the amplitude of the dither, as was shown in chapter 3. If this amplitude drifts, the quantizer is not exactly linearized. However, if the maximum drift of the dither amplitude can be maintained within ten per cent, then the over-all effect of the linearization is to increase the resolution

of the quantizer by a factor of ten. In addition, the system proposed in chapter 4, with a gain added in the input loop and implemented as described in appendix A, makes it possible to control the system to a resolution ten times that determined by the least bit in the counter.

Implementation of a velocity feedback from the quantizer would be very fruitful. As mentioned earlier, a quantizer can be considered as a frequency modulator. If the output pulses from the quantizer were fed to a Shannon rack decoder,[13 and 14] the output from the Shannon rack decoder would then be an analog voltage proportional to the first derivative of the output variable. With this implementation and a second order plant, it would be possible to define an optimum controller since information on all output state variables would be available. The linearized relay system as used in this thesis lends itself readily to description by vector matric difference equations. Having the equations in this form allows stability investigations by the second method of Lyapunov, and the investigations carried out by Nelson[15] can be applied to approximate a minimum time controller for response to step inputs. There are many other sophisticated techniques that can be applied to the analysis of this system provided information on the rate of change of the output can be obtained.

APPENDIX A

In this appendix, a detailed description of the implementation for the system is given.

Figure 24 shows a detailed block diagram of the basic system. The bidirectional counter performs the function of registering the error in the binary number system to an integral number of quanta. It accomplishes this task by adding input pulses $r(t)$ and subtracting feedback pulses $\Omega^*(t)$. The feedback pulses are originated by the quantizer block labeled Q^*. This quantizer emits direction-sensitive pulses. The input pulses are assumed to be obtained from magnetic tape or some other source. The diode matrix following the counter decodes the error from the binary number system to the decimal system. The output from the diode matrix is gated to the circulating register. This register sets the saturation level for the system and gates the pulses which turn off the relay. A pulse is gated from the circulating register to turn off the relay when the bit in the circulating register corresponds to the decimal equivalent of the error. The clock driving the circulating register is used to turn the relay on when the first bit in the circulating register is set. The output from the quantizer Q is a signal that is proportional to distance between quanta points. This signal is summed with the wave form provided by the sawtooth

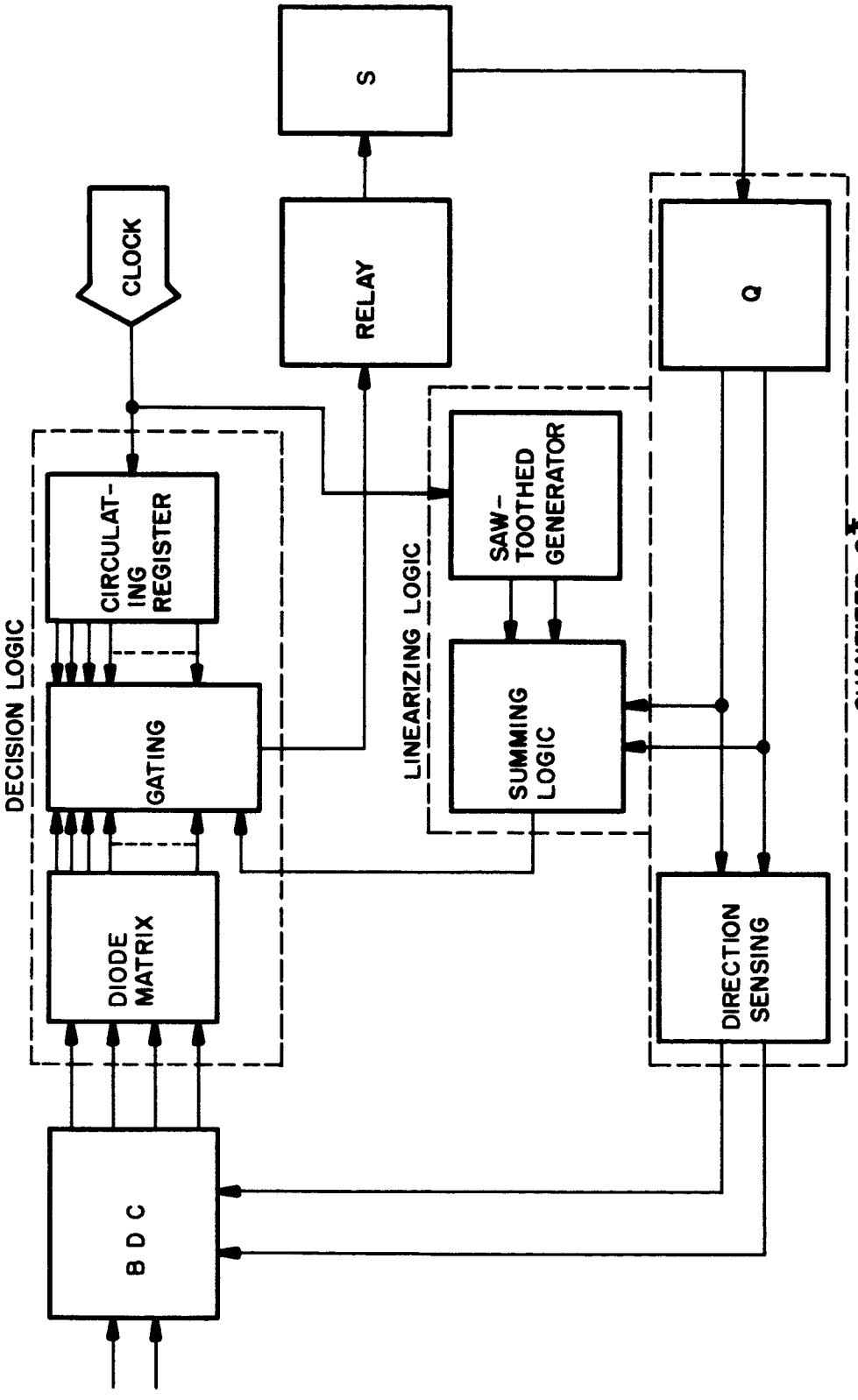

FIG.24 DETAILED BLOCK DIAGRAM

generator and is then used to alter the turnoff point of the relay to account for the quantization error. The sawtooth generator is driven by the same clock that is used to drive the circulating register. This causes the quantizer dither frequency to be much greater than the effective relay dither frequency. Each of these separate circuits will be presented in detail,and timing diagrams, where necessary, have been shown in the following sections of this appendix.

Quantizer and Direction-sensing Circuit

The quantizer used for this system was purchased from W. and L. E. Gurley. It is a photoelectric system with two photoelectric cells positioned so that there is a 90^{o} phase difference between their respective outputs. This phase difference allows the direction of rotation to be sensed. Between the photocell and the light there is an aperture which causes a linear variation in the light intensity that reaches the photocell. The output from this quantizer is shown in figure 26. It may be seen that the output is not exactly a triangular wave but, in the regions from 45^{o} to 135^{o} and from 225^{o} to 315^{o} on each trace, the output is proportional to the amount of rotation. This fact allows these portions on each trace to be used as a position feedback signal. The manner in which these are utilized is discussed later in this chapter.

Since the portion from 45^{o} to 135^{o} is used to indicate the distance between the quanta points, this forces the quanta points

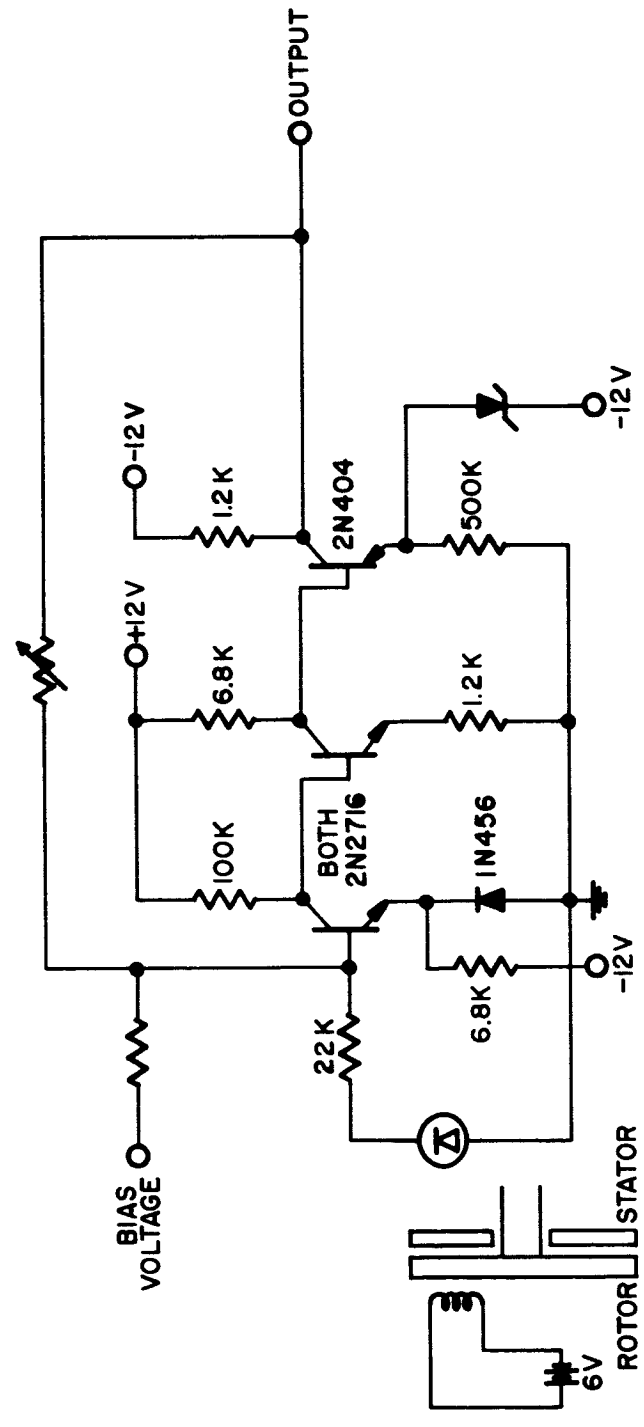

FIG. 25 SCHEMATIC DIAGRAM OF PHOTOELECTRIC QUANTIZER AND AMPLIFIER

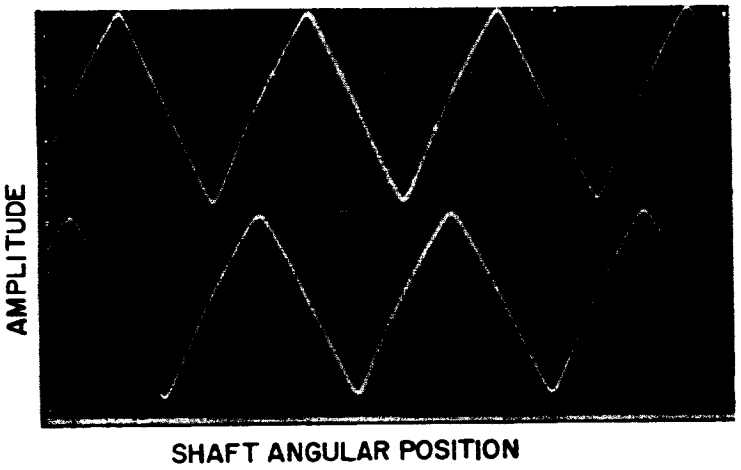

FIG. 26 QUANTIZER OUTPUT TRACES

to be located at $(45 + \frac{n\pi}{2})$ degrees of rotation, where n = 0, 1, 2, 3 . . . The output wave form must be converted into a square wave to be compatible with the bidirectional counter. This conversion is accomplished by use of a threshold device which has the characteristics of an ideal relay. A Schmitt trigger is used to accomplish this task, and the circuit is shown in figure 27. Figure 27 shows the schematic diagram of its operation. The point -D is the trigger level. It was necessary to use two triggers on one line in order to accommodate the requirement for pulses at two separate levels. As shown in figure 28, signal A operates two triggers, A_{1T} and A_{2T}. A_{1T} is turned on at $(45 + n\pi)$ degrees and is turned off at $(315 + n\pi)$ degrees. A_{2T} is turned on at $(135 + n\pi)$ degrees and is turned off at $(225 + n\pi)$ degrees, where n = 0, 1, 2, 3 . . .

Figure 29 shows the logical implementation of the direction-sensing circuit. In order to sense the direction of rotation, signal B is converted to a square wave by trigger B_T. The threshold of this element is set so that it triggers at $(0 + n\pi)$ degrees. This threshold is determined by the requirement that there must not be coincidence between a change in the state of B_T and a change in the state of either A_{1T} or A_{2T}.

The logical equations required to determine the direction of rotation are given below:

Forward: $f = \alpha_{A1}\overline{B} + \alpha_{A2}\overline{B} + \beta_{A2}B + \beta_{A1}B$

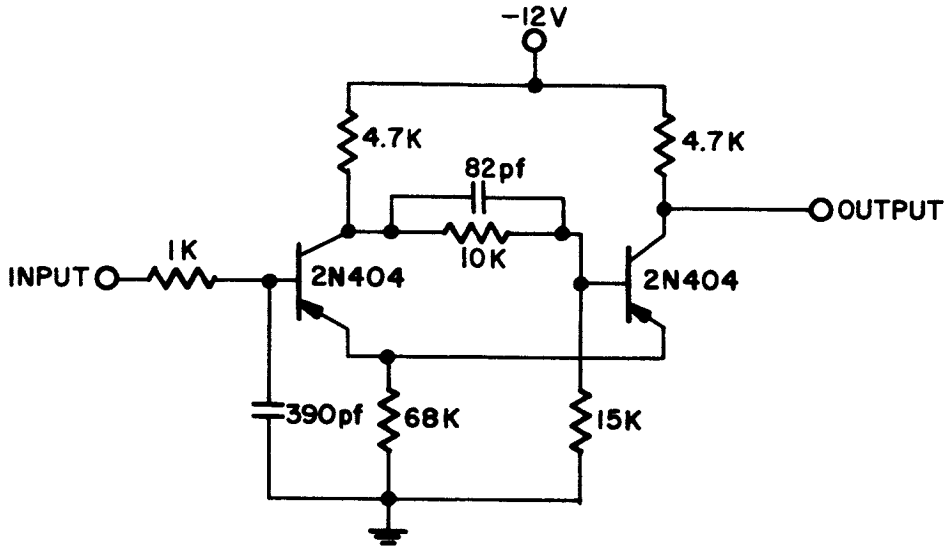

A: CIRCUIT DIAGRAM

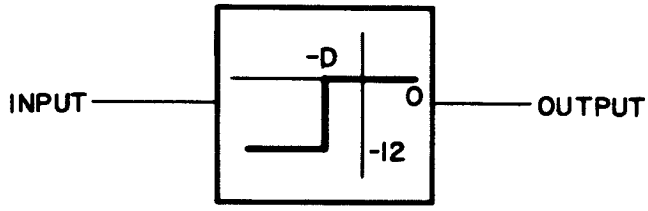

B: SCHEMATIC DIAGRAM

FIG. 27 SCHMITT TRIGGER

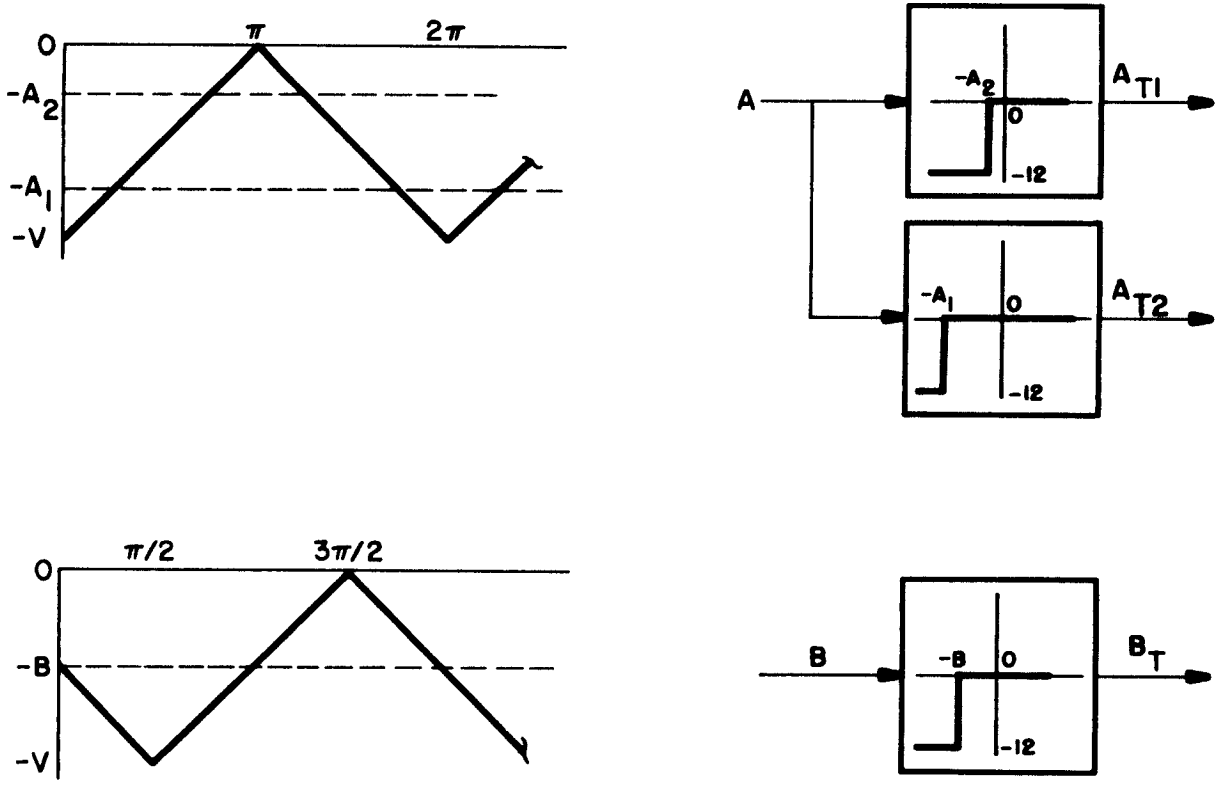

FIG. 28 TRIGGER LEVELS REQUIRED FOR QUANTIZER OUTPUT

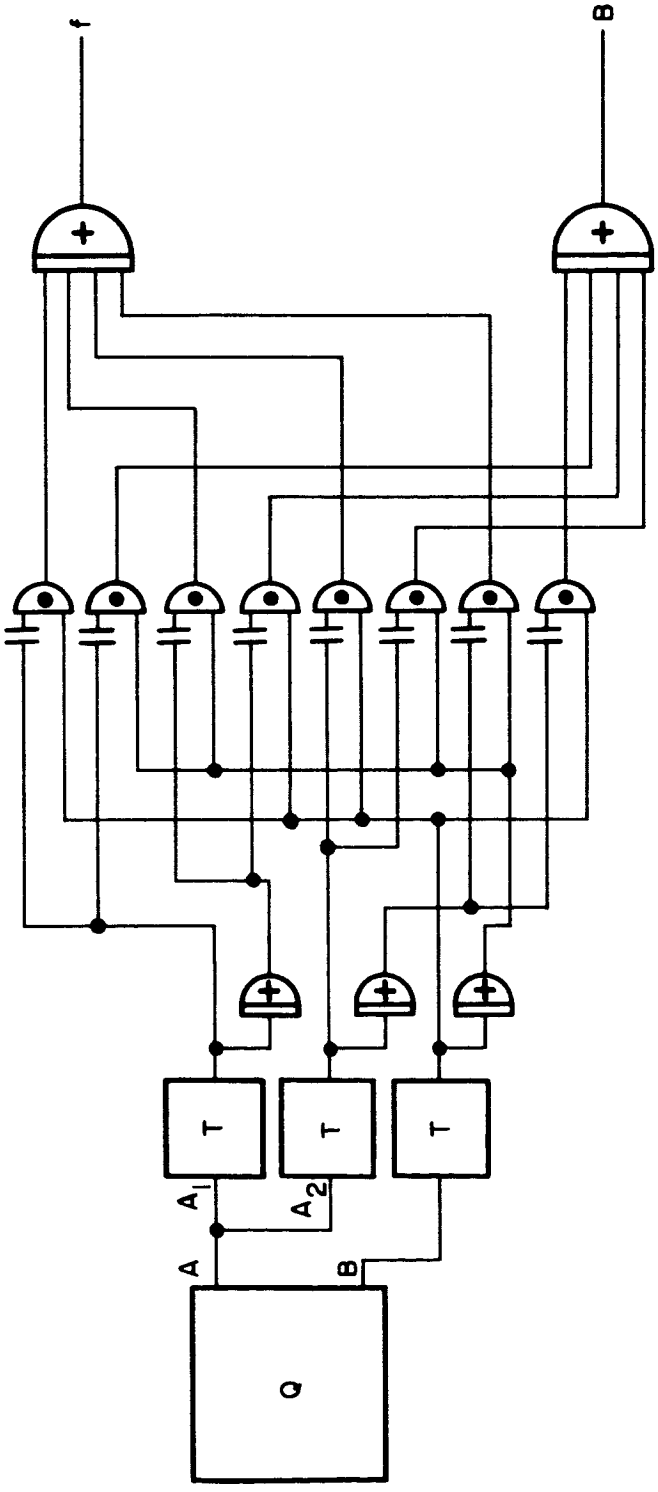

FIG.29 DIRECTION SENSING CIRCUIT

Backward: $B = \alpha_{A1}B + \alpha_{A2}B + \beta_{A2}\overline{B} + \beta_{A1}\overline{B}$

Where: α represents a positive transition of the trigger

β represents a negative transition of the trigger

B represents the ON state of the trigger B_T

Bidirectional Counter and Anti-coincident Circuitry

The logical implementation of the bidirectional counter and the anti-coincident circuitry is shown in figure 30. Since the bidirectional counter must accept pulses from two separate sources and must account for every single pulse, it is necessary to include circuitry which will prevent two pulses from arriving at the input to the counter simultaneously. Any circuit designed to accomplish this task must refrain from forcing the definition of coincidence between pulses.

The circuit used, as shown in figure 30, employs four memory stages. Two of these bits are for the input pulses and two are for the feedback pulses. Since both the input and the feedback have positive and negative pulses, it is necessary to have a memory bit for each direction. The input or feedback pulses set the appropriate flip-flop, and the clock shown in the circuit resets the flip-flops in a given sequence. Since it is impossible to have coincidence of a positive and a negative pulse in the input signal, both input flip-flops may be reset simultaneously. This same reasoning applies to the feedback

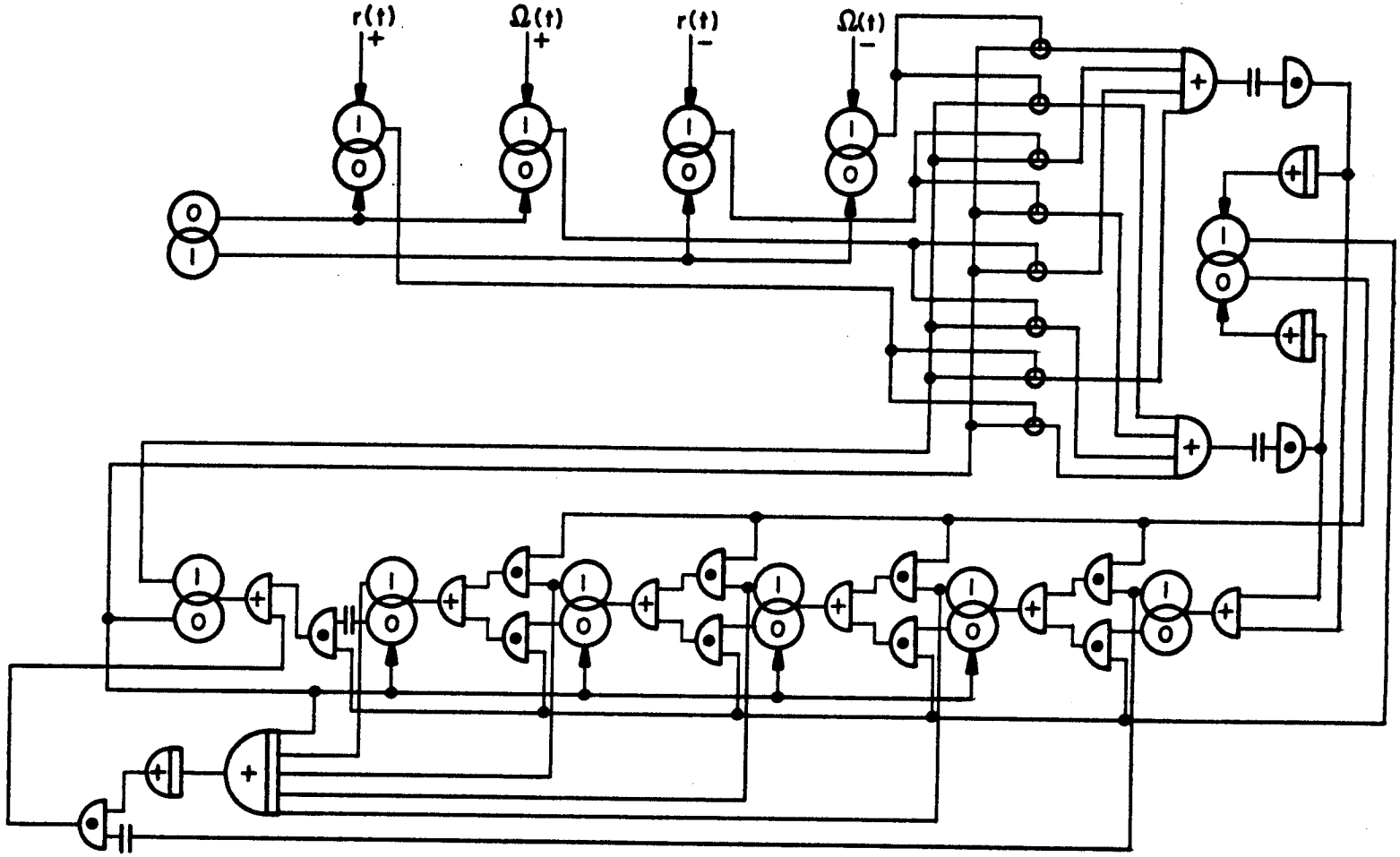

FIG. 30 BIDIRECTIONAL COUNTER AND ANTI-COINCIDENT GATE

line. This allows one output from the clock to reset the input flip-flops and the other output to reset the feedback flip-flops since these outputs are 180^{o} out-of-phase with each other. The frequency of this clock must be, at a minimum, equal to the maximum possible frequency of input or feedback pulses. The clock used in this report is operated at 250 kilocycles, and the maximum frequency of either input or feedback pulses has been shown in chapter 5 to be equivalent to a pulse repetition rate of four kilocycles. A pulse is then registered in the counter when any of these memory bits has been reset by the clock.

The counter consists of five bits, allowing maximum possible count in binary of 64, with one extra bit to register the sign of the error. The optimum number of bits for a bi-directional counter in this circuit is determined by the maximum expected error in the system. This maximum error would occur when the system starts from rest to follow the maximum input rate. Figure 31 shows the transient portion of this response, indicating a maximum error of 18 quanta. In order to accommodate this maximum error safely, five memory bits were necessary. If the error in the system exceeds the maximum count of the bidirectional counter, pulses would not be counted or the counter would dump and indicate a count of zero. (The maximum count in the counter would occur when all the bits of the counter were set. At this point, if there were one more pulse to increase the count, the next state of the

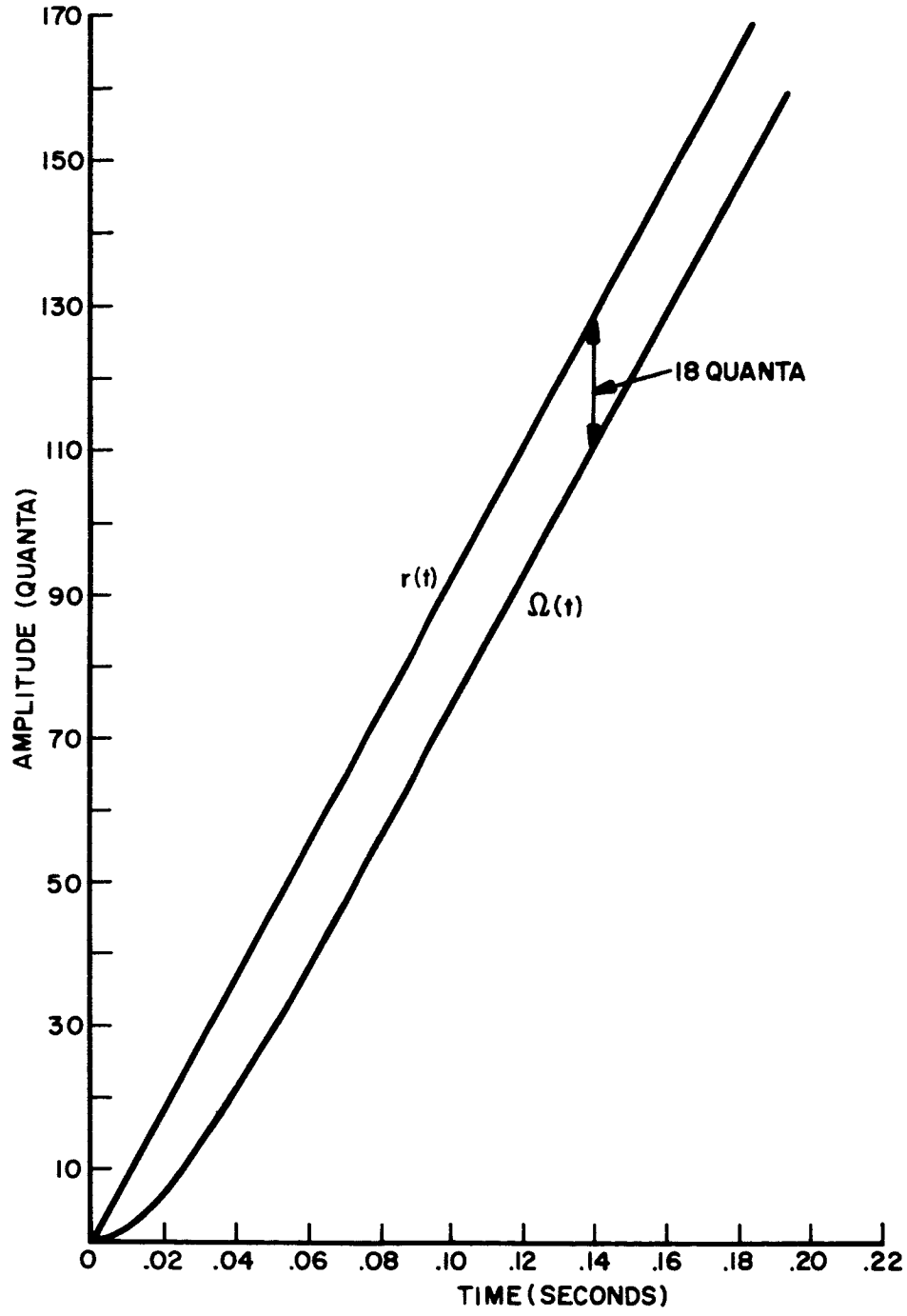

FIG. 31 SYSTEM RESPONSE TO MAXIMUM INPUT RATE

counter would be all zeros. Therefore, the counter would go from maximum error to zero error with one pulse.) This situation can be easily detected and protected against by the inclusion of one extra bit. This extra bit would flash a warning light when it was set, indicating difficulty within the system. The other possibility is simply to forbid input pulses that would count the counter beyond its maximum, incurring a loss of information. It is important to note that any error exceeding the maximum capacity of the counter would indicate that there were troubles within the system.

If the system is to follow step inputs, the maximum step to be allowed might exceed the maximum error determined by the above procedure and would indicate the need for extra counter capacity. This, however, can be easily bypassed by implementing the step inputs that would exceed the maximum capacity of the counter in a manner apart from the presetting of the counter with the maximum step. In other words, this could be accomplished by using several step inputs or by implementing a step input as a maximum pulse rate input.

Decision Logic

Figure 32 shows the logical implementation of the decision logic block consisting of a diode matrix, converting the error from a binary number to a decimal number, and a circulating register. The circulating register is a ten-bit

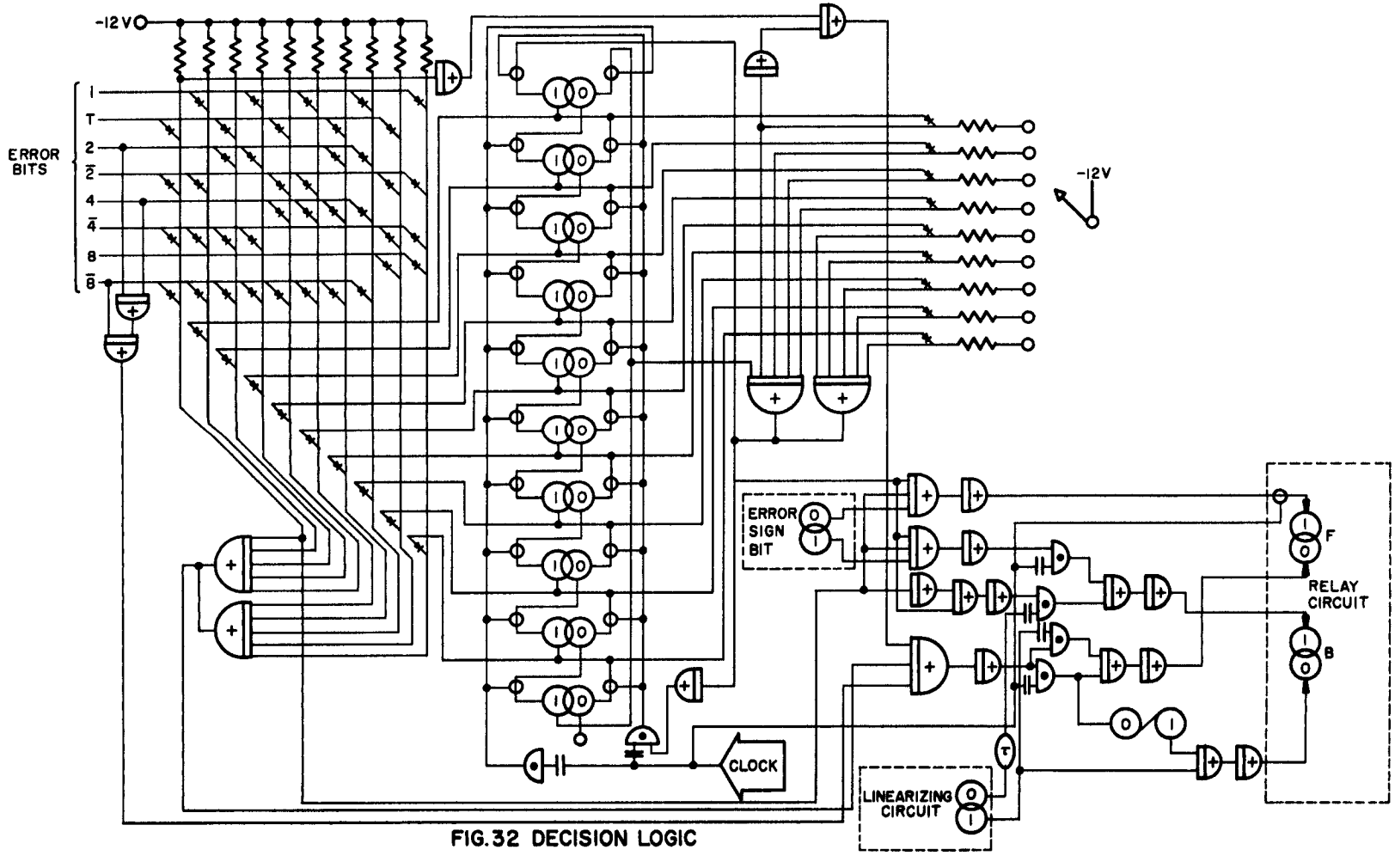

FIG. 32 DECISION LOGIC

shift register which circulates one bit. The clock pulse that sets the first bit of this register is used to turn on the relay, providing there is a non-zero error in the system. The bits of the circulating register have been gated with the output from the binary-to-decimal converter so that, when there is coincidence between the n^{th} bit of the register and the error, the next clock pulse will reset the relay. If the error is equal to or greater than ten, the relay will not be turned off since the next clock pulse will be a command to set the relay. There is a decade switch provided which allows the circulating register to recirculate after n bits, where n = 1, 2, 3 . . . 10. This sets the saturation level at n. The frequency of the dither signal used to linearize the relay, as discussed in chapter 3, is therefore equal to 1/n times the frequency of the clock driving the circulating register. The two flip-flops, F and B, transfer the error sign information to the relay. Two memory bits are needed here to implement a dead zone relay. If an ideal relay is desired, only one would be required. The set and reset logic for the relay is given below, where the letters refer to the least four bits of the bidirectional counter, as indicated in figure 30.

$$\text{Reset } F = \{\bar{8}\bar{4}\bar{2}1C_1 + \bar{8}\bar{4}2\bar{1}C_2 + \ldots + MC_{n-1}\}\overline{\{8(4+2)\}}\bar{S}$$

$$\text{Set } F = (M+1)C_n\bar{S}$$

Where: M is the binary equivalent of (n - 1)

S is the sign of the error: S for negative error

$\overline{S}$ for positive error

C_n is the nth circulating register bit

The reset and set equations for the flip-flop B are identical to the above with $\overline{S}$ replaced by S.

The set and reset logic, as described above, are for a system with no linearization of the quantizer. When the linearizing circuitry has been added, it is necessary to modify this circuitry to accommodate the linearizing signal, which is described in the following section.

Linearizing Circuit

The linearizing circuitry is shown in figure 33 and consists of a sawtooth wave generator, a summing circuit and a trigger element. The circuit for the sawtooth wave generator is shown in figure 34. This circuit uses a unijunction relaxation oscillator and a simple a-c amplifier to invert the signal. The clock input to this wave generator drives the generator at the clock frequency, provided the relaxation frequency is lower than the driving frequency. From figure 24, it can be seen that the clock driving this wave generator is the same clock used to drive the circulating register. Thus, the wave frequency is equal to n times the dither frequency for the relay, where n is the saturation level for the relay.

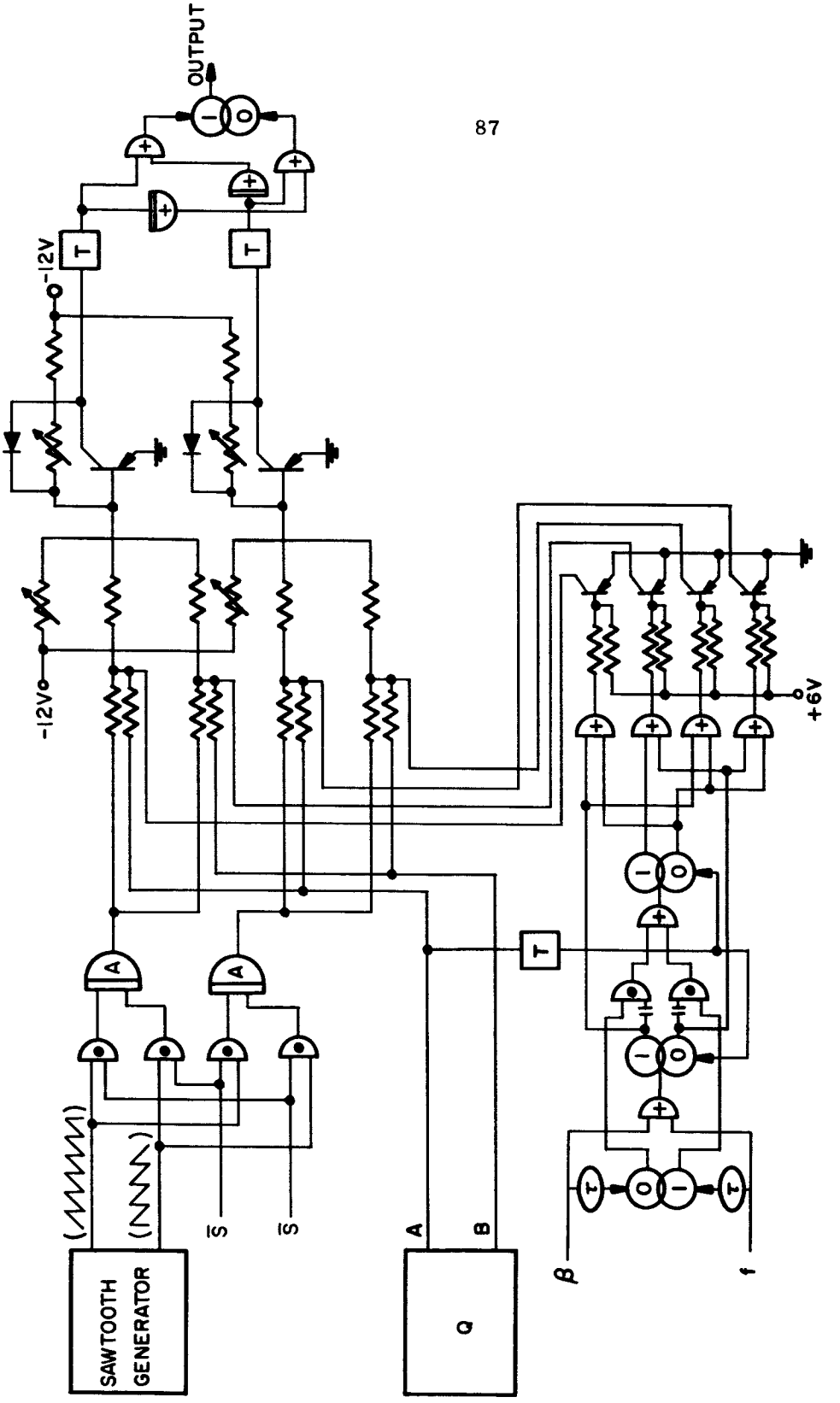

FIG. 33 LINEARIZING CIRCUIT

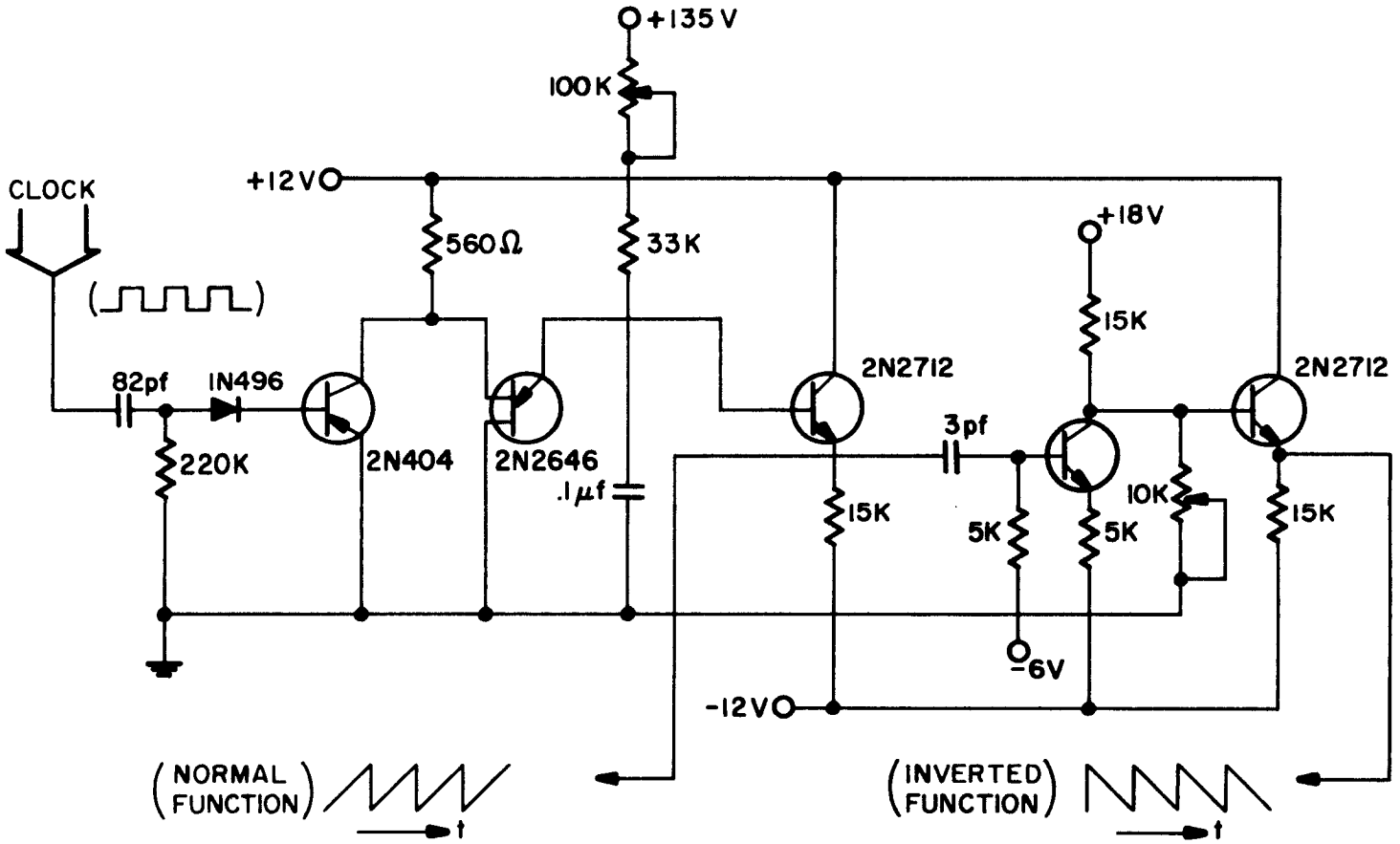

FIG. 34 SAWTOOTH WAVE GENERATOR

Figure 35 plots the quantizer output with the dither added as a function of time, assuming that the system is running at a constant velocity. The dither frequency has been shown to be ten times greater than the quantizer output frequency. In the system, this is the minimum frequency ratio that can exist between these two signals, which validates the usage of the dual input describing function in chapter 3. For half of the cycle, the proportional quantizer output is an increasing function, and the normal wave form is added. For the other half of the cycle, the proportional output is a decreasing function, and the dither signal must be subtracted. The inverted dither effects this subtraction. The decision as to which signal, summation or subtraction, is to be used is shown in the following logical equations. These equations have been derived from figure 28 and from the definition of forward and backward directions of rotation.

$$\{A + d(t)\} = \alpha_{A1}$$

$$\{A - d(t)\} = \beta_{A2}$$

$$\{B + d(t)\} = \alpha_{A2} f + \beta_{A1} B$$

$$\{B - d(t)\} = \beta_{A1} f + \alpha_{A2} B$$

Where: α represents a -12 to 0 volt transition of the trigger output

β represents a 0 to -12 volt transition of the trigger output

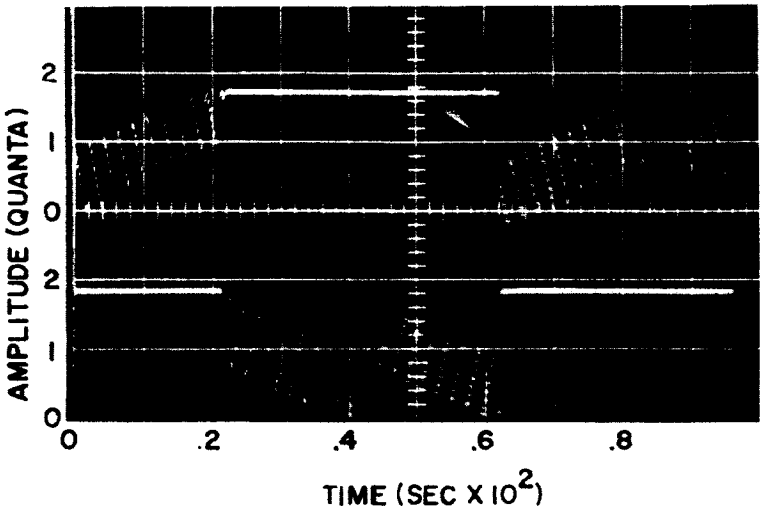

FIG. 35 QUANTIZER OUTPUT PLUS DITHER

A and B are ouputs from quantizer Q

These equations represent the analog quantity $\{A + d(t)\}$, etc., as a boolean variable. To implement this function, a special "and" gate was designed to accommodate both analog and boolean variables, as shown in figure 36. When C is -12 volts, the inverse of $\{A + d(t)\}$ will be available at D; when C is grounded, there will be no transference of $\{A + d(t)\}$. It is possible to add more stages to the circuit provided only one input at a time is activated. With more than one stage, the unit performs an "either/or" function, which can be expressed in "and/or" logic, as follows:

$$D = (A + B + C + \ldots)(\overline{AB})(\overline{AC})(\overline{BC})(\overline{ABC})(\ldots)$$

In order to obtain a function which will provide the proper gating for the appropriate signals, an observation can be made on the sequence for these signals. Table 1 shows the sequence for the forward and backward directions of rotation. It is shown that these sequences are the reverse of each other. Table 2 shows that the state at $(\Omega \pm \pi/2)$ is dependent only upon the state and direction of rotation at Ω.

The two-bit binary bidirectional counter with a diode matrix binary-to-decimal converter was used to implement the above sequence. This circuit is shown in figure 33 . The input

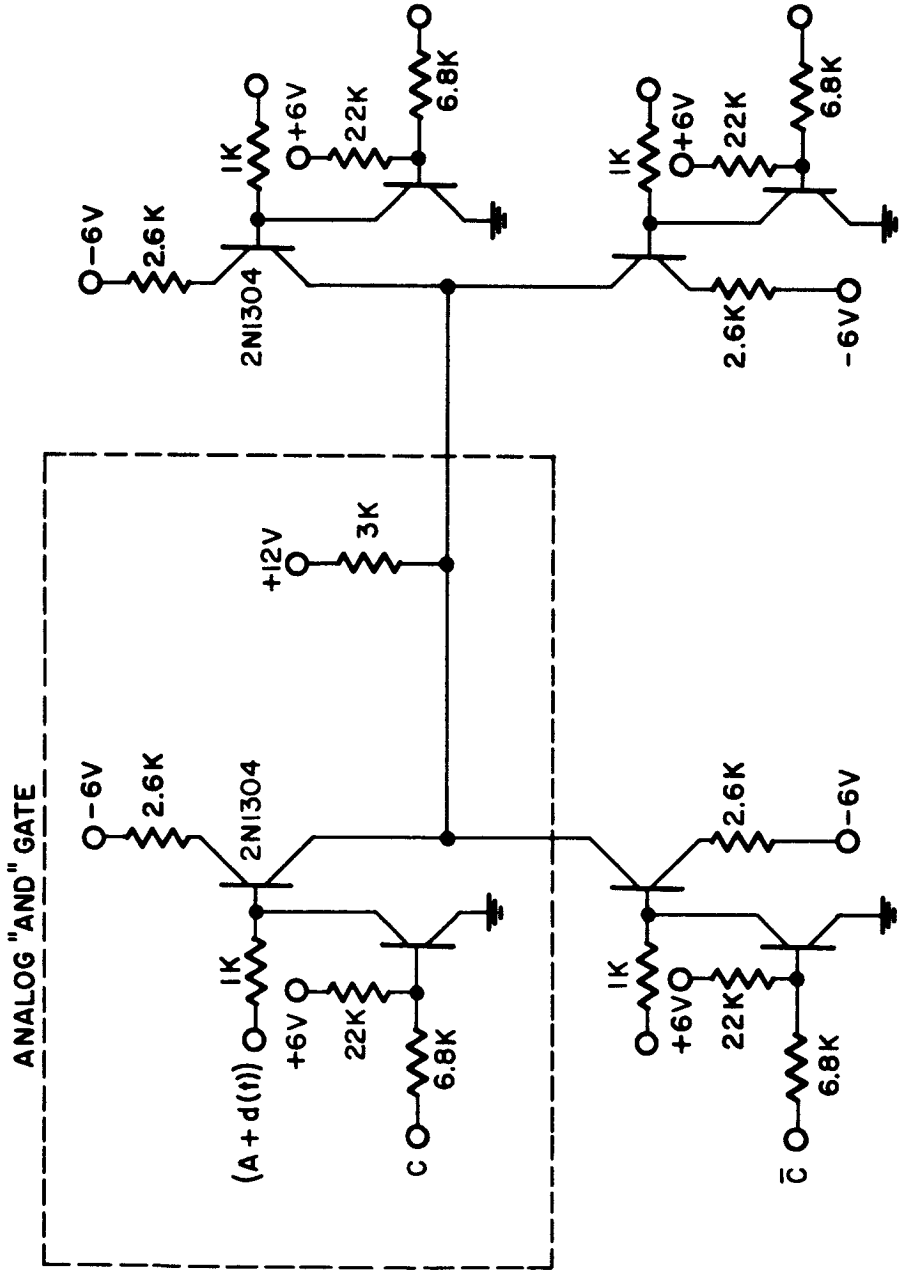

FIG. 36 MULTI-INPUT ANALOG "EITHER-OR" GATE

TABLE 1

DITHER SEQUENCE FOR THE DIRECTIONS OF MOTION OF THE OUTPUT VARIABLE

Forward		Backward	
{A + d(t)}	(1)	{A + d(t)}	(1)
{B + d(t)}	(2)	{B - d(t)}	(4)
{A - d(t)}	(3)	{A - d(t)}	(3)
{B - d(t)}	(4)	{B + d(t)}	(2)
{A + d(t)}	(1)	{A + d(t)}	(1)

TABLE 2

DITHER STATE TRANSITIONS AS A FUNCTION OF THE PLANT OUTPUT (Ω)

Ω	$\Omega + \pi/2$	$\Omega - \pi/2$
{A + d(t)}f	{B + d(t)}f	{B + d(t)}B
{A - d(t)}f	{B - d(t)}f	{B - d(t)}B
{B + d(t)}f	{A - d(t)}f	{A - d(t)}B
{B - d(t)}f	{A + d(t)}f	{A + d(t)}B
{A + d(t)}B	{B - d(t)}f	{B - d(t)}B
{A - d(t)}B	{B + d(t)}f	{B + d(t)}B
{B + d(t)}B	{A + d(t)}f	{A + d(t)}B
{B - d(t)}B	{A - d(t)}f	{A - d(t)}B

to flip-flop D, used to gate forward or backward counts, is delayed such that any pulse indicating a reversal in direction of rotation is counted by the counter before the count direction levels are changed.

Both the normal and inverted sawtooth dither wave forms are needed for linearization with positive and negative error. The dither is added to a signal proportional to the plant output, but the linearization is achieved by altering the quantized error signal. The quantizer input-output relationship must be redefined when the results of quantization of the feedback signal are observed in the forward loop. Figure 37 shows the quantizer Q* input-output relationships as observed in the forward loop. The dither must be subtracted at this point.

Figure 37 also shows the means of implementing the dither with both a positive and a negative error of Δ. With a positive error, the normal dither form is subtracted; with a negative error, the inverted dither is subtracted. The output from the quantizer plus dither has also been shown for one cycle of the dither. The following equations show that the average output from the quantizer is equal to the actual error assumed. If, however, the normal wave form were subtracted from the negative error, the average output would be $(\Delta - 1)$ rather than $-\Delta$.

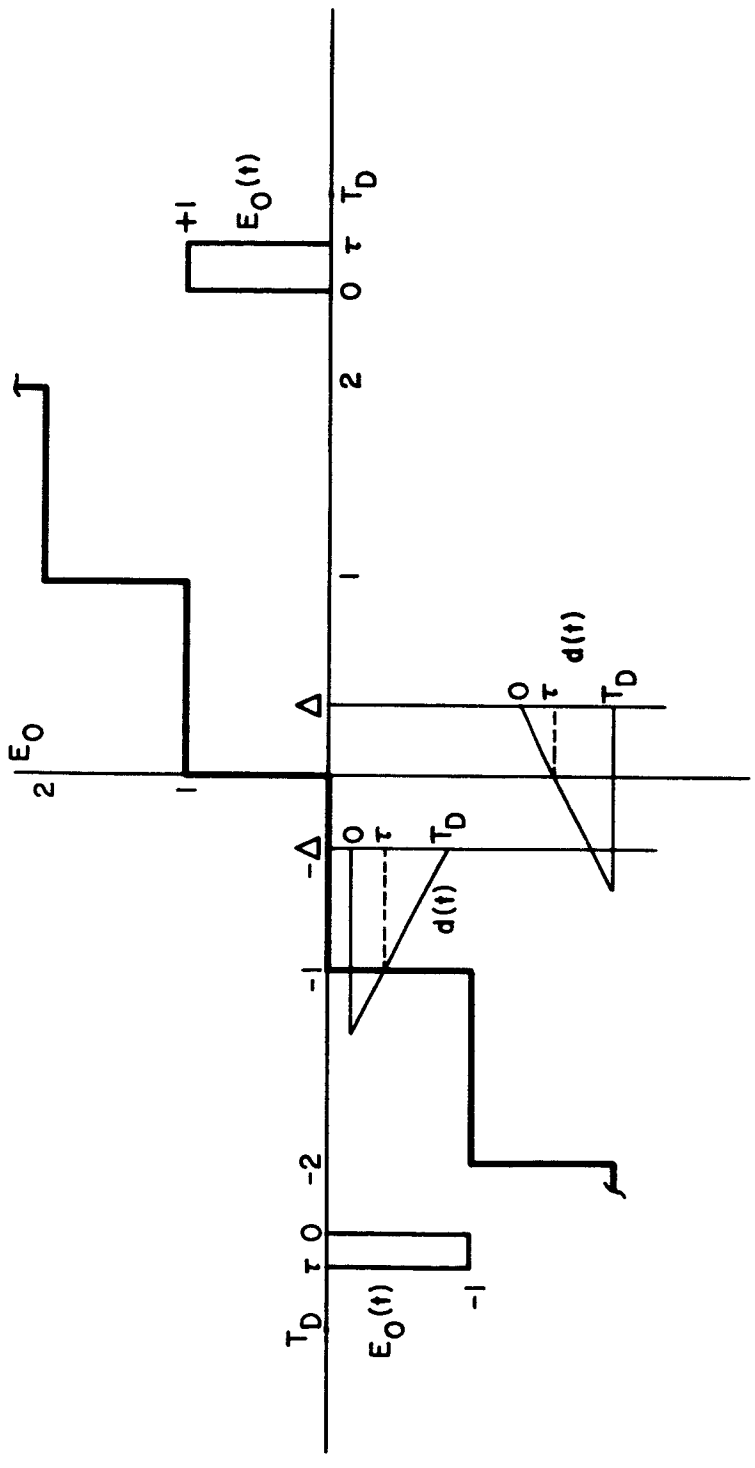

FIG.37 ILLUSTRATING THE NEED FOR INVERTING THE DITHER WHEN THE SIGN OF THE ERROR CHANGES

$$d(t)_N = \frac{t}{T_d} - \sum_{n=0}^{\infty} u(t - nT_d)$$

$$d(t)_I = -\frac{t}{T_d} + \sum_{n=0}^{\infty} u(t - nT_d)$$

Therefore: $$E^{+}_{0\ ave} = \frac{1}{T_d}\int_{\tau}^{T_d} dt = \frac{1}{T_d}(T_d - \tau)$$

Where: $\tau = T_d(1 - \Delta)$

Therefore: $$E^{+}_{0\ ave} = \Delta$$

$$E^{-}_{0\ ave} = \frac{1}{T_d}\int_{0}^{\tau} - dt = \frac{-\tau}{T_d}$$

Where: $\frac{\tau}{T_d} = \Delta$

Therefore: $$E^{-}_{0\ ave} = -\Delta$$

As shown in figure 33, the output from the summation process is converted to a square wave by a trigger. The threshold of this trigger is set equal to a level corresponding to one quanta. The change in state of the trigger is used to reset the relay. The logic required is different when the error is positive than when it is negative. When the error is positive, this signal turns off the relay when it occurs, as the reset gate for the relay flip-flop for a positive error is gated open at this time by the combined decision logic circuitry. However, when

the error is negative, this reset line is not gated open, and the signal from the trigger on the leading edge of the sawtooth wave form is used to gate open the reset line. Hence, when the summation of the dither and the signal from the quantizer are equal to one quanta, the relay will then be reset. This problem arises because the error indication by the bidirectional counter is always greater than or equal to the actual error that exists when there is a positive error. It is always equal to or less than the actual error when the sign of the error is negative. The circuit used to change from the normal to the inverted wave form is shown in figure 33. It performs an "either/or" function.

Figure 38 shows a timing diagram for the relay operation for both positive and negative errors. The time delay in relay closing τ has also been indicated in figure 33. This figure clearly shows the difference in operation between a positive and a negative error.

The quantized error stored in the bidirectional counter is always greater than the actual error, due to the definition for the quantizer, shown in figure 37. For positive errors, the relay must be turned off by the compensating signal before it would be normally turned off by the circulating register output. As shown in figure 38, the reset level is set to gate either the clock pulse occurring with a coincidence between the circulating register and the bidirectional counter or a pulse from the linearizing circuit.

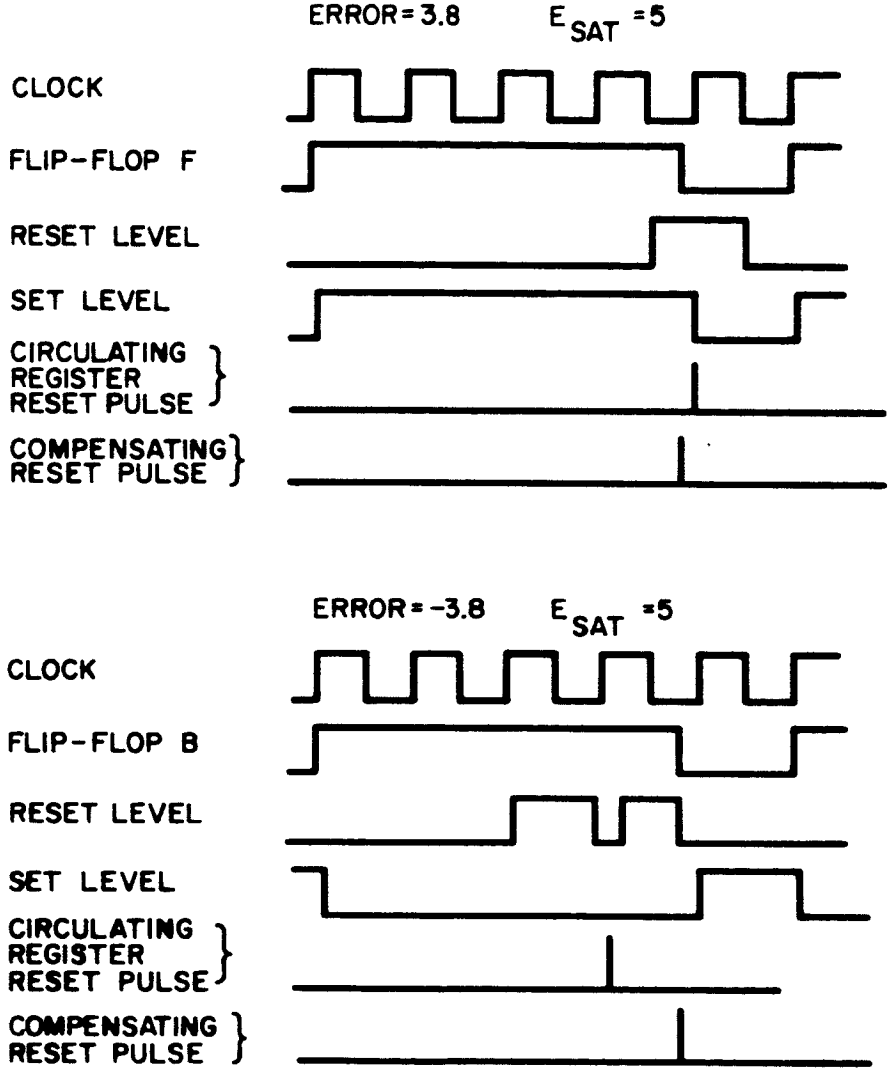

FIG. 38 TIMING DIAGRAM FOR SET AND RESET PULSES TO THE RELAY

In order to minimize the circuitry, this same register is used for negative errors. The compensating signal is now used to delay the turnoff of the relay beyond the time that the circulating register output pulse would normally turn it off. Since the normal reset gating level is not available, other means are used to gate the compensating pulse at the proper time.

Relay

Figure 39 shows the configuration used for the input to the armature of the motor. This is a solid state relay which provides a zero source impedance when the power is turned off. The source impedance is essentially zero when the relay is turned on, due to the zener diode regulated power supply. This relay is capable of being driven at frequencies of up to four kilocycles, which is much greater than the system band pass.

Compensating Scheme for Reducing Output Ripple

Figure 18 of chapter 4 shows a system with a gain in the input line. This gain was introduced to allow an increase in the range of input rates that the system will follow and still keep the output ripple below a given maximum. This refinement was not implemented in this thesis since the implementation duplicates the circuitry used to control the relay and uses the same reasoning to effect the error as was used in the section describing the linearization of the quantizer.

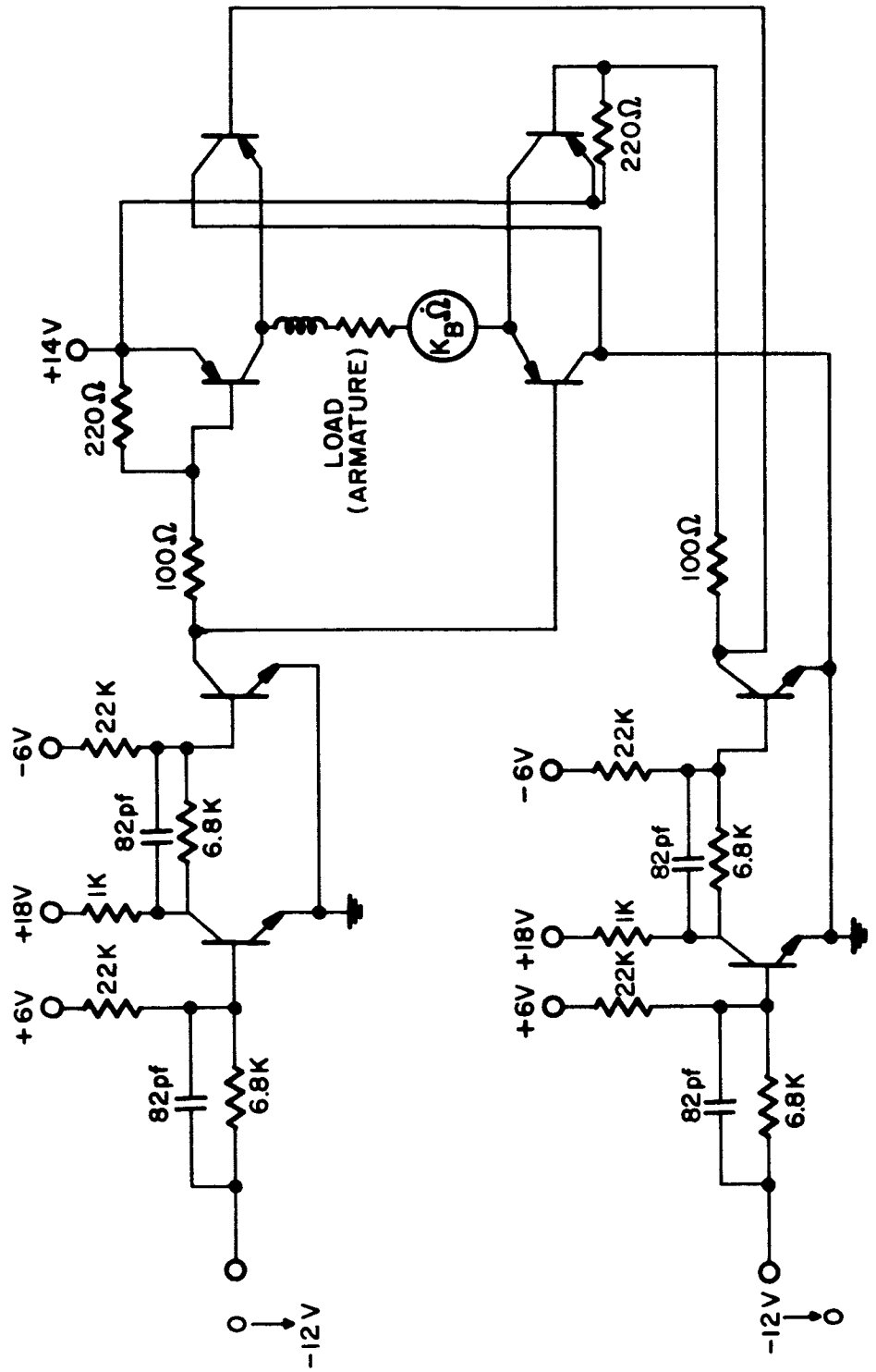

FIG. 39 CIRCUIT DIAGRAM FOR RELAY

Figure 40 shows the suggested block diagram. The capacity of the bidirectional counter C_1 is equal to the gain M. This counter sends one pulse to the bidirectional counter C_2 for every M reference pulses r(t). The count in this counter C_1 represents the quantization error of the reference input. This quantization error is accounted for by the decision logic block number two. This block is identical to the decision logic block described previously. The clock frequency driving this block, however, must be 1/M times the frequency of the clock number one.

The pulse that is gated out from the decision logic block number two will be used to turn the relay on early in the case of a positive error and to delay the turning on of the relay in the case of a negative error. The reasoning behind this is the same as was presented for the linearizing signal from the quantizer.

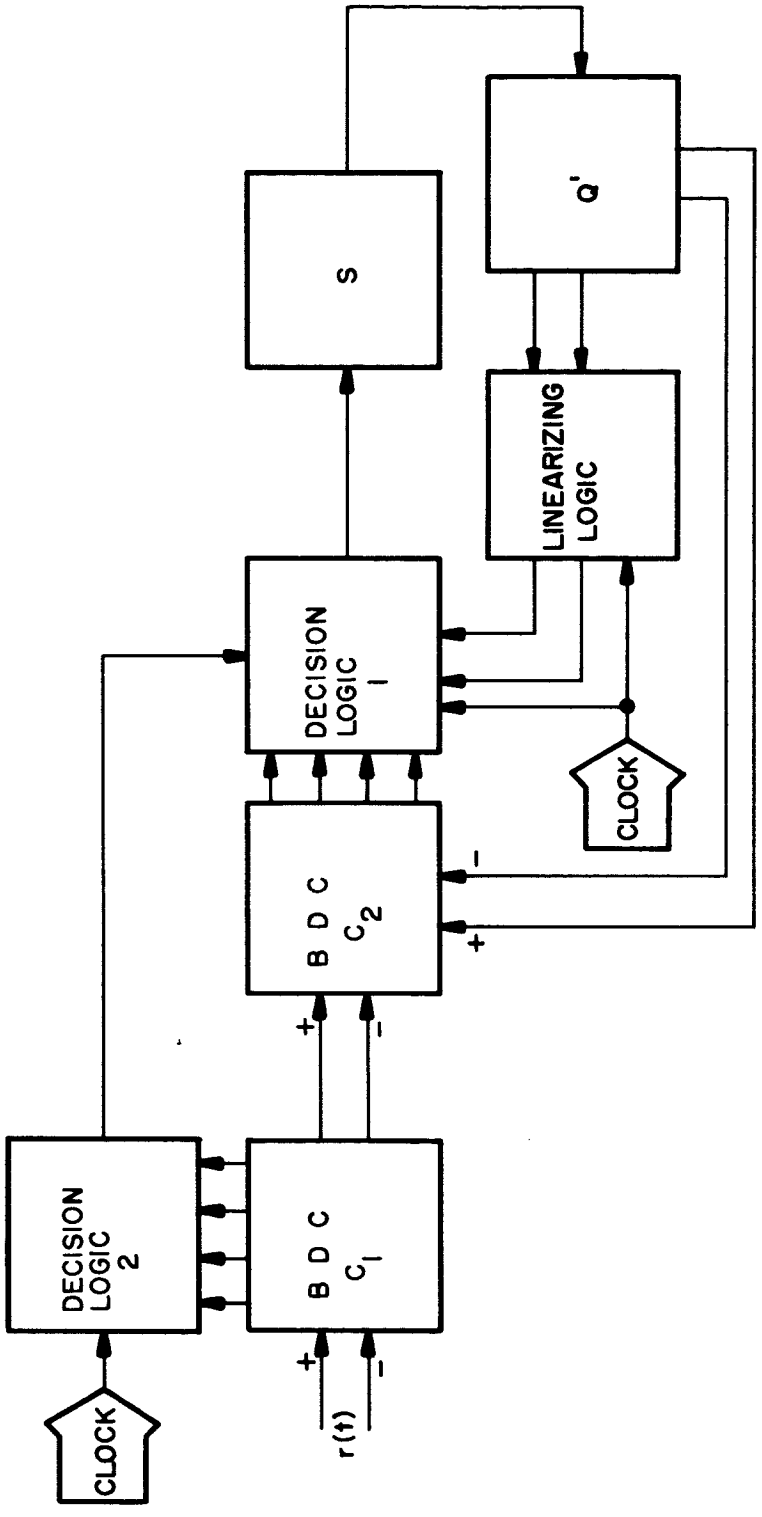

FIG. 40 BLOCK DIAGRAM FOR IMPLEMENTATION OF WEIGHTING THE REFERENCE PULSES

APPENDIX B

The standard logical component circuit diagrams used in this report are shown in this appendix.

Nor Gate

The nor gate satisfies the following logical function:

$$0 = \overline{(A_1 + A_2 + A_3 + \ldots + A_n)}$$

Figure 41 shows the symbolic representation. Figure 41B shows the circuit used to implement this function. To obtain an "or" function, it is necessary to use a "not" element, which is simply a single input nor gate.

Gated Pulse Generator

The gated pulse generator serves the function of an "and" gate for a pulse and a level. The circuit is shown in figure 42

Time Delay Element

For short time delays, a gated pulse generator serves a useful function. A level change from -12 volts to 0 volts can be delayed using a simplified gated pulse generator. Since the "and" function is not needed, one transistor can be deleted from the gated pulse generator circuit to form the circuit shown in figure 43. It is possible to have a multi-input delay, which is

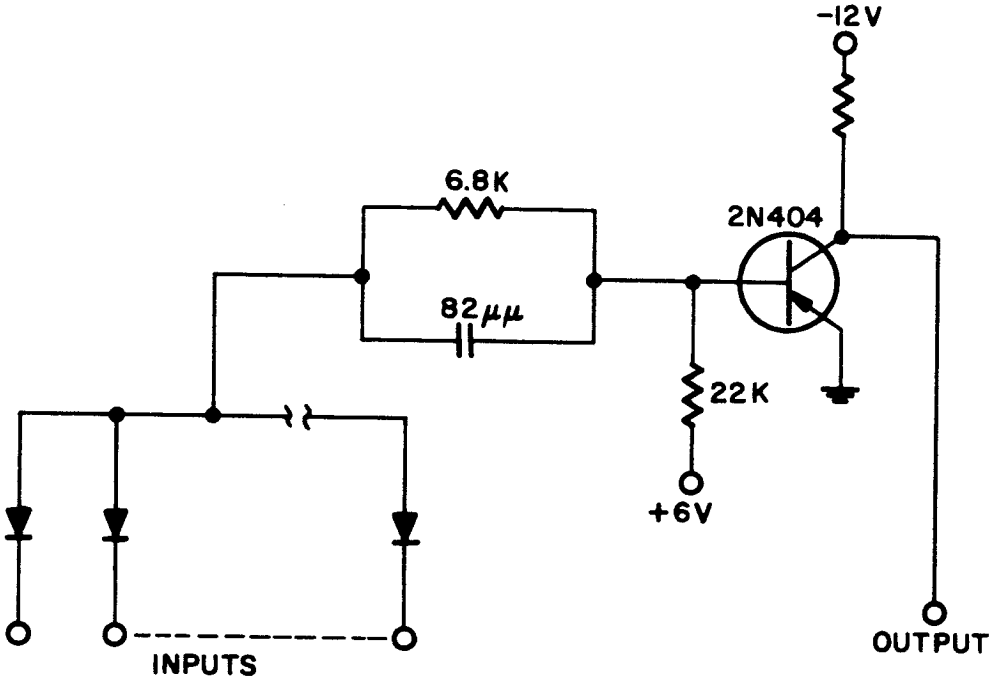

FIG. 41 NOR GATE

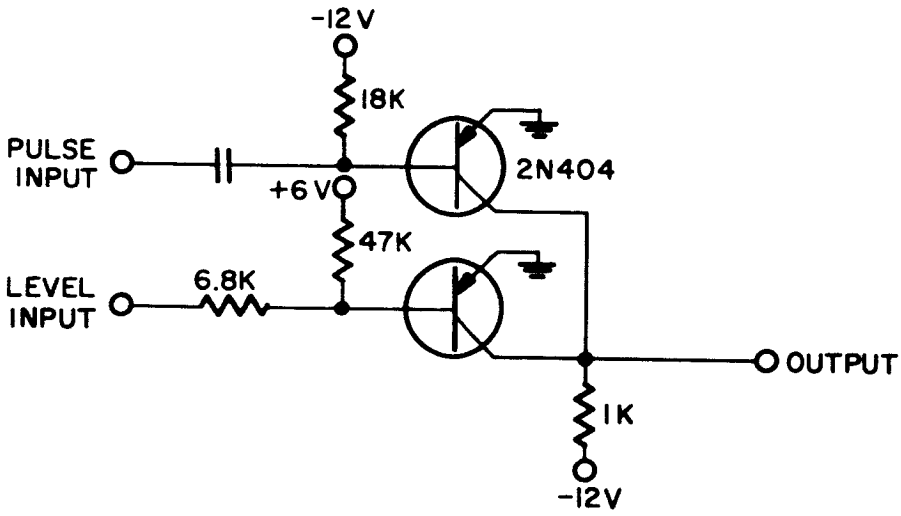

FIG. 42 GATED PULSE GENERATOR

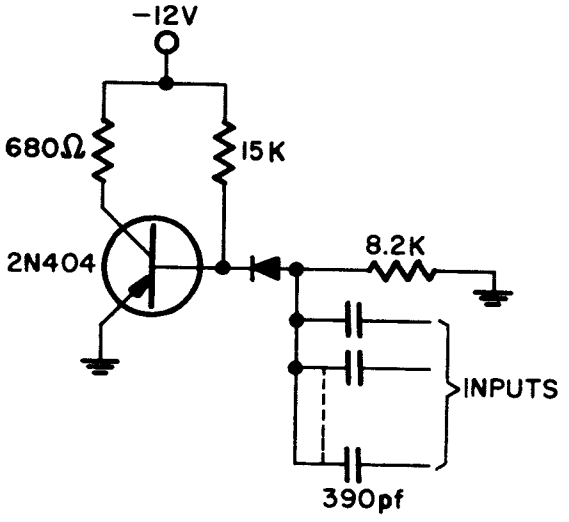

FIG. 43 MULTI-INPUT DELAY

an "or" gate, as shown, for delaying -12 to 0 volt level changes on each input line. This is only satisfactory if the separate inputs cannot occur simultaneously.

Free-running Multivibrator

The free-running multivibrator, shown in figure 44, is used as a "clock". The frequency of this "clock" can be varied easily by adjusting C and R. The output is a square wave operating between -12 and 0 volts.

Flip-flop

The circuit for the memory bit used (flip-flop) is shown in figure 45. This circuit can be used with separate set and reset pulses or, by joining the set and reset input lines, it serves as a trigger element which changes state for every input pulse. The unit operates on a level change from -12 to 0 volts.

Figure 46 shows the circuit used in the counter. It is a two-bit bidirectional counter, and it is possible to mount this on one printed circuit card for a 15 pin connector. This compacting of components serves a useful function in minimizing the number of printed circuit boards required for the total circuit.

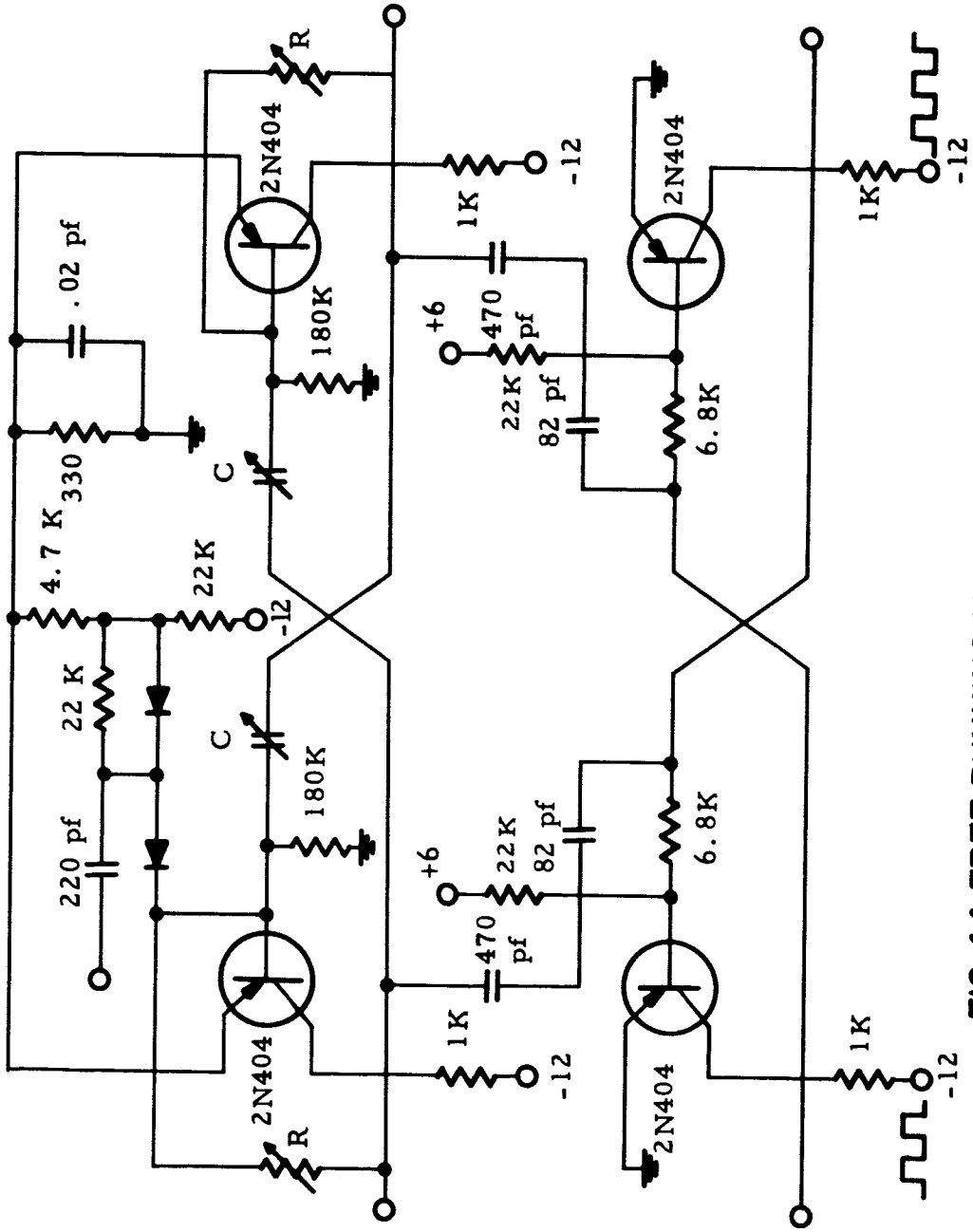

FIG. 44 FREE RUNNING MULTIVIBRATOR

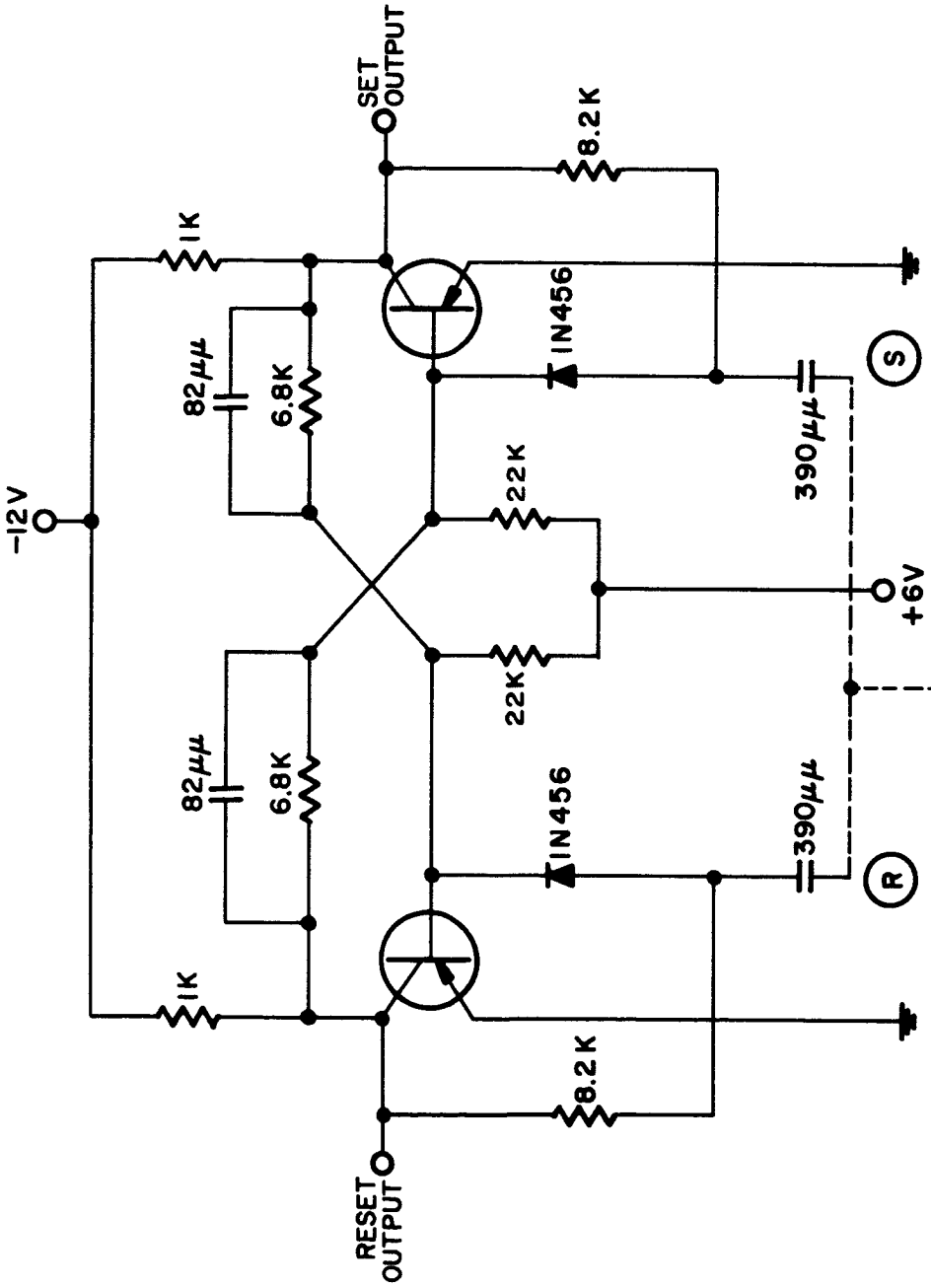

FIG. 45 FLIP-FLOP

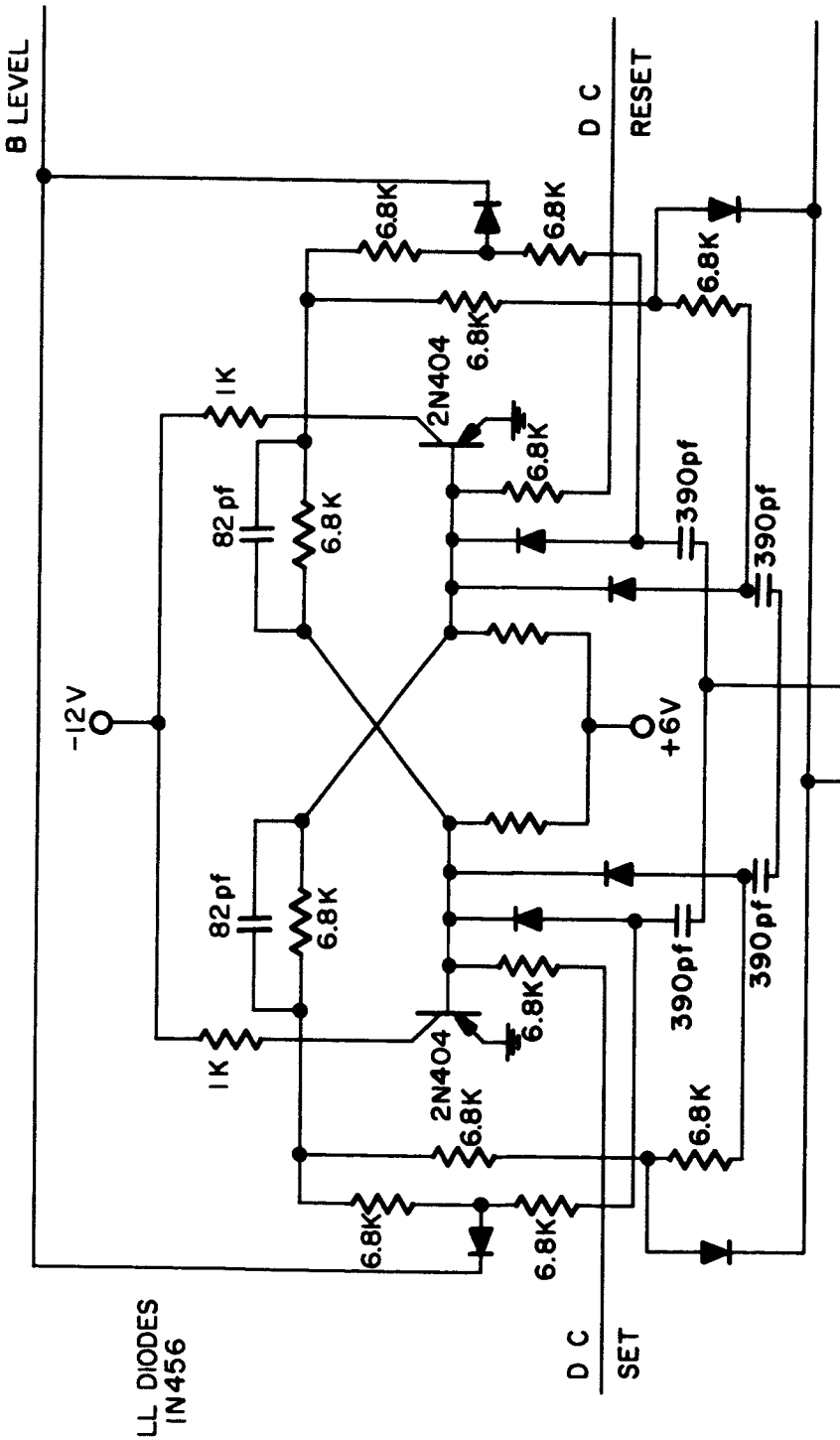

FIG. 46 TWO BIT BIDIRECTIONAL COUNTER

APPENDIX C

The method for determining the transfer function for the d-c motor used in chapter 5 is developed below:

Figure 47 shows the schematic diagram of a d-c motor with armature control. From this schematic, the following equations can be written:

$$\tau = K_t i_a = J\frac{d^2\Omega}{dt^2} + D\frac{d\Omega}{dt} + T_L \qquad \text{(C-1)}$$

Where: τ = output torque (ft.lb.)

K_t = torque constant (ft.lb./amp.)

i_a = armature current (amp.)

J = armature inertia (ft.lb. sec.^{2})

D = damping coefficient (ft.lb./rad./sec.)

Ω = armature position (rad.)

T_L = load torque (ft.lb.)

$$V_{bemf} = K_B\frac{d\Omega}{dt} \qquad \text{(C-2)}$$

Where: V_{bemf} = voltage produced by the armature (volts)

K_B = constant (volts/rad./sec.)

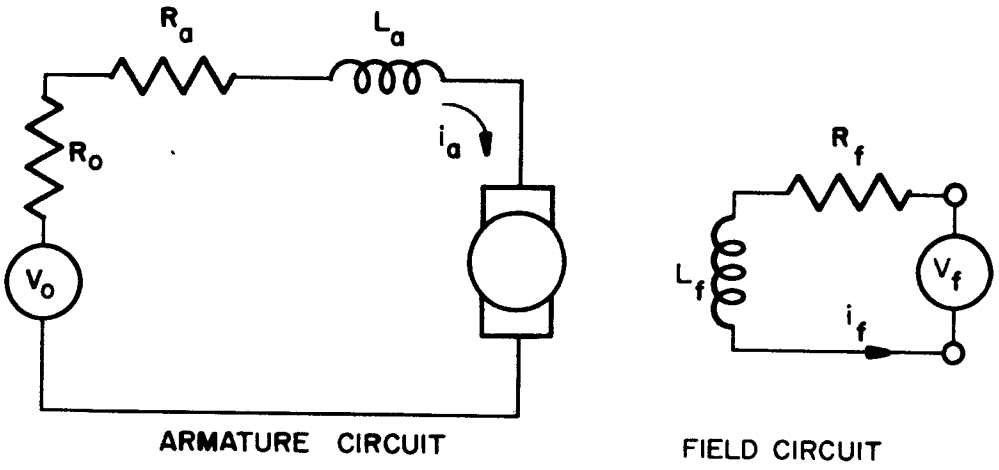

FIG. 47 MODEL OF D-C MOTOR WITH ARMATURE CONTROL

$$V_o = (Z_o + R_a) i_a + \frac{L_a di_a}{dt} + K_B \frac{d\Omega}{dt} \qquad (C-3)$$

Where: V_o = armature input voltage (volts)
R_a = armature resistance (ohms)
Z_o = source voltage (volts)
L_a = armature inductance (henries)

Figure 48 shows a plot of output torque vs armature current for zero velocity. The constant K_t can then be calculated from equation C-1:

$$K_t = \frac{T_L}{i_a} = 0.134$$

Figure 49 shows a plot of the open-circuit armature voltage vs speed of rotation. K_B can then be calculated from equation C-2:

$$K_B = \frac{V_{bemf}}{d\Omega/dt} = 0.182$$

Figure 50 plots the load torque vs the speed of rotation. These curves were obtained by static tests. Therefore,

$$\frac{d^2\Omega}{dt^2} = 0 \qquad \text{and} \qquad \frac{di_a}{dt} = 0$$

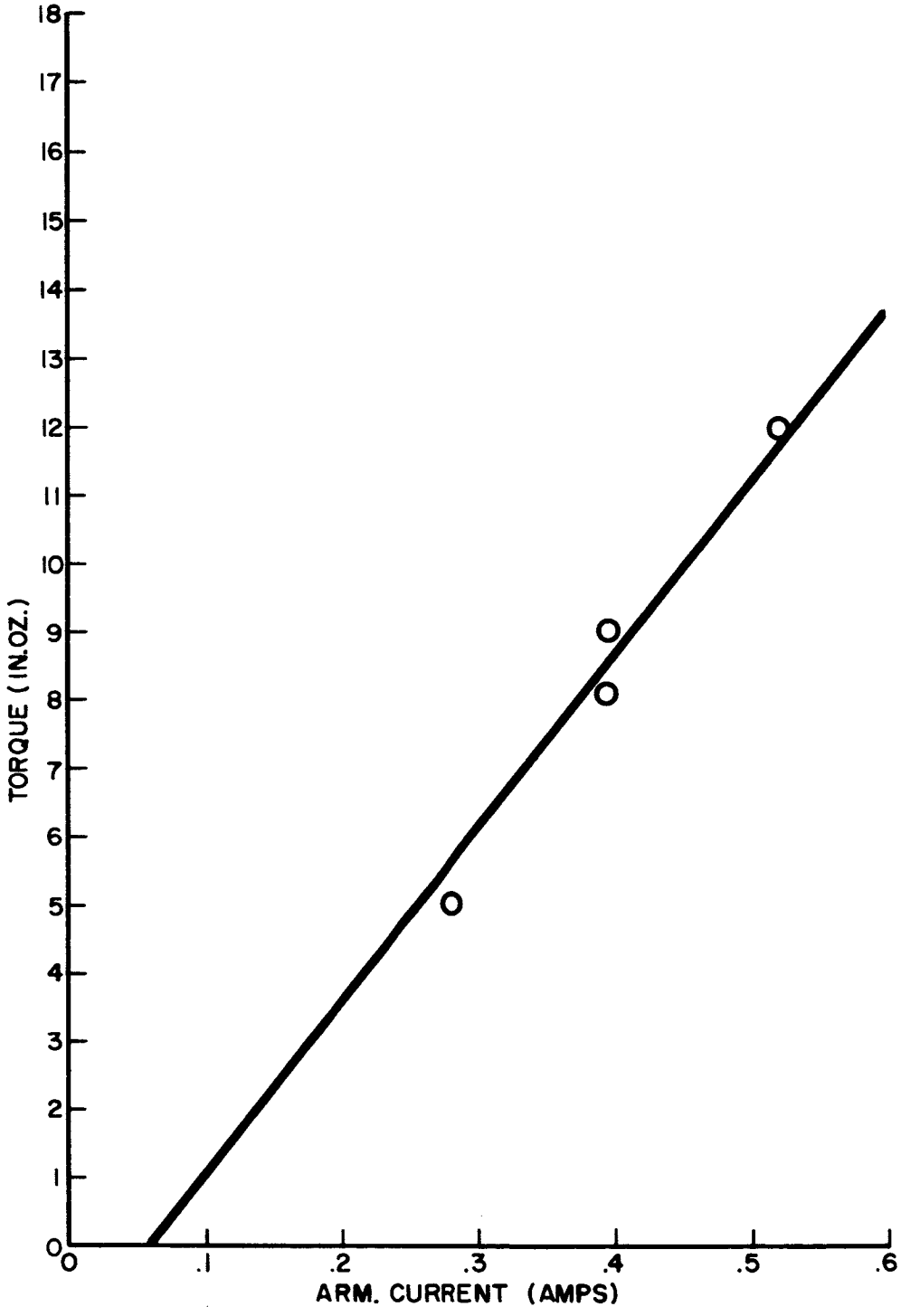

FIG. 48 LOCKED ROTOR TEST

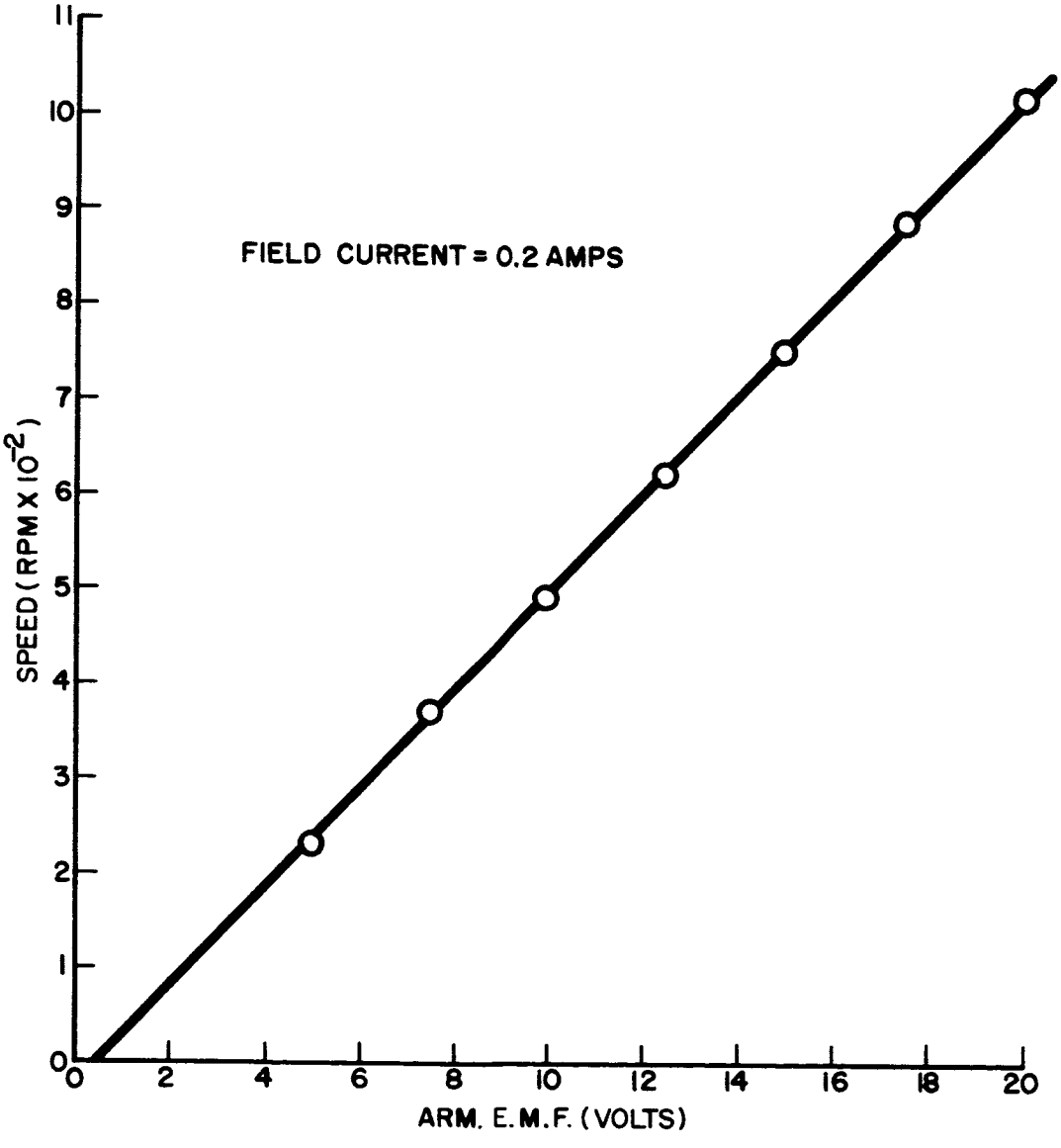

FIG. 49 ARMATURE BACK E.M.F. VS. SPEED

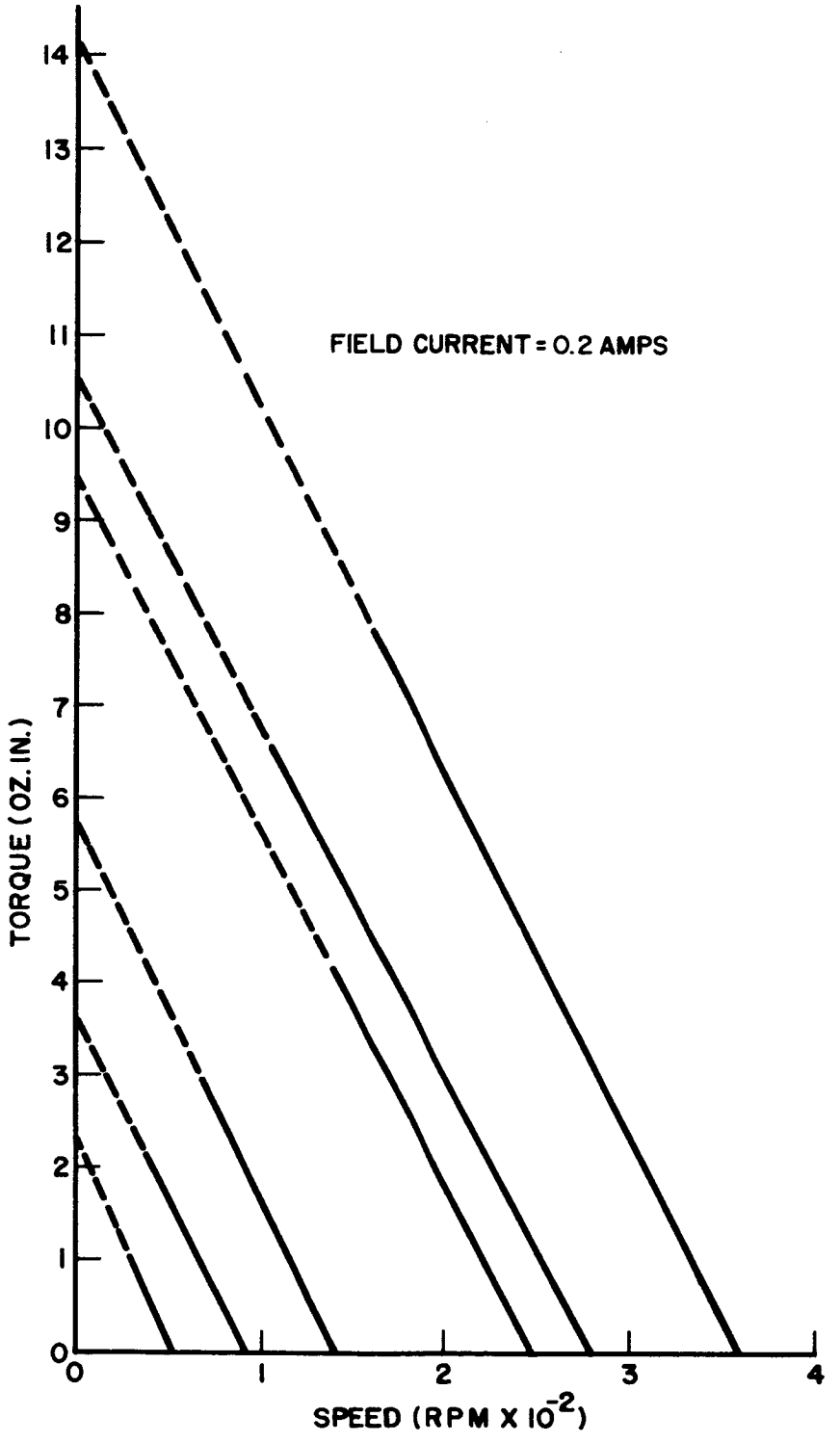

FIG. 50 TORQUE VS. SPEED

Therefore, equation C-1 can be written as:

$$T_L = K_t i_a - D\frac{d\Omega}{dt}$$

and equation C-3 becomes:

$$i_a = \frac{V_o}{Z_o + R_a} - \frac{K_B}{Z_o + R_a}\frac{d\Omega}{dt}$$

Combining these two equations,

$$T_L = \frac{K_t V_o}{Z_o + R_a} - \frac{K_B K_t}{Z_o + R_a} + D\frac{d\Omega}{dt}$$

By assuming that the curves in figure 50 are straight lines, D can be determined from the slope as follows:

$$\frac{-\tau}{d\Omega/dt} = \frac{K_B K_t}{Z_o + R_a} + D$$

The source impedance Z_o is zero, and the average armature resistance can be determined by rotating the armature, with no field voltage present, and allowing an ohmmeter to average the resistance. The value obtained was 25 ohms. Knowing the armature resistance, K_B and K_t, the drag coefficient may be determined as follows:

$$D = \frac{-\tau}{d\Omega/dt} - \frac{K_B K_t}{R_a} = 0.0014$$

The transfer function can be obtained from equations C-1, C-2 and C-3. By Laplace transforming and combining these equations,

$$\frac{\Omega}{V_a} = \frac{K_t}{(JS^2 + DS)(R_a + L_a S) + K_t K_B S}$$

The denominator polynomial contains two terms as yet not determined: J and L_a. Both of these values were measured and were as follows:

$$J = 0.9 \times 10^{-4} \text{ ft.lb. sec.}^2$$
$$L_a = 0.6 \times 10^{-4} \text{ henries}$$

They are both of the same order of magnitude; however, investigation of the denominator polynomial shows that it is permissible to ignore L_a. The coefficient of S^2 in the expansion of the denominator polynomial is independent of L_a since

$$DL_a \ll R_a J$$

Also, the coefficient of S^3 is very small, and its only influence

is to place one pole comparatively far out on the negative real axis in the S plane. The locations of the other two poles are essentially unaffected by L_a.

Therefore, the transfer function is:

$$\frac{\Omega}{V_a} = \frac{K_t}{JS^2 + DS + K_t K_B S}$$

$$= \frac{2.26}{S(0.0379S + 1)}$$

APPENDIX D

The computer program used to generate figures 16 and 17 is given. This program was written by Paul King, graduate student, Case Institute of Technology.

```
-        RUN        35018.0,        (300,030)
-N ALG TESTX
REAL A,B,C,D,TR,T,ET,M,N,OT,DT,K,DH,DL
REAL ARRAY Y(1..9 ),X(1..1010,1..2)      $ INTEGER I,J,L
FOR K=1.0,2.5,5.0,7.5,10.0,15.0,20.0 DO BEGIN
A=0.0$
READ(Y)$
D=SQRT(K-0.25)$
FOR I=(1,1,9)  DO BEGIN TR=Y(I)$ IF Y(I) EQL 0.0 THEN GO TO BACK$
A=0.5*SIN(D*TR)-D*COS(D*TR)+D*EXP(0.5*TR)$
B=0.5*EXP(0.5*TR)-0.5*COS(D*TR)-D*SIN(D*TR)$
C=D*(1.0+EXP(TR)-2.0*EXP(0.5*TR)*COS(D*TR))$
M=EXP(0.5*TR)*SIN(D*TR)$
N=1.0-EXP(0.5*TR)*COS(D*TR)$
DT=TR/500$ T=0.0$
FOR J=(1,1,501) DO BEGIN
X(J,1)=(EXP(0.5*(TR-T))*(A*COS(D*T)+B*SIN(D*T))/C)+T/TR  $
X(J,2)=K*EXP(0.5*(TR-T))*(M*COS(D*(TR-T))+N*SIN(D*(TR-T)))/C$
T=T+DT$ END$
FOR L=1 DO BEGIN  DH=-1000000$ DL=1000000$
FOR J=(1,1,501) DO BEGIN
DH=MAX(X(J,L),DH)$ DL=MIN(X(J,L),DL)$ END$
WRITE(D,K,TR,DH,DL,DH-DL)$ END$
BACK.. END$ END$
FINISH$
-N XQT TESTX
2.5 3.5 5.0 7.0 9.0 11.0 12.0 13.0 0.0
```

LIST OF REFERENCES

1. Sorensen, A. A. "Linear Control Using ON-OFF Controllers," Electro-Technology (April, 1963), pp. 99-101.

2. Thaler, George J., and Pastel, Marvin P. Analysis and Design of Nonlinear Feedback Control Systems. New York: McGraw-Hill Book Company, Inc., 1962, pp. 253-291.

3. Taft, Charles K. "Theory of Pulse-Data Systems Applied to an Input Self-Adaptive Pulse-Data System," Ph.D. Thesis. Cleveland: Case Institute of Technology, 1960.

4. Seshu, Sundaram, and Balabanian, Norman. Linear Network Analysis. New York: John Wiley and Sons, Inc., 1959.

5. Waidelich, D. L. "The Steady State Operational Calculus," Proceedings of the Institute of Radio Engineers (February, 1946), pp. 78-83.

6. Loeb, J. M. A General Linearizing Process for Nonlinear Control Systems Automatic and Manual Control. New York: Academic Press, Inc., 1952, pp. 275-83.

7. Furman, G. G. "Removing the Noise from the Quantization Process by Dithering: Linearization," Paper No. 63-WA-31. (Paper presented at the Winter Annual Meeting of The American Society of Mechanical Engineers, at Philadelphia, Pa., Nov. 17-22, 1963.)

8. Gibson, John E. Nonlinear Automatic Control. New York: McGraw-Hill Book Company, Inc., 1963, pp. 402-24.

9. Boyer, R. C. "Sinusoidal Signal Stabilization," M.S. Thesis. Purdue University, 1960.

10. D'Azzo, John J., and Houpis, Constantine H. Feedback Control System Analysis and Synthesis. New York: McGraw-Hill Book Company, Inc., 1960.

11. Taft, Charles K. "Discontinuous Control Theory," (A series of lectures presented at Case Institute of Technology, Cleveland, Spring, 1963.)

12. Graham, Dunstan, and McRuer, Duane. Analysis of Nonlinear Control Systems. New York: John Wiley and Sons, Inc., 1961.

13. Ninke, W. "A Shannon-Rack Decoder for a Digital Servomechanism," M.S. Thesis. Cleveland: Case Institute of Technology, 1961.

14. Susskind, Alfred K. (ed.) Notes on Analog-Digital Conversion Techniques. New York: John Wiley and Sons, Inc., 1957.

15. Nelson, Winston L. "Pulse-Width Relay Control in Sampling Systems," Transactions of the ASME Journal of Basic Engineering, Paper No. 60-JAC-4, 1960.